creative commons
COMMONS DEED

저작자표시-비영리-변경금지 2.0 대한민국

이용자는 아래의 조건을 따르는 경우에 한하여 자유롭게

- 이 저작물을 복제, 배포, 전송, 전시, 공연 및 방송할 수 있습니다.

다음과 같은 조건을 따라야 합니다:

**저작자표시**. 귀하는 원저작자를 표시하여야 합니다.

**비영리**. 귀하는 이 저작물을 영리 목적으로 이용할 수 없습니다.

**변경금지**. 귀하는 이 저작물을 개작, 변형 또는 가공할 수 없습니다.

- 귀하는, 이 저작물의 재이용이나 배포의 경우, 이 저작물에 적용된 이용허락조건을 명확하게 나타내어야 합니다.
- 저작권자로부터 별도의 허가를 받으면 이러한 조건들은 적용되지 않습니다.

**저작권법에 따른 이용자의 권리는 위의 내용에 의하여 영향을 받지 않습니다.**

이것은 이용허락규약(Legal Code)을 이해하기 쉽게 요약한 것입니다.

Disclaimer

dCollection

이학박사 학위논문

# Characterization of two growth regulatory genes, *pod1* and *NitFhit*

## 성장 조절 유전자 *pod1*과 *NitFhit*의 기능 규명

2021 년 8 월

서울대학교 대학원

생명과학부

전 경 호

# 성장 조절 유전자
# *pod1*과 *NitFhit*의 기능 규명

지도 교수 정 종 경

이 논문을 이학박사 학위논문으로 제출함
2021 년 8 월

서울대학교 대학원
생명과학부
전 경 호

전경호의 이학박사 학위논문을 인준함
2021 년 8 월

위 원 장 _____

부위원장 _____

위 원 _____

위 원 _____

위 원 _____

# Characterization of two growth regulatory genes, *pod1* and *NitFhit*

Professor Jongkyeong Chung

Submitting a Ph.D. Dissertation of
Biological Sciences

August, 2021

Graduate School of Biological Sciences
Seoul National University
Biological Sciences Major

Kyoungho Jun

Confirming the Ph.D. Dissertation written by
Kyoungho Jun
August, 2021

Chair _____
Vice Chair _____
Examiner _____
Examiner _____
Examiner _____

# Abstract

# Characterization of two growth regulatory genes, *pod1* and *NitFhit*

**Kyoungho Jun**

**Dept. of Biological Sciences**

**The graduate School**

**Seoul National University**

Through proper regulation of cell proliferation and apoptosis, tissues maintain their shapes and functions. Losing the balance between cell proliferation and cell death often results in diseases such as cancer. The Hippo pathway is a typical signaling mechanism that governs tissue homeostasis by regulating both cell proliferation and apoptosis. In part I, I studied the regulatory mechanisms of the Hippo pathway. To find a new regulator of the pathway, I listed potential candidates for the Hippo pathway from interactome databases and conducted the

genetic screening for validation. As a result, I found that *pod1* could be a previously unknown regulator of the Hippo pathway and examined whether *pod1* overexpression or mutations in *Drosophila* exhibits any phenotypes related to the pathway. I observed that *pod1* suppressed cell growth-related phenotypes such as changes in body weight, wing size, cell proliferation, and apoptosis. Therefore, I tested the genetic interaction between *pod1* and each component of the Hippo pathway. Firstly, Pod1 directly controls Yki activity through the Hippo pathway and is an upstream regulator of the core kinase complex of the pathway. Further genetic interactions with the membrane adapter complex showed that Pod1 is a downstream target of the complex. Based on these genetic data in *Drosophila*, I examined the physical interaction of CORO7, the mammalian homolog of Pod1, with the Hippo pathway components and found that CORO7 specifically interacts with SAV1, MST2, and LATS1. Furthermore, I observed that the core kinase complex doesn`t assemble in the absence of CORO7, indicating that CORO7 is essential for the complex formation. Finally, I also found that the tyrosine kinase SRC is an upstream regulator of Pod1 and regulates the Hippo pathway. In Part II, I discovered that NitFhit, the naturally occurring fusion protein between Nit1 and Fhit in *Drosophila*, positively regulates cell growth of the enterocyte. I found that *NitFhit* null fly is lighter than the wild-type and shows defects in food uptake and excretion. *NitFhit* expression in the enterocyte positively regulated the thickness of the intestinal wall and increased the resistance to starvation. Genetic evidence suggested that removal of hydrogen peroxide by Catalase can restore the defects of *NitFhit* knockout and ferredoxin reductase is necessary for NitFhit to regulate the intestinal wall thickness in *Drosophila*. In conclusion, I found two independent pathways controlling tissue growth. *pod1* is a novel regulator of the Hippo pathway modulating cell proliferation and death. Besides the tumor suppressor function, *NitFhit* in the enterocyte promotes cell growth thereby affecting the intestinal wall thickness. Since dysfunction of cell proliferation and

growth is the cause of multiple diseases such as cancer, my research revealing the mechanisms of cell proliferation and growth suggests new therapeutic mechanisms for the above diseases.

**Keywords:** Pod1, Hippo pathway, cell proliferation, core kinase complex, NitFhit, enterocyte.

***Student number*:** 2014-25024

# TABLE OF CONTENTS

# List of Figures

## List of Tables

# Background

## Background

Tissue growth refers to the size increase of the tissue during embryonic development, post-natal growth, and tissue regeneration. Tissue growth occurs through cell proliferation which consists of two parallel steps, cell growth that cell increases its mass, and cell division which grown cell divides into two smaller cells thereby increasing the number of cells (Neufeld et al., 1998; Su and O'Farrell, 1998; Thompson, 2010). Continuous division without cell growth results in the increase of cell number without volume, making cells smaller. Cleavage of the zygote to form a blastula during early embryonic development is a typical example of this process. Therefore, cell growth must precede cell division for cell proliferation and tissue growth to occur. In contrast, tissues can rarely grow by cell growth alone without cell division. Cells perform biosynthesis and increase their size according to their genome content. Since most cells are monoploidy having one copy of the genome, there is a limit to increasing the cell size. But after endo-replication cells become polyploidy with multiple copies of their genome, and increases their size further than monoploidy cells without cell division. Such examples are the growth of neurons during axonal pathfinding in nervous system development and epithelial cell growth of the intestine in the human or fat body and salivary gland development in *Drosophila*.

Cell growth is an increase in the volume and contents of a cell (Neufeld et al., 1998). Cell growth occurs when the cellular anabolic pathways synthesizing biomolecules such as protein and lipid exceed the catabolic pathways such as the biomolecule degradation by proteasome, lysosome, or autophagy. For the anabolic pathways to overwhelm the catabolic pathways, plenty of nutrients and growth factors generated by food uptake should be provided.

Treating the growth factor such as insulin/IGF-1 family or treating amino acids to the cell directly activates the PI3K/AKT/mTOR signaling pathway which is most famous for regulating cell growth (Saxton and Sabatini, 2017). The mTOR signaling pathway elevates mRNA transcription activity by promoting ribosome biogenesis through directly phosphorylating and activating S6-kinase (Xie et al., 2018). Also, the mTOR pathway elevates the translation activity by inhibiting 4E-BP, a known inhibitor of eukaryotic translation initiation factor eIF4E (Josse et al., 2016). Elevated mRNA transcription and protein translation activity promote cell growth by increasing protein synthesis including enzymes required to break down and absorb the nutrients. In contrast, nutrients deficiency, physical stress blocking cell expansion, or harmful chemical stress such as reactive oxygen species make cells prefer the catabolic pathway for survival, resulting in cell growth inhibition (Day and Suzuki, 2006; Levayer, 2020).

Ordinary tissues maintain their shape and homeostasis by keeping the balance between cell proliferation and programmed cell death called apoptosis (Bao et al., 2020). Severe DNA damages causing mutations in genes and defects in signaling pathways controlling cell growth, division, and death often result in continuous cell proliferation and abnormal tissue growth, ultimately leading to tumorigenesis (Feitelson et al., 2015).

# Material and Methods

## Material and Methods

### *Drosophila* strains and genetics

All *Drosophila* strains were maintained at 25°C. $w^{1118}$ strains were used for the wild-type control. Following *Drosophila* strains were used in this study: *GMR*-GAL4 [Bloomington Drosophila Stock Center (BDSC) 9146], *MS1096*-GAL4 (BDSC 8860), *Heat-shock*-GAL4 (BDSC BL2077), *Hedgehog*-GAL4 (BDSC 67046), *Cg*-GAL4 (BDSC 7011), *tubulin*-GAL4 (BDSC 5138), *Esg*-GAL4 (extracted from BDSC 84324), *Su(H)GBE*-GAL4 (BDSC 83377), *Myo1A*-GAL4 (extracted from BDSC 84307), UAS-*eGFP* (BDSC 5430), UAS-*pod1* (BDSC 8801), UAS-*pod1*:*GFP* (BDSC 8800), UAS-$pod1^{RNAi}$ [Vienna Drosophila Resource Center (VDRC) 108886], UAS-$yorkie^{RNAi}$ (BDSC 34067), UAS-*Yorkie*:*GFP* and UAS-$Yorkie^{S168A}$:*GFP* (from Dr. Ken Irvine), UAS-*Scalloped* (BDSC 9374), UAS-$warts^{RNAi}$ (VDRC 9928), UAS-*warts* (BDSC 44250), UAS-$Hippo^{RNAi}$ (from Dr. Georg Halder), UAS-$mats^{RNAi}$ (VDRC 17716), UAS-*salvador* (from Dr. Nicolas Tapon) UAS-$salvador^{RNAi}$ (BDSC 28006), UAS-$merlin^{RNAi}$ (VDRC 7161), UAS-$kibra^{RNAi}$ (BDSC 31755), UAS-$expanded^{RNAi}$ (BDSC 34968), UAS-$src64B^{RNAi}$ (BDSC 62157), UAS-*NitFhit*:*FLAG* (from Otmar Huber), UAS-*SOD2* (BDSC 24494), UAS-*Catalase* (BDSC 24621), and UAS-$dare^{RNAi}$ (VDRC 38683).

### Protein sequence comparison

Full amino acid sequences of each protein were obtained from NCBI. Protein sequence comparison was conducted using Multiple Sequence Alignment by CLUSTALW (https://www.genome.jp/tools-bin/clustalw) and GeneDoc program.

**Generation of *Drosophila* NitFhit, human Nit1, and human Fhit transgenic fly**

NitFhit, N-terminal Nit domain of *Drosophila* NitFhit, C-terminal Fhit domain of *Drosophila* NitFhit, human nitrilase 1, and human Fhit DNA were cloned into C-terminal HA-tagged pUAST vector and injected to $w^{1118}$ embryos.

**Generation of *pod1* and *NitFhit* knockout *Drosophila* using the CRISPR/Cas9 system**

Following guide-RNAs were used for *pod1* knockout *Drosophila* generation: 5′CTTCGCCTCCGCCTTGGGCACAAT and 3′AAACATTGTGCCCAAGGCGGAGGC.

Following guide-RNAs were used for *NitFhit* knockout *Drosophila* generation: 5 CTTCGGGCTTGG ACGGCGAGTTAA and 3’ AAACTTAACTCGCCGTCCAAGCCC.

Guide RNAs were ligated into pU6 chi-RNA vector and injected with pBS-Hsp70-Cas9 into $w^{1118}$ embryos.

**Measurement of the *Drosophila* body weight**

Three 5-day-old flies of each genotype were taken in EP-tubes respectively. The total body weight of three flies was divided into the average for the body weight of one fly for statistical analysis.

**Wing mounting**

*Drosophila* wings were mounted using Gary's Magic Mountant, a mixture of Canada balsam and methyl salicylate (4:1 v/v).

**Wing and intestine imaging**

Images of adult *Drosophila* wings and intestines were taken by Leica DM750 equipped with ICC50E (Leica) using 5× (numerical aperture: 0.15) chroma objectives. Data acquisition was performed using Leica Application Suite, version 4.10.0 (Leica).

**Quantification of the *Drosophila* wing size and intestinal wall thickness**

The *Drosophila* wing size and intestinal wall thickness were quantified using ImageJ program. To quantify the intestinal wall thickness, images of the intestinal wall were taken and the average distances between actin filament at 5 randomly distributed points were measured.

**Adult *Drosophila* imaging**

Adult *Drosophila* imaging was performed using Stemi 2000-C (Zeiss) and Axiovision Rel 4.8 (Zeiss).

**Immunostaining**

For the antibody staining in the imaginal eye disc, imaginal wing disc, and fat body, wandering larvae were dissected in PBS and then fixed with 4% paraformaldehyde for 20 min. For the antibody staining in the adult *Drosophila* intestine and mitochondria in the thorax, 7-days-old adult flies were dissected in PBS and then fixed with 4% paraformaldehyde for 1 h. Samples were washed two times with PBS with 0.1% Triton X-100 (0.1% PBST), permeabilized with 0.5% PBST, again washed with 0.1% PBST, and incubated with 3% bovine serum albumin in 0.1% PBST. The primary antibody was treated with the noted ratios for overnight at 4°C. On the next day, the primary antibody solution was removed, and samples were washed by 0.1% PBST three times and incubated 2 h at room temperature with the tetramethylrhodamine- or 647-conjugated secondary antibodies (Jackson, 1:200; Invitrogen, 1:200). The tissues were washed in 0.1% PBST three times and then washed in PBS twice shortly and mounted on a glass slide with 80% PBS + glycerol solution. Images were taken using the Zeiss 10 program. Following antibodies and chemical were used: disc-large [4F3, Developmental Studies Hybridoma Bank (DSHB), 1:200], DE-cadherin (DCAD2, DSHB; 1:200), a-phospho histone 3 (06-570, upstate, 1:200), KDEL (ab1223, abcam, 1:200), HA (6E2, Cell signaling, 1:200), Nit1 (3A11, GeneTex, 1:200), Phalloidin (P1951, Sigma, 1:200), 488-conjugated streptavidin (ab272187, abcam, 1:200), and Hoechst (33258, Invitrogen, 1:400).

**TUNEL assay**

For the TUNEL assay, wandering larvae were dissected in PBS and then fixed with 4% paraformaldehyde for 20 min. Samples were washed one time with 0.1% PBST, then incubated with 0.1% PBST containing 0.1 M sodium citrate at 60°C for 30 min, washed with 0.1% PBST

two times, permeabilized with 0.5% PBST, and washed with 0.1% PBST. Samples were incubated with a mixture of enzyme solution and label solution (1:9 v/v) from the below kit at 37°C for overnight. On the next day, the mixture solution was removed, and samples were washed by 0.1% PBST three times and then washed in PBS twice shortly and mounted on a glass slide with 80% PBS + glycerol solution. Images were taken using the Zeiss 10 program. The following kit was used: In Situ Cell Death Detection Kit, TMR red (Roche, 12156792910).

**Heat shock–induced gene expression in *Drosophila***

For heat shock-induced gene expression using *Heat-shock*-GAL4, 3-days-old flies were incubated at 30°C for 24 h.

**RNA isolation and real-time PCR**

Total RNA was isolated from *Drosophila* using Trizol reagent. Complementary DNA was synthesized by reverse transcription using oligo (dT) and subjected to real-time PCR with SYBR green PCR-Mix (Bioneer, Korea). The relative abundance of *diap1* mRNA was calculated by normalization to *rp49* mRNA. The following primer pairs were used: *diap1* (5′-GCCACCGTATCGATATAGAGC-3′ and 5′-CCAACGACTCGACGCTGG-3′); *rp49*: (5′-GCTTCAACATGACCATCCGCCC-3′ and 5′-GCGCTTCTTGGAGGAGACGCCG-3′). Data were obtained from five independent experiments and shown as the average mean ± S.D.

**ATP assay**

Two 7-day-old flies were homogenized in 100 µl of cell lysis reagent. The samples were incubated at RT for 5 minutes and centrifuged at 10,000 rpm for 1 min. 5 µl of supernatants were used for protein concentration by BCA method. The samples were diluted to 5 µg/ml protein concentration and mixed with luciferase reagent (50 µl: 50 µl). Luminescence was measured using Tecan-infinite 2000 pro and Tecan-i control 1.9 software. Reagents from the following kits were used: ATP Bioluminescence Assay Kit HS II (11699709001, Roche), Pierce™ BCA Protein Assay Kit (23325, Thermo Scientific).

**CAFÉ assay**

Two 7-day-old flies were incubated in the vial filled with 1% agarose for water supply. The vial at the side was drilled to make a hole to avoid suffocation. 10 µl of 10% sucrose solution with green dye was provided using a rubber lid and two capillaries. The amount of food uptake at the first day of incubation was excluded due to adaptation. Following reagents were used: Sucrose (S5-500, Fisher), Green-dye (LEAF GREEN, AmeriColor), Capillary (53432-706, VWR).

**Food uptake and excretion rate quantification**

Ten 7-day-old flies were incubated in the vial filled Kimwipes soaked with water for 24 h. Flies were transferred to the vial with 3M paper containing 100 µl of 10% sucrose solution with green dye for 1, 2, and 12 h. The amount of food uptake was quantified according to the quantification index. 12 h-fed flies were transferred to the vial filled with Kimwipes soaked

with water again for 24 h. Then, the number of flies still containing dyed solution in the abdomen was counted.

**Starvation assay**

Twenty 7-day-old flies was incubated in the vial filled with Kimwipes soaked with water each and the number of dead flies were counted every 12 h.

**Crop contraction rate quantification**

7-day-old flies were anesthetized briefly and dissected in PBS to incise the abdomen. The crop contraction number of wakening flies was counted per minute five times repeatedly, with 30 sec of rest between each counting. The average contraction rate of 5 times quantification was calculated.

**Mammalian cell culture and transfection**

HEK293T and MDA-MB-231 cells were maintained in DMEM containing 10% of fetal bovine serum. HEK293T and MDA-MB-231 cells were treated with dasatinib (50 nM or 250 nM) for 1 h or 2 h, respectively (Sigma-Aldrich; CD S023389). Plasmids were transfected with the polyethylenimine reagent. HEK293T cells were provided by Dr. John Blenis and MDA-MB-231 cells by Dr. Dae-sik Lim. A nontargeting siRNA was used for siRNA control (Bioneer, 1003). *CORO7* siRNA (Bioneer, 5′-CACCTTGTGTCTACTGGAT-3′ and 5′-

ATCCAGTAGACACAAGGTG-3′) was transfected to HEK293T cells and MDA-MB-231 cells using the RNAiMAX reagent (Invitrogen) according to the manufacturer's protocol.

**Plasmids**

The mammalian expression plasmids for human LATS1/2, MST1/2, and SAV1 were gifts from Dr. Dae-sik Lim (KAIST, Korea). CORO7 plasmid was purchased from Sino Biological (Beijing) and cloned in pcDNA3-hemagglutinin (HA), pcDNA3.1-Flag, and pcDNA3-Myc vector. Plasmids for truncated forms of genes were generated by PCR and cloned in pcDNA3-HA or pcDNA3.1-Flag expression vectors. *SRC* plasmid was purchased from Addgene and cloned into pcDNA3-HA vector. CORO7, and SRC mutants were generated by site-directed mutagenesis. All constructs were confirmed by DNA sequencing.

**Immunoblotting and immunoprecipitation**

Cells were lysed in lysis buffer (150 mM NaCl, 20 mM Tris, pH 7.4, 1 mM EGTA, 1 mM EDTA, 1% NP-40, 2.5 mM sodium pyrophosphate, 1 mM Na3VO4, 10% glycerol, and protease inhibitors). Equivalent protein quantities were subjected to SDS-PAGE and transferred to nitrocellulose membranes. Membranes were blocked with 5% bovine serum albumin and 0.1% Tween-20 containing TBS for 1 h at room temperature and then incubated with the indicated primary antibodies at 4°C overnight, followed by the appropriate HRP-conjugated anti-mouse/anti-rabbit secondary antibodies (Jackson) at room temperature for 1 h. Immunoreactive bands were visualized with enhanced chemiluminescence. Relative signal intensities of immunoblots were analyzed using Image Studio Lite 5.2 software (LI-COR

Biosciences). For immunoprecipitation, cells grown in 21.5 $cm^2$ culture plates were collected and lysed in 0.5 ml lysis buffer–containing protease inhibitors for 30 min at 4°C. After 12,000 g centrifugation for 15 min, the lysates were immunoprecipitated with 2 μg of specific antibody overnight at 4°C, and 30 μl protein A/G agarose beads were washed and then added for an additional 1 h. Thereafter, the precipitants were washed five times with lysis buffer, the immune complexes were boiled with loading buffer for 5 min, and analyzed by SDS-PAGE. The following antibodies were used for immunoblotting and immunoprecipitation: antibodies against HA (MBL Life Science; M132-3), Flag (MBL Life Science; M185-3L), Flag (CST; 2368), CORO7 (Abcam; ab117446), YAP (Santa-Cruz; sc-101199), p-YAP (CST; 4911), LATS1 (CST; 3477), tubulin (DSHB; E7), SAV1 (CST; 13301), p-Tyr (CST; 9411), and IgG (Millipore; 2896738).

**Statistical analysis**

All experiments were repeated at least three times, and all scatter graphs with bars were expressed as mean ± S.D. The Student's two-tailed t test was used. Prism 8 (Graphpad) was used for the statistical analyses.

# Results and Discussions

# Part I

# Characterization of Pod1 as a regulator of the Hippo signaling pathway

# Introduction

## The Hippo pathway

The Hippo pathway was initially discovered in *Drosophila melanogaster* during a mosaic-based screening for cell growth regulators (Justice et al., 1995; Xu et al., 1995). Sequential identification of tumor suppressor gene *Warts* (*wts*), *Salvador* (*sav*), *Hippo* (*Hpo*), and *mats* and research about the interaction between these genes established the currently known signaling pathway that is the master regulator of organ growth and tissue homeostasis (Harvey et al., 2003; Kango-Singh et al., 2002; Lai et al., 2005; Pantalacci et al., 2003; Tapon et al., 2002; Udan et al., 2003). The Hippo pathway regulates cell proliferation and apoptosis through co-transcription factor YES-associated protein [YAP, Yorkie (Yki) in *Drosophila*] (Huang et al., 2005; Sudol, 1994) and the core kinase complex consisting of mammalian sterile 20-like kinase 1/2 [MST1/2, Hpo in *Drosophila*], salvador family WW domain-containing protein 1 (SAV1, Sav in *Drosophila*), MOB kinase activator 1 (MOB1, mats in *Drosophila*), and large tumor suppressor kinase 1/2 [LATS1/2, Wts in *Drosophila*] (Harvey and Tapon, 2007). Under the growth-inhibitory condition, LATS1/2 of the core kinase complex phosphorylates YAP and inhibits its translocation to the nucleus (Hao et al., 2008). Phosphorylated YAP is retained in the cytosol by chaperone protein 14-3-3, and finally degraded by β-transducin repeat-containing E3 ubiquitin protein ligase (Dong et al., 2007; Zhao et al., 2010; Zhao et al., 2007). But under the favorable condition for cell to grow, the Hippo pathway is inhibited and YAP migrates to the nucleus and binds to the transcription factor transcriptional enhanced associate domain [TEAD, Scalloped (Sd) in *Drosophila*] to

express downstream genes required for cell cycle progression, cell proliferation, and inhibition of apoptosis, such as *diap, cycE, e2f1* (Goulev et al., 2008; Wu et al., 2008; Zhang et al., 2008).

**Regulatory mechanism of the Hippo pathway**

It is reported that the membrane adaptor complex, composed of NF2 [Merlin (Mer) in *Drosophila*], KIBRA (Kibra in *Drosophila*), and WILLIN [Expanded (Ex) in *Drosophila*] transfer extracellular activating signals to the core kinase complex by physical binding (Hamaratoglu et al., 2006; Yu et al., 2010; Zhang et al., 2010). Especially, NF2 among those three components is necessary for activating the core kinase complex, but the exact molecular mechanism is unclear. Upon growth-inhibitory signals, MST1/2 forms a dimer and auto-phosphorylates its activation loop (Zheng et al., 2017). Activated MST1/2 binds to and phosphorylates the scaffold protein SAV1 (Callus et al., 2006; Scheel and Hofmann, 2003). Next, SAV1- MST1/2 complex binds to and phosphorylates another scaffold protein MOB1, promoting its binding to the kinases LATS1/2 (Ni et al., 2015; Praskova et al., 2008). This complex composed of SAV1-MST1/2-MOB1-LATS1/2 is termed the core kinase complex of the Hippo pathway (Harvey and Tapon, 2007). LATS1/2 in the core kinase complex go into structural changes, phosphorylate themselves at their activation loop, and become active status to phosphorylate YAP (Hergovich et al., 2006).

Many upstream environmental cues regulate the activity of the Hippo pathway (Panciera et al., 2017). Nutrient and growth factor inhibits the Hippo pathway through GPCR (Yu et al., 2012). Mechanical stress such as cell-cell contact or cell-adhesion activates the Hippo pathway through spectrin and Rho-controlling actin filament homeostasis (Chang et al., 2019; Machnicka et al., 2014; Qiao et al., 2017). Other mechanical stress such as cell junction

activates the Hippo pathway through Scribble, Fat, and Dachsous (Verghese et al., 2012; Willecke et al., 2008). The Hippo pathway recognizes the cell polarity changes through Crumb and Disc large homolog1 (DLG1) (Chen et al., 2010; Meignin et al., 2007).

**The Hippo pathway as a therapeutic target**

Malfunctions of the Hippo pathway cause continuous cell proliferation despite the above cell growth inhibitory conditions, leading to disease development such as cancer (Harvey et al., 2013). For example, there is a report that hyperactivation of YAP in the mouse causes cancer by inhibiting apoptosis (Eder et al., 2020). Indeed, many genetic mutations of Hippo pathway components, such as NF2, had been reported in various cancer cell types (Gareth and baser, 2001). Several drugs targeting the Hippo pathway, such as MST inhibitor XMU-MP-1, are under development to cure the Hippo pathway-derived tumors (Dey et al., 2020).

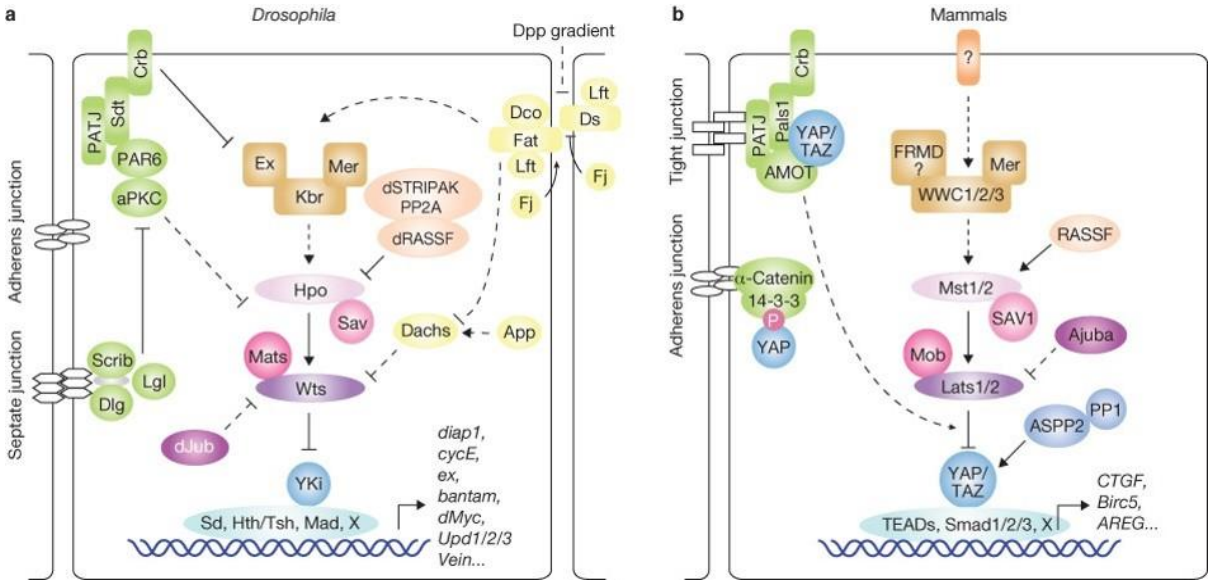


**Figure 1. An overview of the Hippo pathway.**

Adopted from Bin Zhao, Karen Tumaneng & Kun-Liang Guan (Zhao et al., 2011).

**The coronin superfamily**

Coronin7 (CORO7, Pod1 in *Drosophila*) is the only member of group III of the coronin superfamily, containing two WD40-repeat domains (Liu et al., 2016). Other members of the coronin superfamily from CORO1 to CORO6 have only one WD40-repeat domain. Instead, CORO7 lacks the C-terminal coiled-coil domain which plays roles in actin binding, complex formation with Arp2/3, and homo-oligomerization (Gatfield et al., 2005). *Drosophila* has two coronin homologs, Coro and Pod1. Coro has only one WD40-repeat domain, representing human CORO1 to CORO3. Pod1 has two WD40-repeat domains, representing human CORO7 (Rybakin et al., 2004). The WD40-repeat domain of the coronin superfamily consists of a seven-bladed β propeller structure (Xu and Min, 2011) which facilitates the protein-protein physical binding, such as the interaction between CORO7 and RacC (Swaminathan et al., 2015).

**Biological functions of the coronin superfamily**

Coronin family was reported to participate in actin-cytoskeleton homeostasis by forming the complex with Arp2/3 (Cai et al., 2007; Machesky et al., 1997). Also, the coronin family plays roles in signal transduction, endosomal trafficking, T cell signaling, and survival of bacteria in macrophages (Ferrari et al., 1999; Jayachandran, 2008). CORO7/Pod1 participates in actin cytoskeleton formation by interacting with Cdc42 and N-WASP (Bhattacharya et al., 2016; Rothenberg et al., 2003). CORO7 is located in the trans-Golgi network to regulate Golgi morphology and post Golgi-trafficking (Bhattacharya et al., 2016). There are few reports about post-translational modification of CORO7. Tyrosine kinase SRC directly phosphorylates 758 Tyr residues promoting the association of CORO7 to the Golgi

(Rybakin, 2008; Rybakin et al., 2008). Poly-ubiquitination by Cul3-KLHL20 ubiquitin E3 ligase activates the function of F-actin assembly and protein trafficking of CORO7 (Yuan et al., 2014).

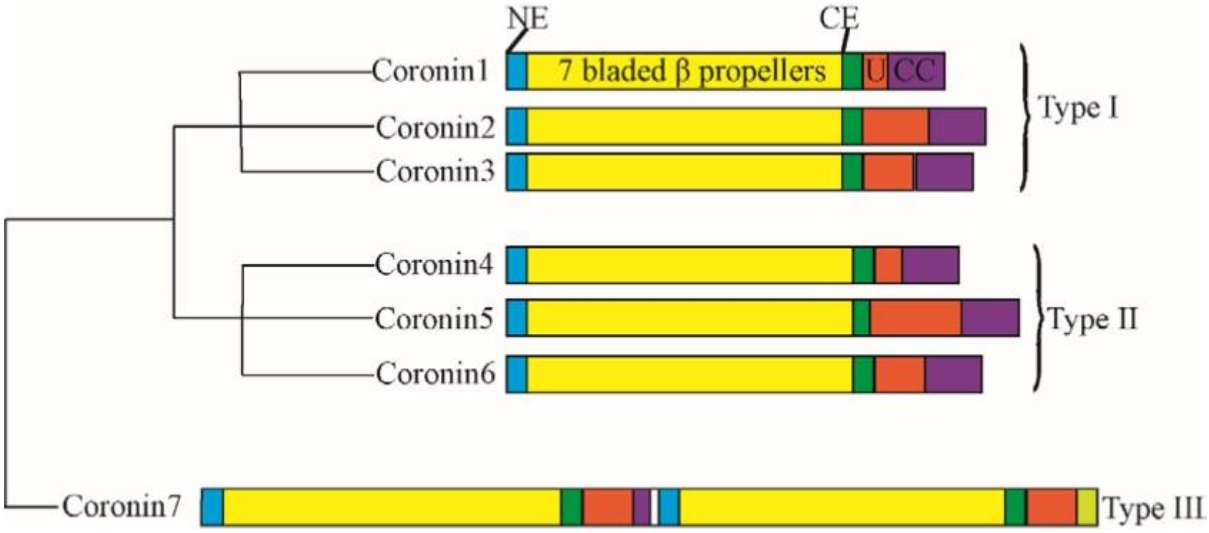


**Figure 2. Structural domains and phylogenetic relationships of mammalian coronins.**

Adopted from Xiaolong Liu, Yunzhen Gao, Xiao Lin, Lin Li, Xiao Han and Jingfeng Liu (Liu et al., 2016).

**SRC tyrosine kinase**

The proto-oncogene SRC is a non-receptor tyrosine kinase encoded by the human *SRC* gene. The human *SRC* gene encodes 536 amino acids and SRC protein consists of an N-terminal myristoyl group, an SH3 domain, an SH2 domain, an SH2-kinase linker, an SH1 domain responsible for kinase activity, and a C-terminal regulatory segment (Brown and Cooper, 1996; Thomas and Brugge, 1997). SRC interacts with RTKs such as IGF-1R, EGFR, and PDGFR (Moon et al., 2002) through SH2 and SH3 domains, and regulates related signaling pathways. Especially, SRC regulates the Hippo pathway to control cell proliferation and apoptosis. At first, SRC was known to inhibit the Hippo pathway indirectly, through modulating the PI3K pathway (Kim and Gumbiner, 2015). In addition, another study revealed that *src64B* in *Drosophila* activates the c-Jun N-terminal kinase signaling to suppress the Hippo pathway (Enomoto and Igaki, 2013; Fernandez et al., 2014). However, recent studies revealed that SRC can directly suppress the Hippo pathway activity, by inhibiting LATS1 and activating YAP via phosphorylation (Lamar et al., 2019; Si et al., 2017). It is known that the regulation of SRC on the Hippo pathway is activated by the adhesion of cells to the extracellular matrix (Byun et al., 2017; Li et al., 2016), one of the Hippo pathway-inhibiting conditions.

Here, to understand the regulatory mechanism of the Hippo pathway, I conducted the genetic screening and found *pod1* to be a novel regulator of the Hippo pathway. Knockout characterization, genetic interaction with the Hippo pathway components, and co-immunoprecipitation assays confirmed that Pod1 directly participates in the Hippo pathway. Moreover, I suggest the tyrosine kinase SRC as an upstream regulator of Pod1 for regulating the Hippo pathway.

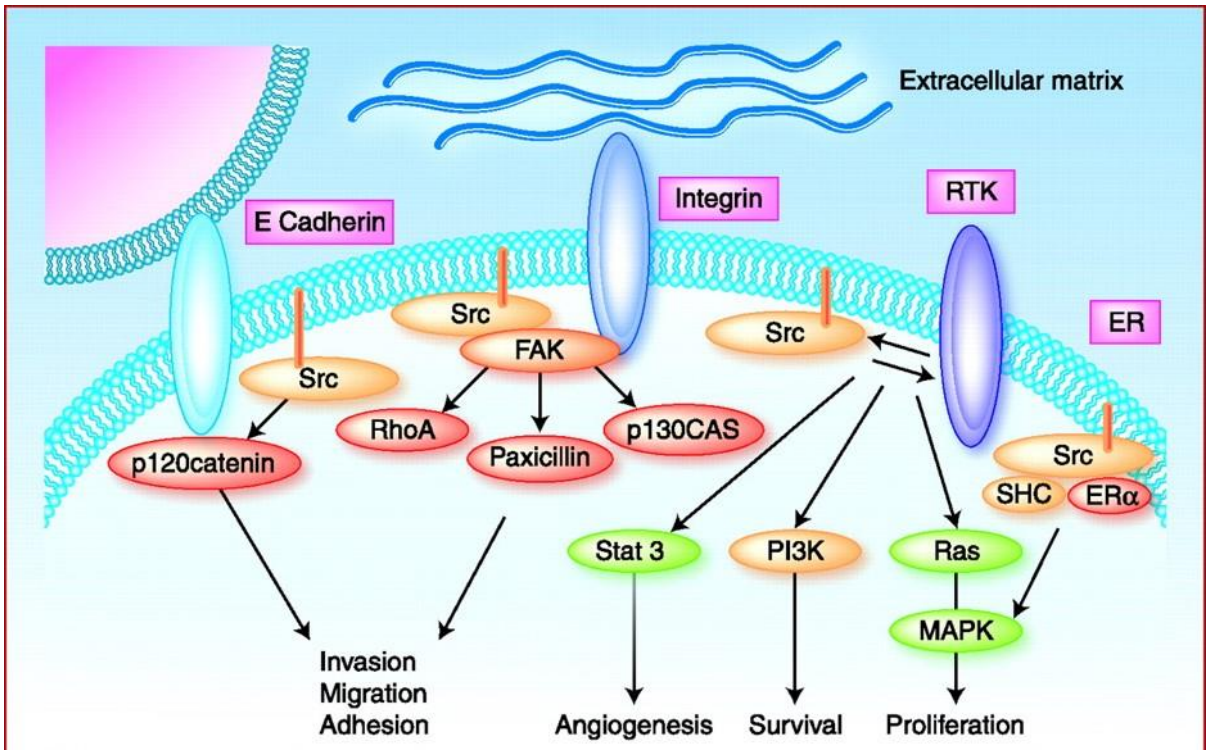


**Figure 3. An overview of the downstream targets of SRC.**

Adopted from Mayer EL and Krop IE (Mayer and Krop, 2010).

# Result

### Genetic screening for finding a new regulator of the Hippo pathway

To identify new regulators of the Hippo pathway, I collected *Drosophila* genes that had been reported to interact with the Hippo pathway from four interactome databases (Biogrid, Bioplex, STRING, DroID) (Table 1). Except for the previously studied regulators, I performed the genetic screening to confirm the correlation between the new regulator candidates and the Hippo pathway (Figure 4). As the Hippo pathway controls the growth of the *Drosophila* eye during development, I chose the *GMR*-GAL4 driver that expresses the transgene specifically in the eye for the screening. The candidates were knocked down or overexpressed alone or under *Hpo* knockdown or *yki* overexpression conditions, representing the Hippo pathway-inhibited status. Of the candidates, only *pod1* (cg4352) negatively regulated the eye size of the fly under both normal and the Hippo pathway-inhibited conditions (Figure 5). Under the normal condition, *pod1* overexpression decreased the eye size whereas *pod1* knockdown didn`t change it. The Hippo pathway inhibition by *Hpo* knockdown or *yki* overexpression induced bigger eyes, which was suppressed by *pod1* overexpression and enhanced by *pod1* knockdown. As a result, I selected *pod1* as a potential regulator of the Hippo pathway.

| Gene | Interacting component | Gene | Interacting component | Gene | Interacting component |
|---|---|---|---|---|---|
| *AGO1* | Hpo | *Fim* | Ft, Mer | *woc* | Mer |
| *Arf79F* | Sav, Hpo | *grn* | Sav | *ref(2)P* | D, Mer |
| *Ars2* | Mer, Fj, Wts | *HLH4C* | Yki, Mer | *Sec31* | Ft, Yki |
| *RnrS* | Ft | *Hrs* | Ft, Fj | *SEMG1* | Sav |
| *trn* | Mer | *igl* | Mer | *SERCA* | Mts, Ds, Fj, Wts, Hpo |
| CG11999 | Fj, Wts | *inc* | Ex | *shrb* | D, Mer |
| CG12645 | Kibra, Sav | *kune* | Sav | *SNCF* | Ft, Mer |
| CG13705 | Ft, Hpo | *(1)G0289* | Mts, Sav, Ds | *Snx17* | Ex |
| CG17841 | Mer | *Lasp* | Ft, Yki | *Spn* | Tao, Mer |
| *Cpsf5* | Sav, Yki | *Mbs* | Dco, Mer | *Tab2* | Kibra, Yki |
| *babo* | Kibra | *mod* | Hpo, Mer | *TER94* | Ft, Mer |
| *CG9581* | Ds, Sav, Yki | *mor* | Sd, Yki, Mer | *tum* | D, Mer |
| *dUfd2* | Mer | *mwh* | Mer | *Ythdf* | Sav |
| *chinmo* | Hpo, Mer | *NXPH2* | FAT5 | *drk* | Ex, Sav |
| *Hel25E* | Ft | *pod1* | D, Mer | | |

**Table 1. Candidate interactors for the Hippo pathway genes from interactome-databases.**

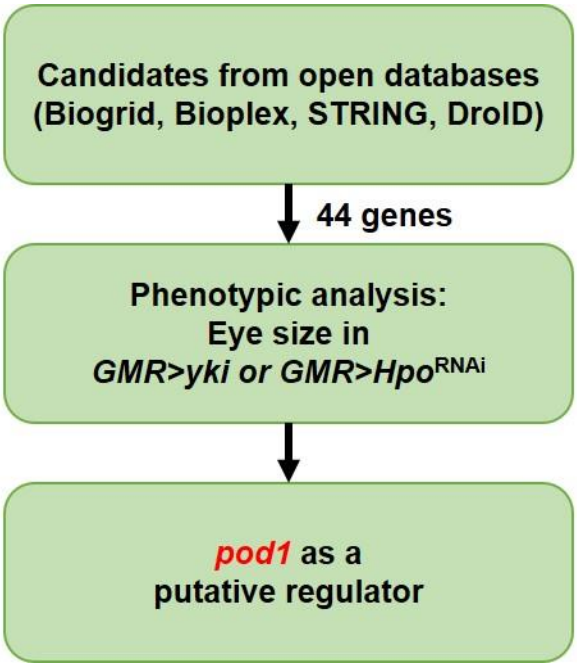


**Figure 4. A schematic diagram of the genetic screen to find the novel regulator of the Hippo pathway.**

44 genes were selected as candidates of the Hippo pathway regulators. Transgenic flies of selected genes were crossed with *GMR*-GAL4, *GMR>yki*, or *GMR>Hpo*$^{RNAi}$. After comparing the eye size of flies, *pod1* was selected as a putative regulator of the Hippo pathway.

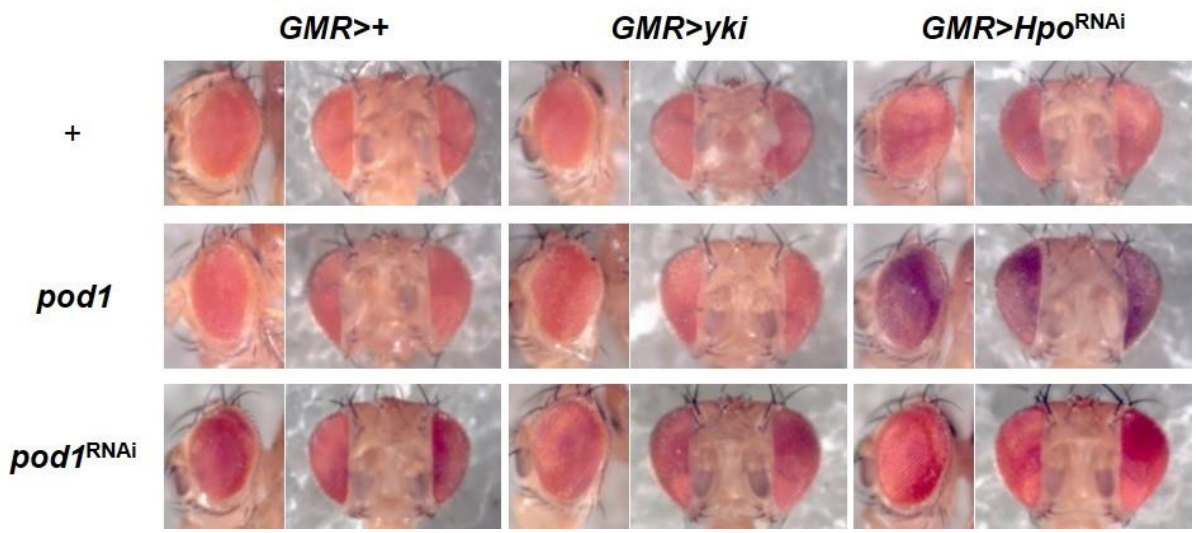


**Figure 5.** ***pod1*** **negatively regulated the eye size of the fly under normal and the Hippo pathway-inhibited conditions.**

Representative images of eyes of indicated genotypes.

**Generation of *pod1* knockout (KO) *Drosophila***

For further inspection of the function of *pod1*, I generated the *pod1* KO fly using the CRISPR/Cas9-system. Targeted DNA deletion using guide-RNA and Cas9 enzyme at the *pod1* exon#1 resulted in a frameshift of the *pod1* genomic DNA sequence (Figure 6), creating a *pod1* KO fly ($pod1^{KO}$) that cannot express the normal Pod1. $pod1^{KO}$ didn`t show any developmental delay or defect.

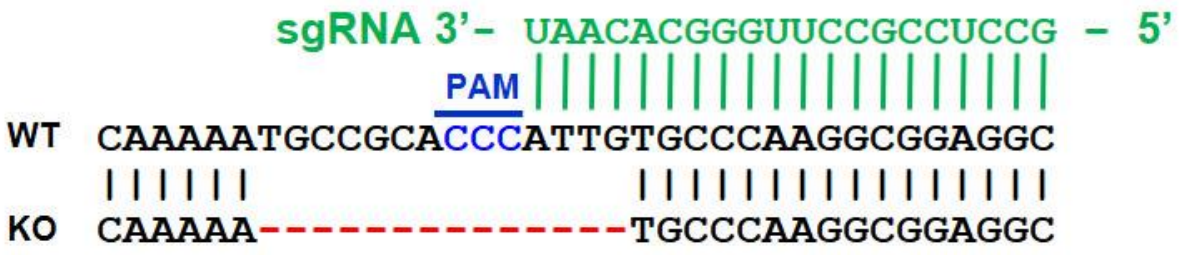


**Figure 6. Genomic DNA sequences of the wild-type (WT) or *pod1*$^{KO}$ (KO) targeted by sgRNA.**

Injecting sgRNA targeting *pod1* exon#1 and Cas9 enzyme resulted in genomic deletion and frameshift of *pod1* exon#1.

**Characterization of *pod1* as a growth regulator**

If *pod1* is indeed a regulator of the Hippo pathway, I expected that $pod1^{KO}$ would exhibit phenotypes associated with the Hippo pathway, such as changes in cell proliferation or death resulting in tissue size changes (Zheng and Pan, 2019). To confirm the idea, I conducted the following experiment. First, I measured the body weight of the $pod1^{KO}$ to compare the overall growth level of $pod1^{KO}$ to that of the wild-type. Both male and female $pod1^{KO}$ were heavier than the wild-type, indicating that *pod1* inhibits the growth of the fly (Figure 7).

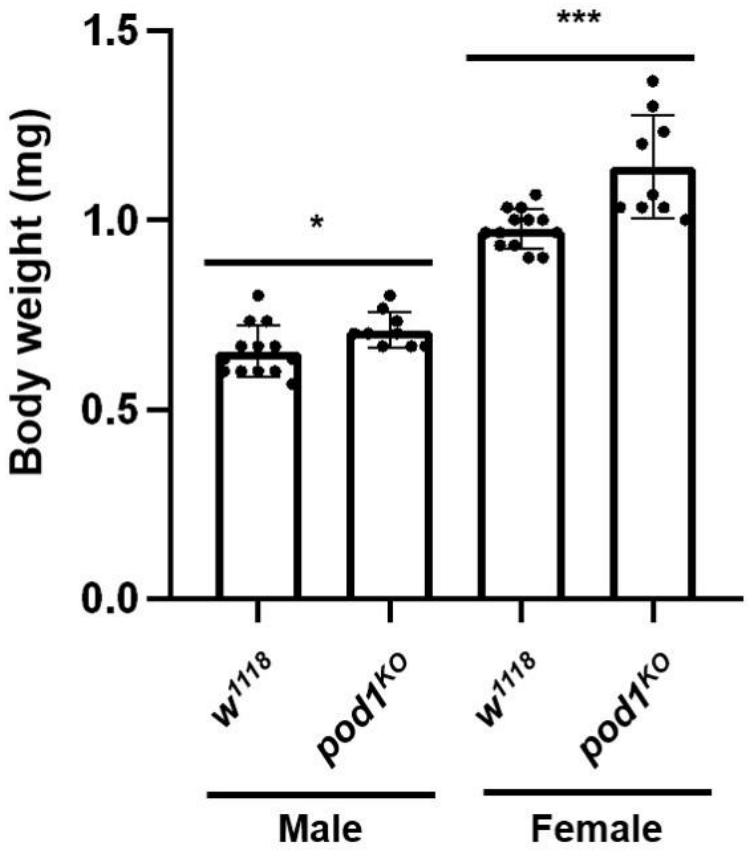


**Figure 7. *pod1$^{KO}$* is heavier than the wild-type.**

Statistical analysis of the body weight of each genotype (*, $p<0.05$; ***, $p<0.001$).

Next, I analyzed the growth of *pod1*$^{KO}$ at the tissue level. Since the fly wing size is a widely used phenotype representing the tissue growth of the fly, I observed *pod1*-dependent wing size changes using two wing-specific GAL4 drivers, *MS1096*-GAL4 and *Hedgehog (Hh)*-GAL4. Wing-specific *MS1096*-GAL4-induced *pod1* overexpression decreased the fly wing size, whereas knockdown and KO increased the wing size (Figures 8 A and B). Furthermore, *MS1096*-GAL4 induced *pod1* overexpression decreased the wing size of *pod1*$^{KO}$, indicating that the wing size change is caused entirely by *pod1*.

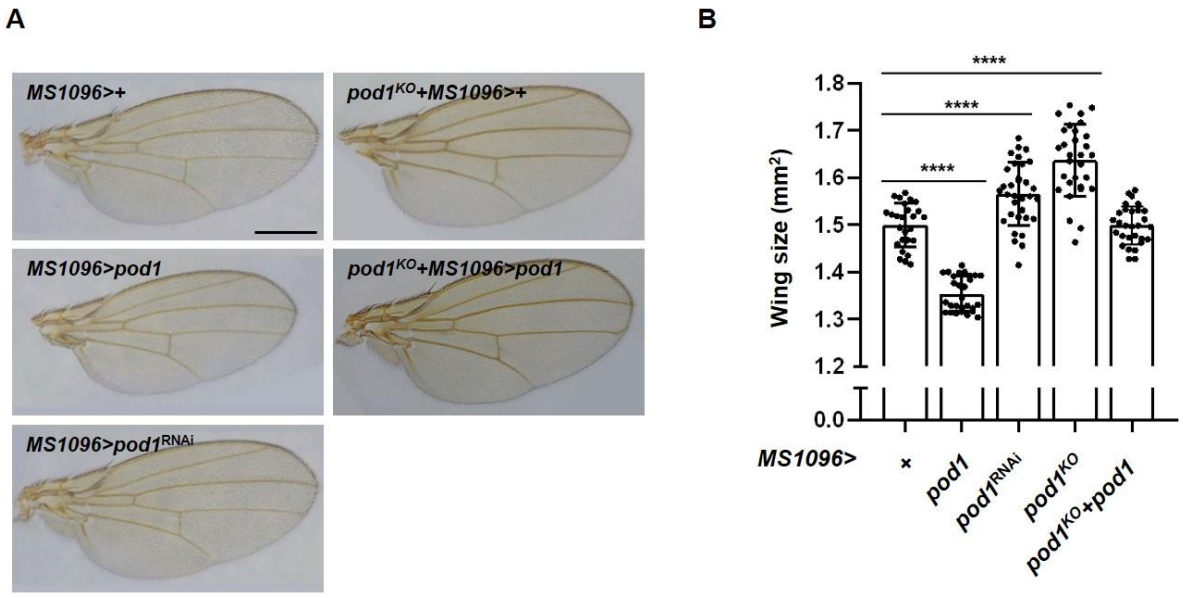


**Figure 8. *pod1* negatively regulates the wing size by *MS1096*-GAL4.**

(A) Representative pictures of wings of indicated genotypes. Scale bar represents 500 μm.

(B) Statistical analysis of the wing size of each genotype in (A) (****, $p<0.0001$).

I analyzed these wing size changes again using the *Hh*-GAL4 which expresses the transgene at the posterior region of the fly wing. *pod1* overexpression by *Hh*-GAL4 also reduced the wing size, consistent with the *MS1096*-GAL4-induced *pod1* overexpression (Figures 9 A and B). However, *pod1* knockdown by *Hh*-GAL4 didn`t result in the particular wing size change. Since *pod1* knockdown increased the eye size only under the Hippo pathway-inhibited condition, I expected that *pod1* knockdown by *Hh*-GAL4 would change the wing size and shape under the Hippo pathway-inhibited condition. *Hpo* knockdown by *Hh*-GAL4 resulted in abnormal wing enlargement at the posterior region (Figure 9 A), rendering it incomparable to the size of the anterior region. *pod1* overexpression suppressed the wing enlargement of *Hpo* knockdown, whereas *pod1* knockdown aggravated this phenotype, resulting in severe damage to the wing shape. In conclusion, I confirmed that *pod1* negatively regulates tissue growth.

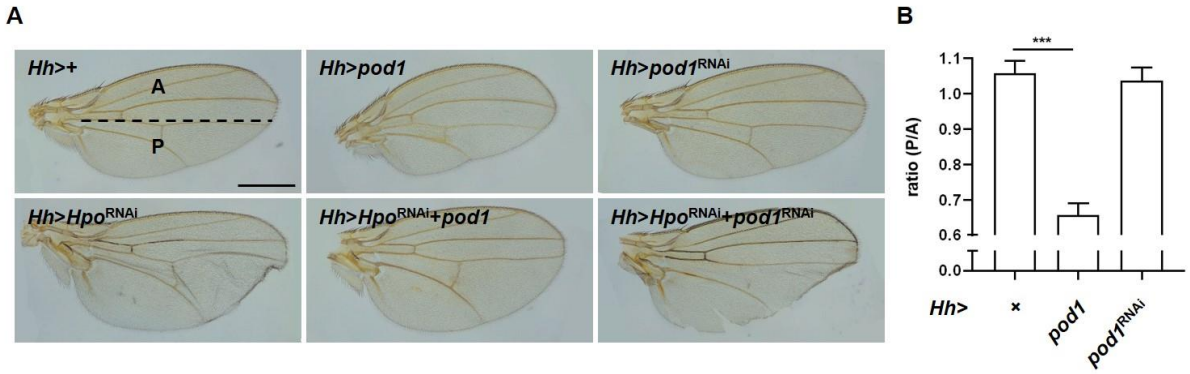


**Figure 9. *pod1* negatively regulates the wing size by *Hh*-GAL4.**

(A) Representative pictures of wings of indicated genotypes. *Hh*-GAL4-induced *Hpo* knockdown resulted in the wing morphology destruction, rendering the size of the anterior and posterior region incomparable. Anterior and posterior regions are indicated. Scale bar represents 500 μm.

(B) Statistical analysis of the ratio of wing sizes between the anterior and posterior region of each genotype in (A) (***, $p<0.001$).

The Hippo pathway controls the organ size by regulating cell proliferation and death (Fallahi et al., 2016). If *pod1* is a regulator of the Hippo pathway, the growth-related phenotype of *pod1* shown earlier would be associated with cell proliferation and death. Using mitosis marker phospho-histone 3 (pH3) and *Hh*-GAL4, I examined the effect of *pod1* on cell proliferation (Figure 10 A). Comparing the ratio of proliferative cells between the anterior and posterior region, I confirmed that *pod1* overexpression reduced the ratio of proliferative cells whereas knockdown increased it (Figure 10 B).

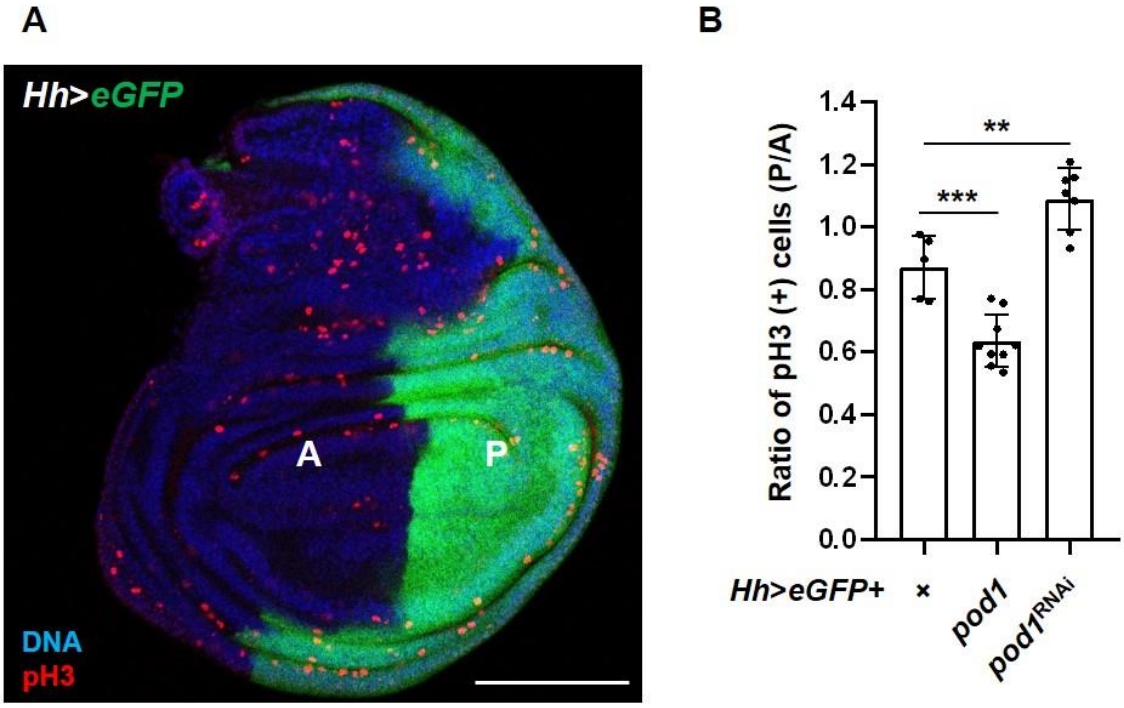


**Figure 10.** ***pod1*** **negatively regulates cell proliferation.**

(A) The representative model for comparing the ratio of anti-pH3-positive (red) cells between the anterior (A) and posterior (P) region in the imaginal wing disc from *Hh*>e*GFP.* GFP represents the posterior region where transgene is expressed. Scale bar represents 100 μm.

(B) Statistical analysis of the ratio of anti-pH3-positive cells between the anterior and posterior region of each genotype (**, $p<0.01$; ***, $p<0.001$).

With the same scheme, I also tested the role of *pod1* on cell death by TUNEL assay (Figure 11 A). *pod1* overexpression elevated cell death whereas knockdown decreased it (Figure 11 B). To summarize, I concluded that *pod1* inhibits tissue growth by regulating cell proliferation and death, like the Hippo pathway.

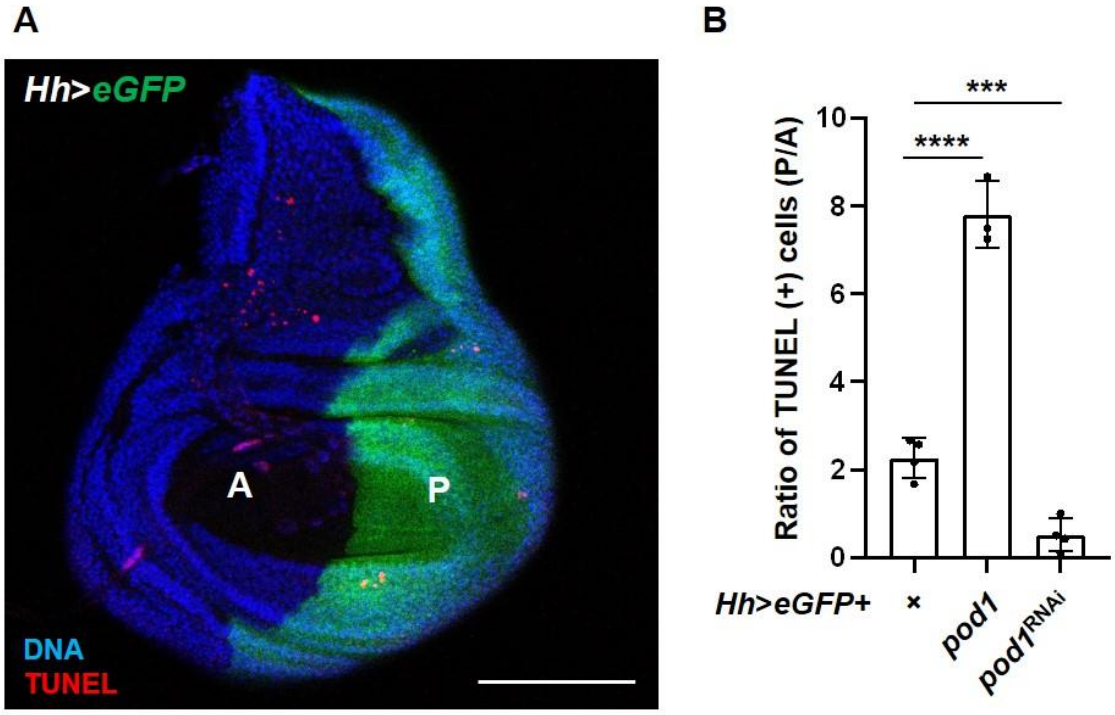


**Figure 11. *pod1* positively regulates cell death.**

(A) The representative model for comparing the ratio of TUNEL-positive (red) cells between the anterior (A) and posterior (P) region in the imaginal wing disc from *Hh*>e*GFP.* GFP represents the posterior region where transgene is expressed. Scale bar represents 100 μm.

(B) Statistical analysis of the ration of TUNEL-positive cells between the anterior and posterior region of each genotype (***, $p<0.001$; ****, $p<0.0001$).

Since the Hippo pathway is known to modulate cell polarity (Chen et al., 2010), I tested whether *pod1* also modulates cell polarity using *Hh*-GAL4 and apical markers, Disc-large and cadherin 2. The wild-type and *pod1* overexpression exhibited ordinary tissue morphology, showing the Disc-large and cadherin2 at the apical line of the wing disc (Figure 12). However, *pod1* knockdown results in cell proliferation above the apical line, indicating a defect in cell polarity control. Inhibition of the Hippo pathway by *Hpo* knockdown showed the same defect as *pod1* knockdown. *pod1* overexpression was sufficient to restore the defect of *Hpo* knockdown whereas concomitant *pod1* knockdown aggravated it. From these data, I discovered that *pod1* positively regulates cell polarity.

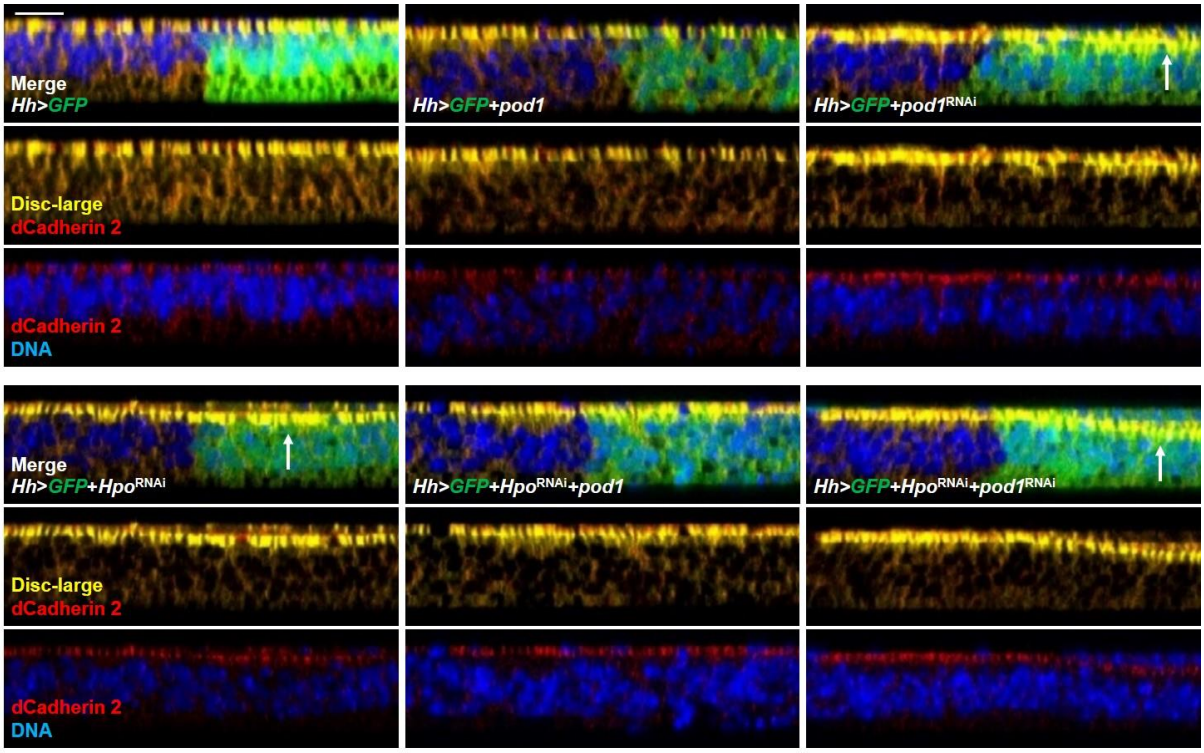


**Figure 12. *pod1* positively regulates the cell polarity.**

Representative images of anti-Disc-large (yellow) and anti-dCadherin2 (red) in the vertical section of the imaginal wing disc from indicated genotypes. GFP represents the GAL4-expressing region where transgene is expressed. Scale bar represents 10 μm.

Lastly, based on the previous study that Pod1 is localized in the ER/Golgi and regulates its morphology and vesicle formation (Bhattacharya et al., 2016; Yuan et al., 2014), I observed the localization of Pod1 and the role of *pod1* on the ER morphology at the two different stages, the late 3$^{rd}$ stage and the wandering stage. The late 3$^{rd}$ stage is the stage when larvae keep eating food to grow, representing the Hippo pathway-inhibited status. The wandering stage represents the Hippo pathway-activated status when larvae halt eating and growth for preparing the pupariation. GFP-tagged Pod1 was expressed by fat body-specific *Cg*-GAL4 for analyzing the Pod1 localization, and the KDEL antibody was used as the ER marker. As a result, I found that most of the Pod1 were localized to the plasma membrane, but some of the protein were localized right next to the ER, probably on the Golgi, at both 3$^{rd}$ and wandering stages (Figure 13 A). The fat body of the wild-type larvae entering the wandering stage formed ER vesicles. *pod1* overexpression promoted earlier vesicle formation at the 3$^{rd}$ stage, whereas *pod1*$^{KO}$ larvae showed delayed ER vesicle formation as entering the wandering stage (Figures 13 A and B). Neither *pod1* overexpression nor KO resulted in the structural defect of the plasma membrane at both stages. Consistent with previous studies, I confirmed the localization of Pod1 on ER/Golgi and the role of *pod1* in regulating the ER/Golgi morphology and vesicle formation.

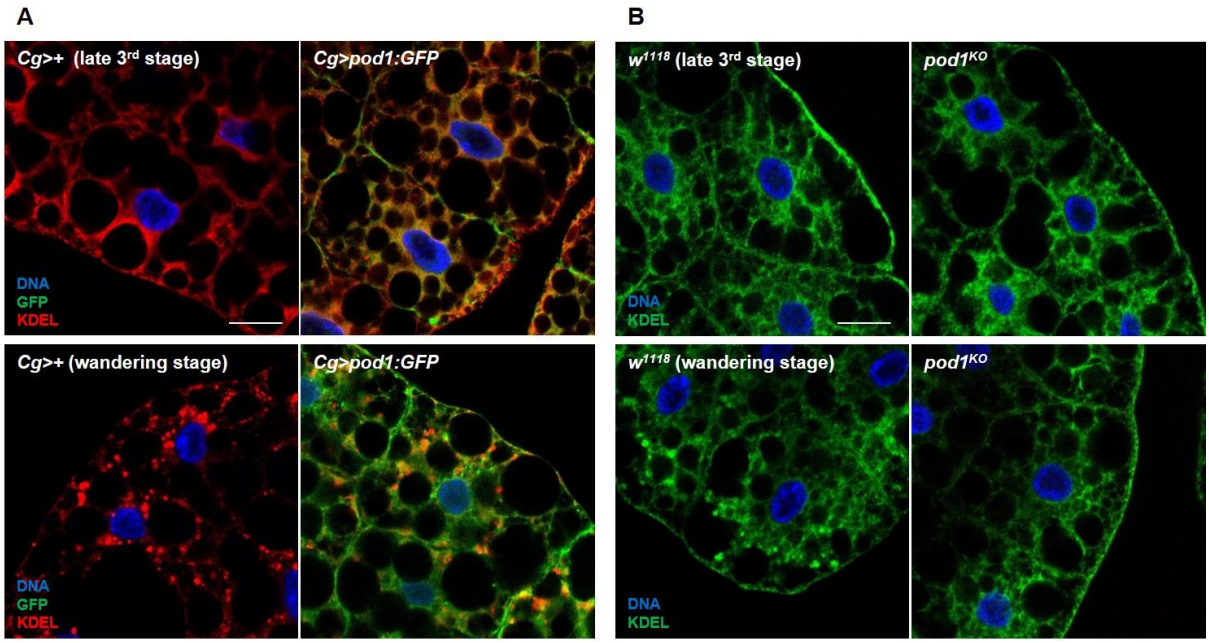


**Figure 13. Subcellular localization of Pod1 and the role of *pod1* in the ER morphology.**

(A) Representative images of anti-KDEL (red) and Pod1:GFP (green) in the fat body from indicated genotypes. Scale bar represents 20 μm.

(B) Representative images of anti-KDEL (green) in the fat body from indicated genotypes. Scale bar represents 20 μm.

**Genetic interaction between *pod1* and *yki***

To verify *pod1* as a regulator of the Hippo pathway, I tested the genetic interaction between *pod1* and each component of the Hippo pathway. First, I started from the most downstream effector of the Hippo pathway, *yki*. *yki* overexpression by *MS1096*-GAL4 resulted in increased wing size, which was suppressed by *pod1* overexpression and enhanced by *pod1* knockdown and KO (Figure 14 A). In contrast, *yki* knockdown blocked the wing development both in the wild-type and $pod1^{KO}$ background (Figure 14 B). Considering these results that *pod1* only regulates the wing size when Yki exists, I expected *pod1* to be an upstream inhibitor of *yki*.

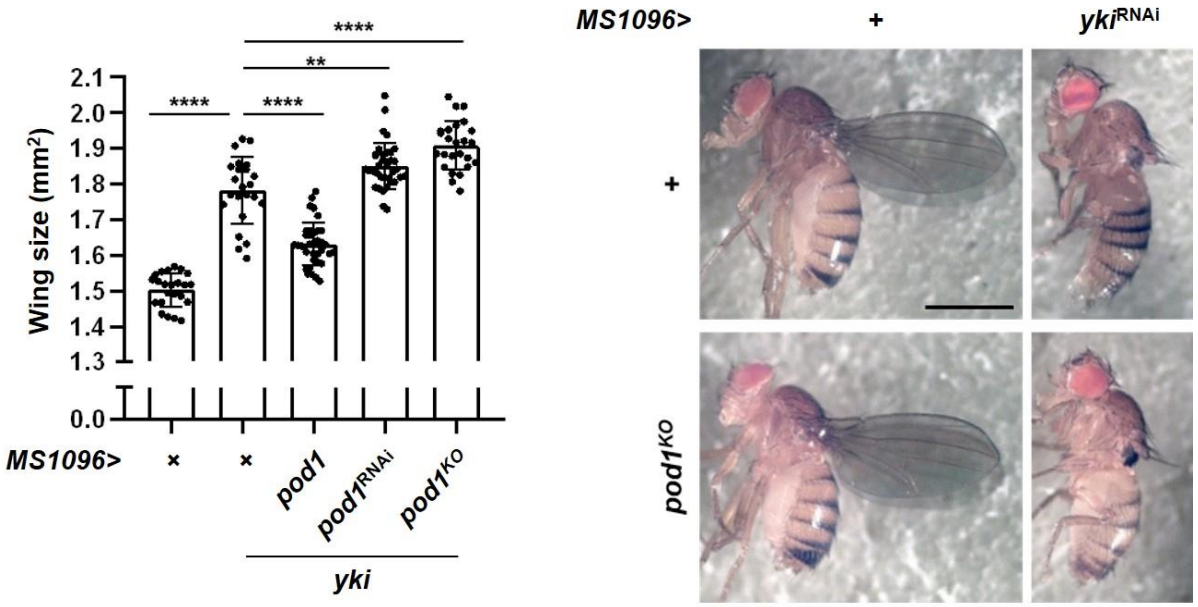


**Figure 14. Genetic interaction between *pod1* and *yki*.**

(A) Statistical analysis of the wing size of each genotype (**, $p<0.01$; ****, $p<0.0001$).

(B) Representative pictures of flies of indicated genotypes. Scale bar represents 500 μm.

The Hippo pathway inhibits Yki activity by Wts-dependent Ser111, 168, and 250 residues phosphorylation (Oh and Irvine, 2009). To confirm the genetic epistasis between *pod1* and *yki,* I tested the role of *pod1* over Yki$^{S168A}$, a partially activated form of Yki in which the Ser168 residue is substituted with alanine to prevent the phosphorylation. Unfortunately, *MS1096*-GAL4-induced *yki$^{S168A}$* overexpression resulted in lethality at pupa-stage, making it impossible to compare the wing size of the adult fly. Instead, I overexpressed *yki$^{S168A}$* in the fly eye using *GMR*-GAL4 and found that *yki$^{S168A}$* overexpression resulted in larger and bumpy eyes than wild-type *yki* overexpression (Figure 15; see also Figure 5). *pod1* overexpression didn`t reduce the eye size but only made the outer surface even, and *pod1* knockdown still slightly increased the eye size. I thought that *pod1* still regulates Yki$^{S168A}$ by Wts-dependent Ser111, 250 residues phosphorylation. If *pod1* is an upstream regulator of *yki,* I assumed that *pod1* could not inhibit the already fully activated Yki in the nucleus. A previous study reported that Yki$^{S168A}$ moves into the nucleus with the binding partner Sd (Ren et al., 2010). Indeed, co-overexpression of *yki$^{S168A}$* and *Sd* increased the eye size of the fly further than *yki$^{S168A}$* overexpression alone, which was affected by neither *pod1* overexpression nor knockdown (Figure 15). In conclusion, I found that *pod1* is an upstream regulator of *yki*.

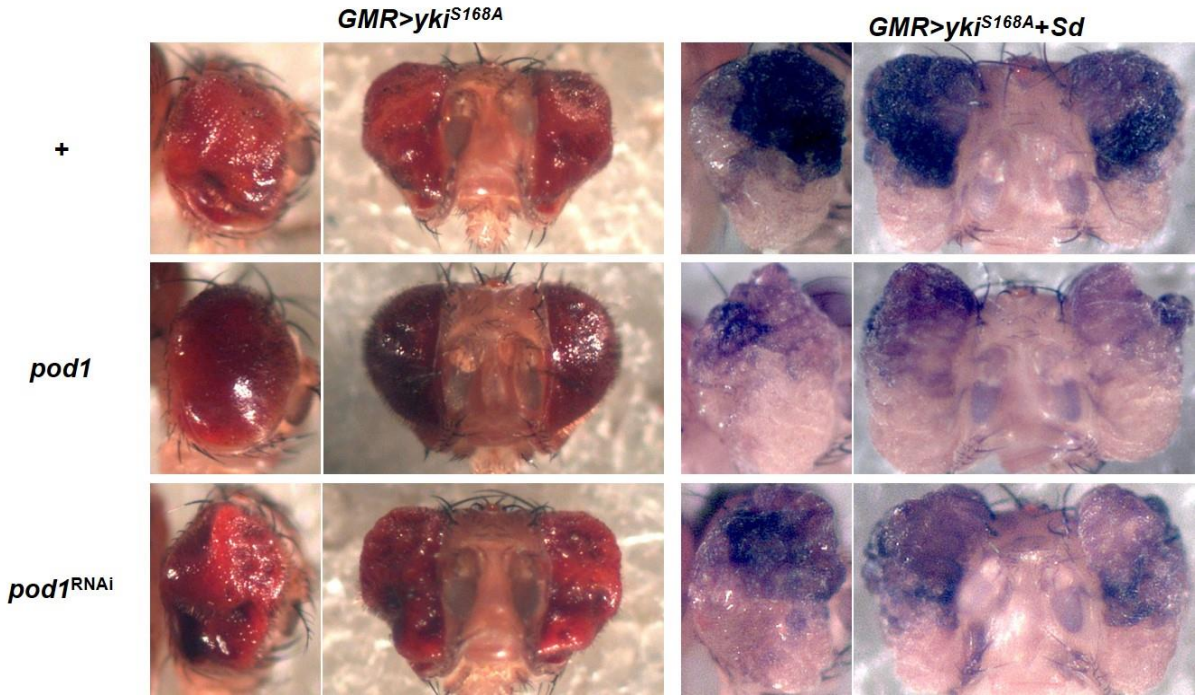


**Figure 15. *pod1* is an upstream regulator of *yki*.**

Representative images of eyes of indicated genotypes. *yki*$^{S168A}$ overexpression induced larger eye compared to *yki* overexpression on Figure 5.

To find out whether *pod1* directly regulates *yki* through the Hippo pathway, I measured Yki activity. First, I observed the localization of Yki and discovered that only $Yki^{S168A}$, but not wild-type Yki, was localized in the nucleus with its binding partner Sd (Figure 16), consistent with the previous report (Ren et al., 2010). However, I confirmed that *pod1* knockdown induced the nuclear trans-localization of wild-type Yki, indicating that *pod1* knockdown had the same effect as substitution of the Ser168 residue of Yki into alanine. From these data, I discovered that Pod1 negatively regulates Yki through the Hippo pathway.

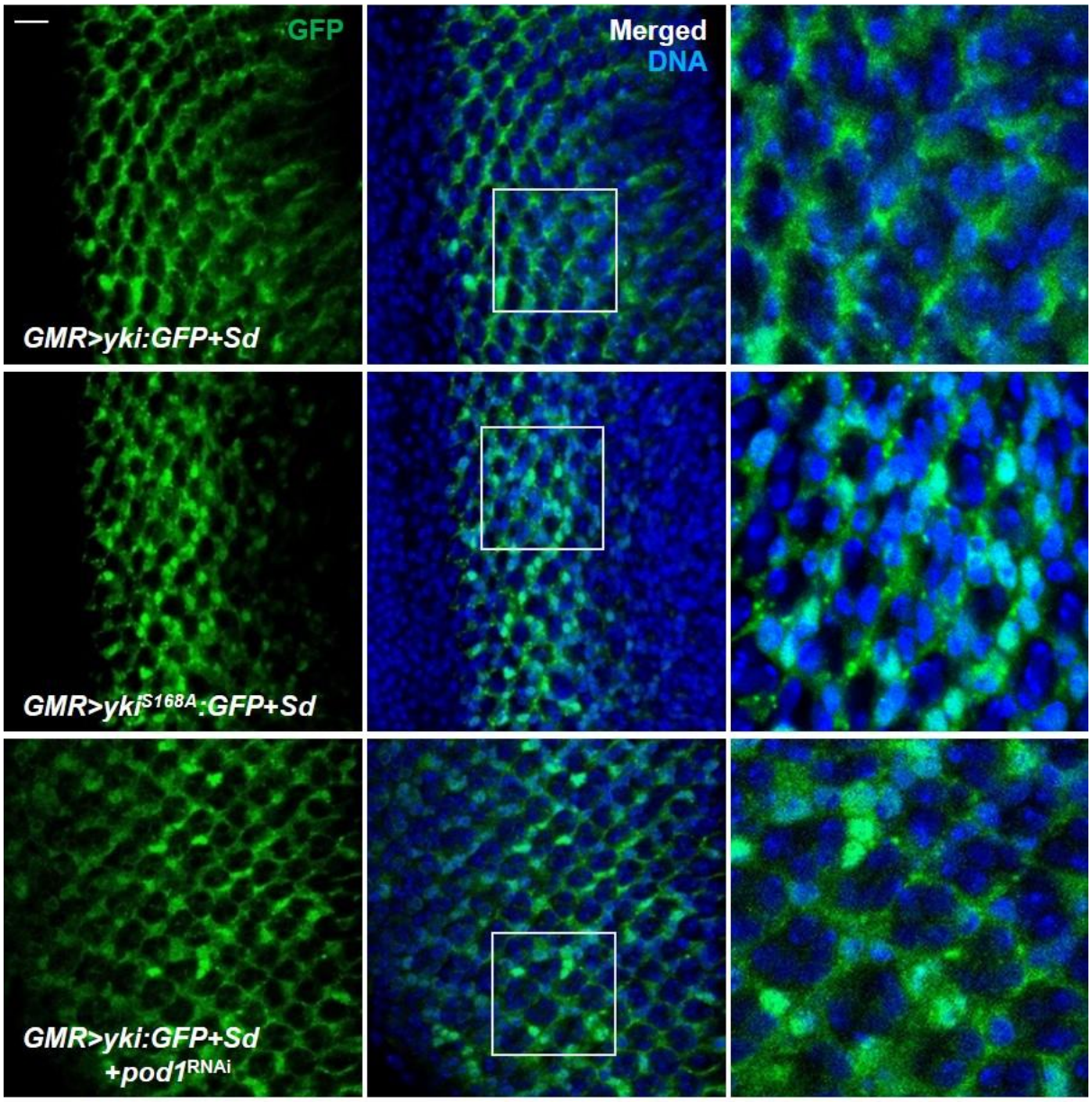


**Figure 16. Pod1 regulates Yki through the Hippo pathway.**

Representative images of Yki:GFP and Yki$^{S168A}$:GFP of the imaginal eye disc from indicated genotypes. Scale bar represents 20 μm.

Co-transcription factor Yki controls the expression of multiple genes related to cell proliferation and death (Yu and Pan, 2018). Therefore, I measured changes in the mRNA expression level of *diap1*, a downstream target gene of Yki, by *pod1* using *Heat-shock (Hs)*-GAL4. Flies were incubated at 30°C before mRNA extraction to induce the heat-shock-induced gene expression. The *diap1* mRNA expression level was down-regulated by *pod1* overexpression and elevated in the *pod1* KO background (Figure 17). Moreover, *pod1* overexpression was sufficient to suppress the elevated *diap1* mRNA expression level of *pod1* KO background, indicating that changes in *diap1* mRNA expression level were dependent on *pod1*. In conclusion, I confirmed that Pod1 directly and negatively regulates Yki through the Hippo pathway.

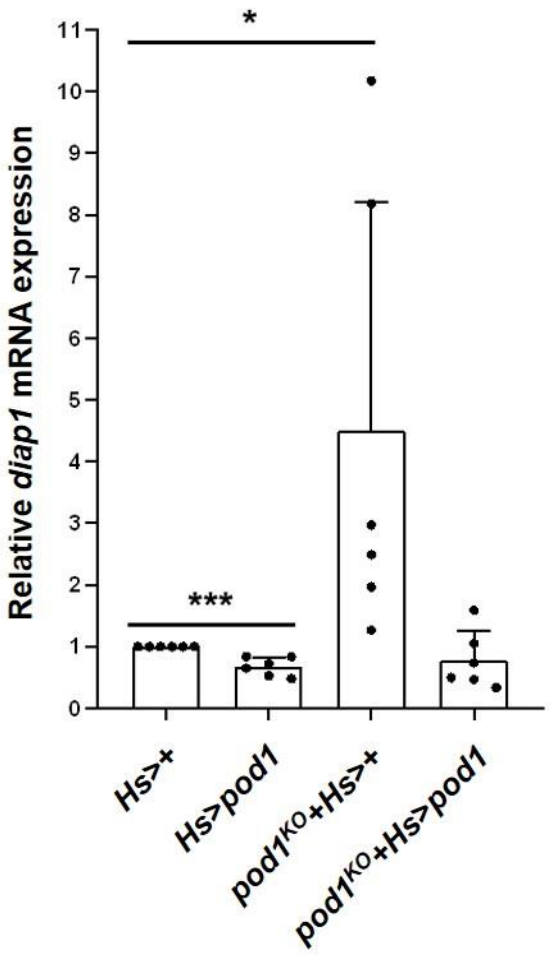


**Figure 17. Pod1 regulates the downstream target of Yki.**

Statistical analysis of the mRNA expression level of *diap1* of each genotype (*, $p<0.05$; ***, $p<0.001$).

**Genetic interaction between *pod1* and *wts*/*hpo*/*sav*/*mats***

Next, I examined the genetic interaction between *pod1* and *wts* which directly phosphorylates Yki (Hao et al., 2008). *wts* overexpression by *MS1096*-GAL4 decreased the wing size of the fly (Figure 18 A). *pod1* overexpression decreased the wing size further, but *pod1* knockdown didn`t alter the *wts* overexpression phenotype. In contrast, *wts* knockdown increased the wing size which was affected by neither *pod1* overexpression nor knockdown. Based on the result that Pod1 decreased the wing size further only when Wts exists, *pod1* seems to be an upstream activator of *wts.*

Since Wts is activated by Hpo-dependent phosphorylation (Chan et al., 2005), I examined the genetic interaction between *pod1* and *Hpo*. *Hpo* knockdown by *MS1096*-GAL4 increased the wing size (Figure 18 A). *pod1* overexpression suppressed the wing size increase by *Hpo* knockdown whereas *pod1* knockdown increased it further. This enhanced wing size increase by simultaneously knocking down two growth-inhibitory genes *pod1* and *Hpo* excludes the possibility of *pod1* being downstream of *Hpo.* In addition, *Hpo* knockdown caused the posterior cross vein (PCV) development defect (Figure 18 B). Although *pod1* alone didn`t cause developmental defects of the wing structure (Figure 8 B), *pod1* overexpression restored the PCV development whereas *pod1* knockdown completely blocked the PCV development under the *Hpo* knockdown background. Taken together, I concluded that *pod1* regulates the Hippo pathway parallel to or above *Hpo*.

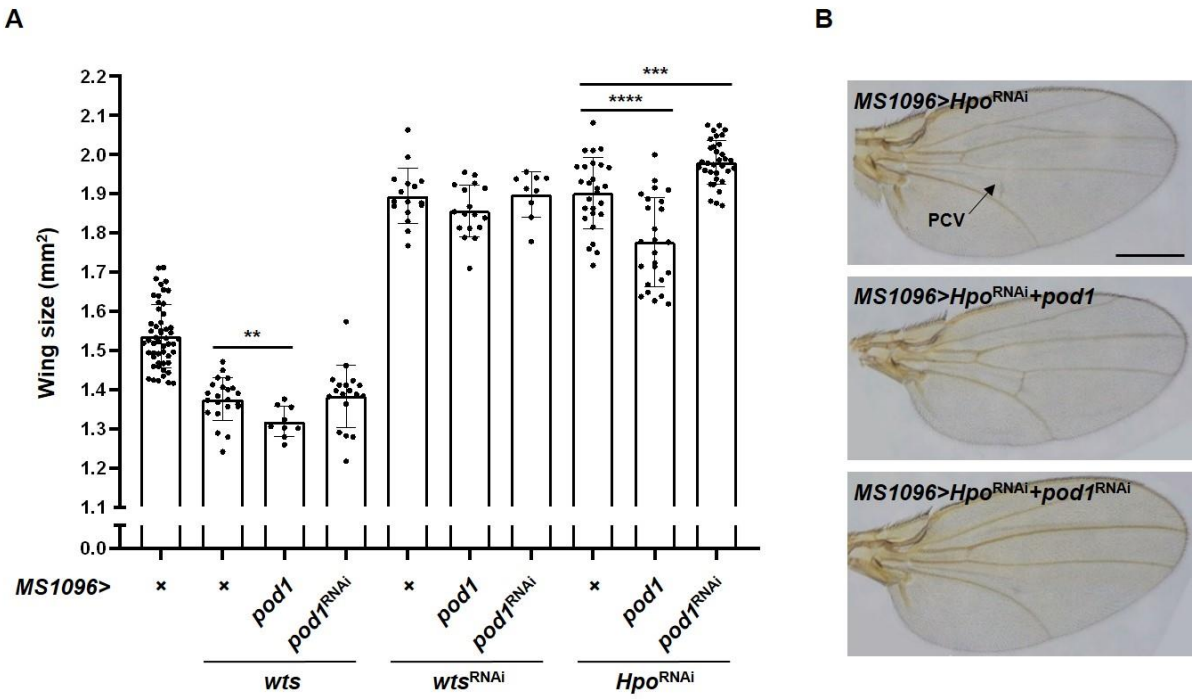


**Figure 18. Genetic interaction between *pod1* and *wts*/*Hpo*.**

(A) Statistical analysis of the wing size of each genotype (**, p<0.01; ***, p<0.001).

(B) Representative images of wings of indicated genotypes. Posterior cross vein (PCV) is indicated. Scale bar represents 500 μm.

*mats* knockdown by *MS1096*-GAL4 increased the wing size (Figure 19). Both *pod1* overexpression and knockdown reduced it, indicating there is no particular genetic epistasis between *pod1* and *mats.*

*sav* knockdown by *MS1096*-GAL4 increased the wing size (Figure 19). *pod1* overexpression suppressed the wing size increase by *sav* knockdown whereas *pod1* knockdown didn`t affect *sav* knockdown-induced wing size increase. *sav* overexpression by *MS1096*-GAL4 decreased the wing size compared to UAS-*sav* control instead of *MS1096*-GAL4 control (Figure 19). *pod1* overexpression decreased the wing size further, whereas *pod1* knockdown didn`t affect wing size decrease by *sav* overexpression. *pod1* knockdown didn`t increase the wing size of *sav* overexpressing flies, denying that *pod1* is downstream of *sav*. However, *pod1* overexpression inhibited the wing size increase by *sav* knockdown, also denying that *pod1* is an upstream regulator of *sav*. Since *pod1* can be interpreted as both upstream and downstream regulators of *sav*, I can only claim the genetic interaction but not the genetic epistasis between *sav* and *pod1* with this data alone. But considering that Sav binds to Hpo to form the core kinase complex (Callus et al., 2006) and that *pod1* seems to regulate the Hippo pathway at or above *Hpo* (Figure 18), *pod1* is predicted to regulate the Hippo pathway at parallel or upstream to the core kinase complex.

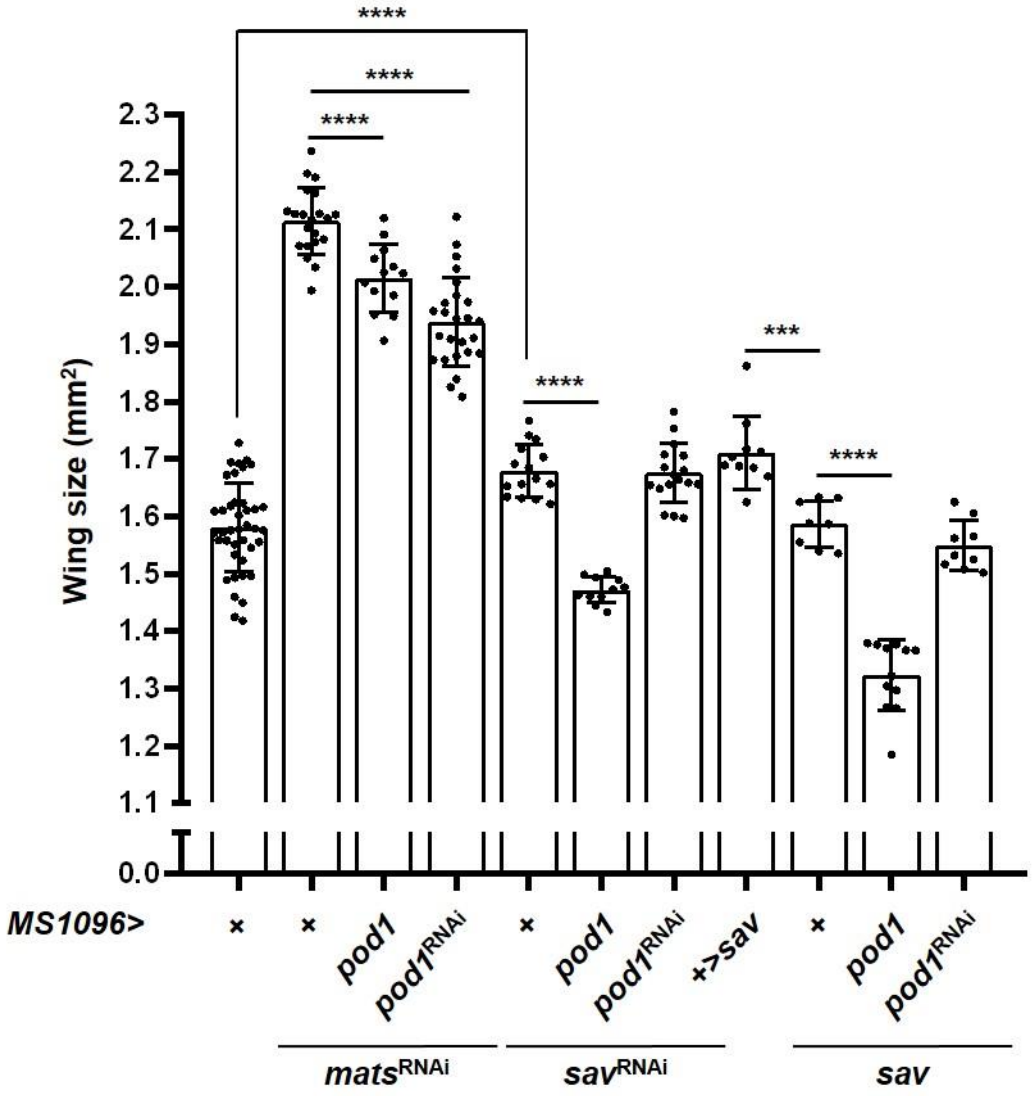


**Figure 19. Genetic interaction between *pod1* and *mats*/*sav*.**

Statistical analysis of the wing size of each genotype (****, p<0.0001).

**Genetic interaction between *pod1* and *mer*/*kibra*/*ex***

The core kinase complex of the Hippo pathway is activated at the membrane by the membrane adaptor complex consisting of Mer, Kibra, and Ex (Hamaratoglu et al., 2006; Yu et al., 2010; Zhang et al., 2010). Given the genetic interaction data above that *pod1* could be an upstream regulator of the core kinase complex, I tested the genetic interaction between *pod1* and *mer, kibra,* and *ex.* Knockdown of *mer*, *kibra*, or *ex* by *MS1096*-GAL4 all increased the wing size (Figure 20). The wing size increase by *mer* and *kibra* knockdown was suppressed by *pod1* overexpression but not affected by *pod1* knockdown, presenting *pod1* as a downstream of *mer* and *kibra.* Neither *pod1* overexpression nor knockdown affected the wing size increase by *ex* knockdown. Considering that *mer*, *kibra*, and *ex* are parallel regulators of the Hippo pathway and that *pod1* seems to be a downstream target of *mer* and *kibra,* it is reasonable to claim that *pod1* and *ex* have no specific genetic interaction rather than *pod1* is an upstream regulator of *ex.* Taken together, *pod1* is expected to be located downstream of the membrane adaptor complex.

Combining all genetic interactions between *pod1* and components of the Hippo pathway, *pod1* seems to locate between the membrane adaptor complex and the core kinase complex.

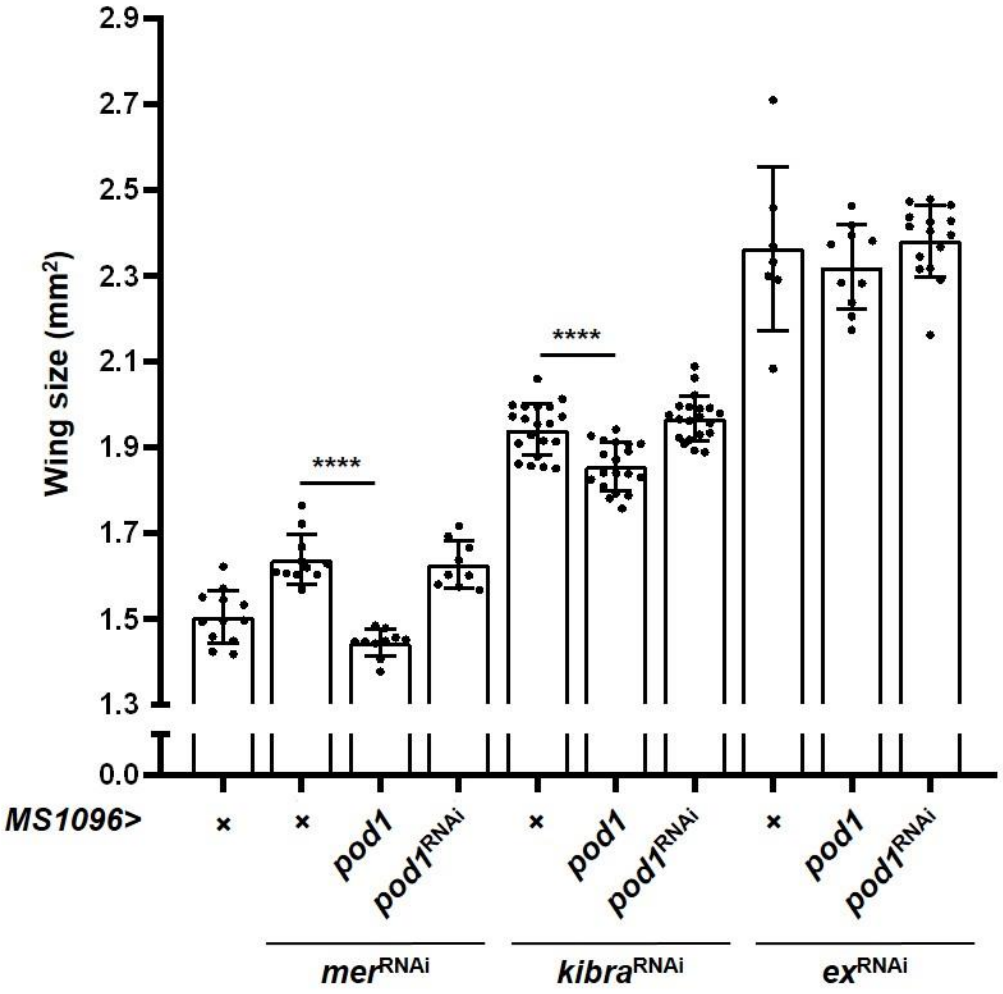


**Figure 20. Genetic interaction between *pod1* and *mer*/*kibra*/*ex*.**

Statistical analysis of the wing size of each genotype (****, $p<0.0001$).

**Physical interaction between CORO7 and MST2, LATS1, or SAV1**

To identify the exact regulatory mechanism of *pod1* in the Hippo pathway, I used the mammalian system and *CORO7,* the mammalian homolog of *pod1.* Because CORO7 consists of two WD-40 repeat domains that facilitate the physical interaction between proteins (Figure 21 A; see also Figure 2) (Liu et al., 2016), I hypothesized that CORO7 regulates the Hippo pathway by physically interacting with other components and conducted co-immunoprecipitation assay between CORO7 and each component of the Hippo pathway. As a result, I discovered that CORO7 directly binds to MST2, LATS1, and SAV1 among components of the Hippo pathway (Figures 21 B - D). Because MST2, LATS1, and SAV1 consist of the core kinase complex with MOB1 (Harvey and Tapon, 2007), I tested whether the binding of CORO7 has a role in the core kinase complex formation. Surprisingly, CORO7 depletion inhibited the physical interaction between MST2, LATS1, and SAV1 (Figure 21 E), indicating that CORO7 is required for the core kinase complex formation.

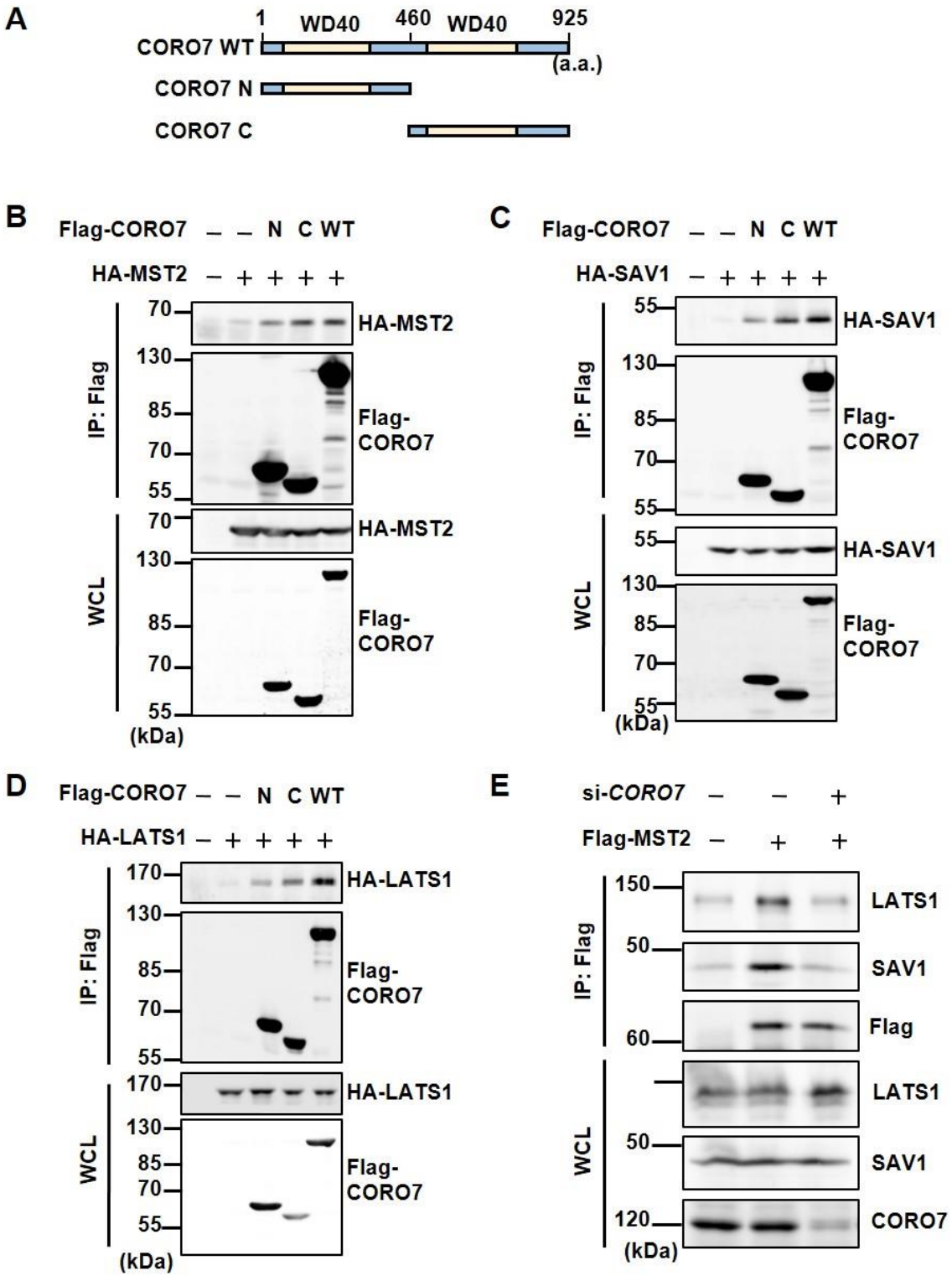


**Figure 21. CORO7 physically interacts with MST2, SAV1, and LATS1.**

(A) Schematic representation of domains and truncated constructs of CORO7.

(B - D) HA-MST2 (B), HA-SAV1 (C), or HA-LATS1 (D) was expressed together with wild-type (WT), N-terminal (N), or C-terminal (C) Flag-CORO7 in HEK293T cells. The lysates were immunoprecipitated (IP) by anti-Flag antibody and immunoblotted with anti-HA and anti-Flag antibodies. The whole cell lysate (WCL) samples were loaded for indicating the expression levels.

(E) Physical interaction between Flag-MST2 and endogenous LATS1 and SAV1 upon si-*CORO7* treatment.

**SRC phosphorylates Pod1/CORO7 to regulate the Hippo pathway**

From experiments so far, I found that Pod1 acts as a scaffold protein for the core kinase complex formation. However, since Pod1 lacks enzymatic activity that controls itself according to upstream signals, I expected that there would be an upstream enzyme regulating Pod1 activity. I used the same scheme used to find *pod1* to find the upstream regulator of *pod1*. From interactome databases, I listed genes that had been reported to interact with *CORO7* or *pod1* (Table 2). Among 13 candidates, human tyrosine kinase SRC had been already studied about its regulation on the Hippo pathway (Enomoto and Igaki, 2013; Li et al., 2016; Si et al., 2017). Based on previous reports, I predicted SRC to be an upstream regulator of Pod1.

| Gene | BioPlex | BioGRID | STRING | DroID |
|---|---|---|---|---|
| *THBS3* | O | O | | |
| *ASB6* | O | O | | |
| *CNTF* | O | O | | |
| *KLHL20* | O | O | O | |
| *SRC* | | O | O | |
| *MYH10* | | O | | O |
| *RHOA* | | O | | |
| *AP1G1* | | O | O | |
| *CUL1* | | O | O | |
| *DAG1* | | O | O | |
| *BUB1* | | O | | O |
| *NF2* | | O | | O |
| *BTBD10* | | O | | O |

**Table 2. Candidate regulators for CORO7 from interactome-databases.**

The databases where interactions between each gene and *pod1* were reported are indicated.

I examined the genetic interaction between *pod1* and *src64B,* a *Drosophila* homolog of human *SRC*, to clarify the genetic epistasis. *src64B* knockdown by *MS1096*-GAL4 decreased the wing size (Figure 22). *pod1* overexpression decreased the wing size further, whereas *pod1* knockdown completely blocked the effect of *src64B* knockdown, increasing the wing size more than the wild-type. From these genetic interactions, I expected *pod1* to be a downstream target of *src64B*.

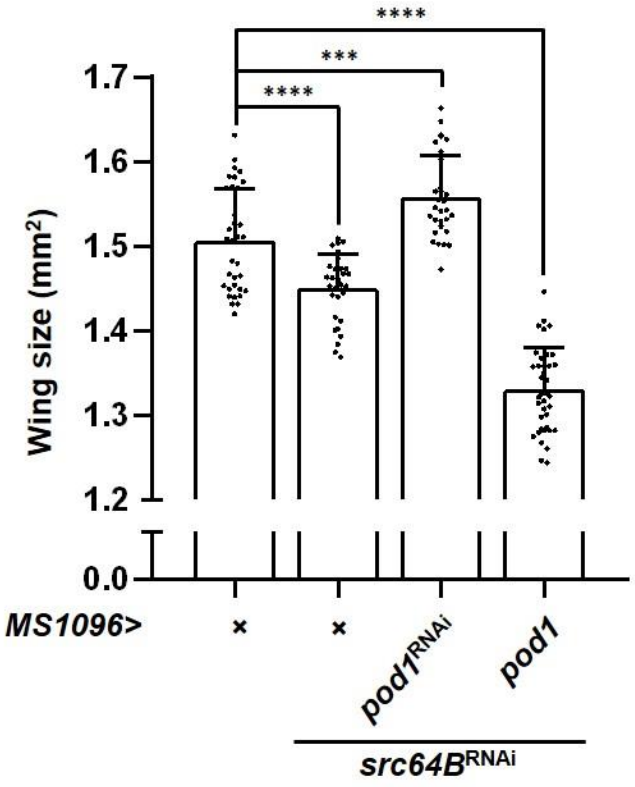


**Figure 22. *pod1* is a downstream target of *src64B*.**

Statistical analysis of the wing size of each genotype (***, p<0.001; ****, p<0.0001).

I tested whether this genetic epistasis is evolutionarily conserved in human and functions to regulate the Hippo pathway. Treatment of cells with the SRC inhibitor dasatinib increased the Hippo pathway-dependent YAP Ser127 residue phosphorylation (Zhao et al., 2007), and CORO7 depletion decreased this YAP phosphorylation in the dasatinib-treated cells (Figure 23). This data shows that CORO7 is a necessary downstream molecule for SRC to regulate the Hippo pathway.

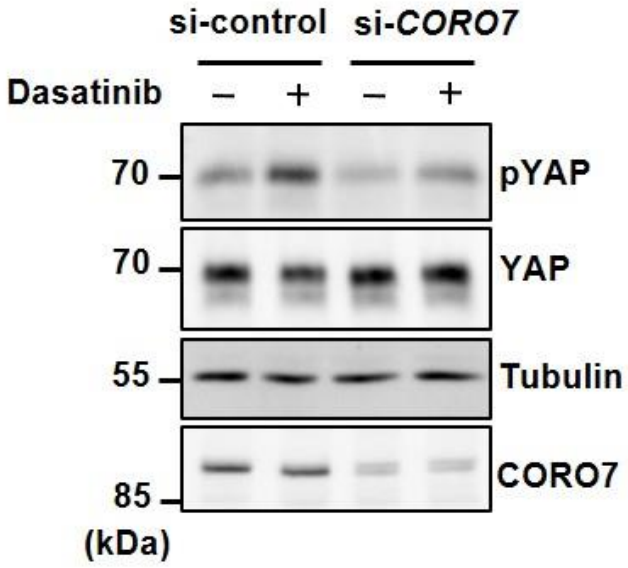


**Figure 23. SRC regulates the Hippo pathway through CORO7.**

siRNA targeting *CORO7* (si-*CORO7*) or nontargeting control siRNA (si-control) was transfected in MDA-MB-231 cells, and 50 nM dasatinib was treated for 1 h as indicated. The cell lysate samples were immunoblotted with anti-pYAP, anti-YAP, anti-tubulin, and anti-CORO7 antibodies.

Based on the enzymatic function of SRC, I predicted tyrosine kinase SRC to regulate CORO7 through tyrosine phosphorylation. Indeed, *SRC* overexpression increased the tyrosine phosphorylation of CORO7, which was inhibited by dasatinib treatment (Figure 24), indicating that SRC directly phosphorylates CORO7.

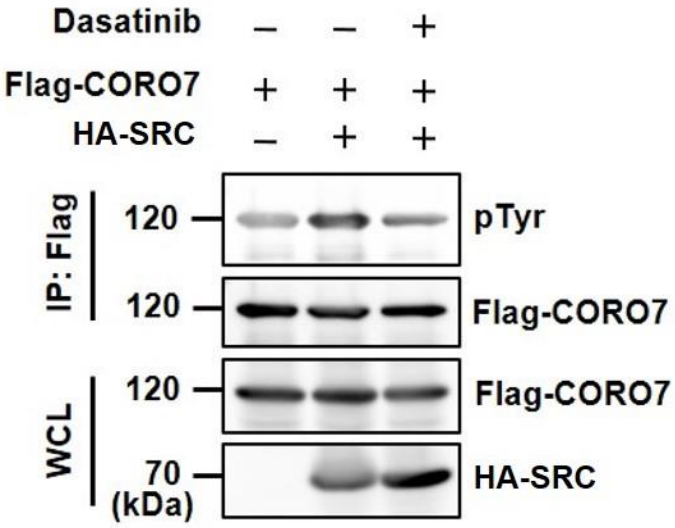


**Figure 24. SRC directly phosphorylates CORO7.**

HEK293T cells expressing Flag-CORO7 and HA-SRC were treated with 250 nM dasatinib for 2 h. The cell lysate samples were immunoprecipitated (IP) with anti-Flag antibody and immunoblotted with anti-pTyr and anti-Flag antibodies. The WCL samples were loaded for indicating the expression levels. WCL, Whole cell lysates.

Next, I screened tyrosine residues at which SRC phosphorylates CORO7. Since regulation of CORO7 by SRC appears to be evolutionarily conserved according to our data so far, I tested the phosphorylation of six evolutionarily conserved tyrosine residues between human CORO7 and *Drosophila* Pod1 (Figure 25). Among these tyrosine residues, I confirmed that combinational mutations of Tyr712, 738, 758 residues of CORO7(3YF) reduced tyrosine phosphorylation of CORO7 (Figure 26), indicating that SRC phosphorylates CORO7 at those three tyrosine residues. Taken together, these data present SRC as a potent regulator of CORO7 controlling the Hippo pathway.

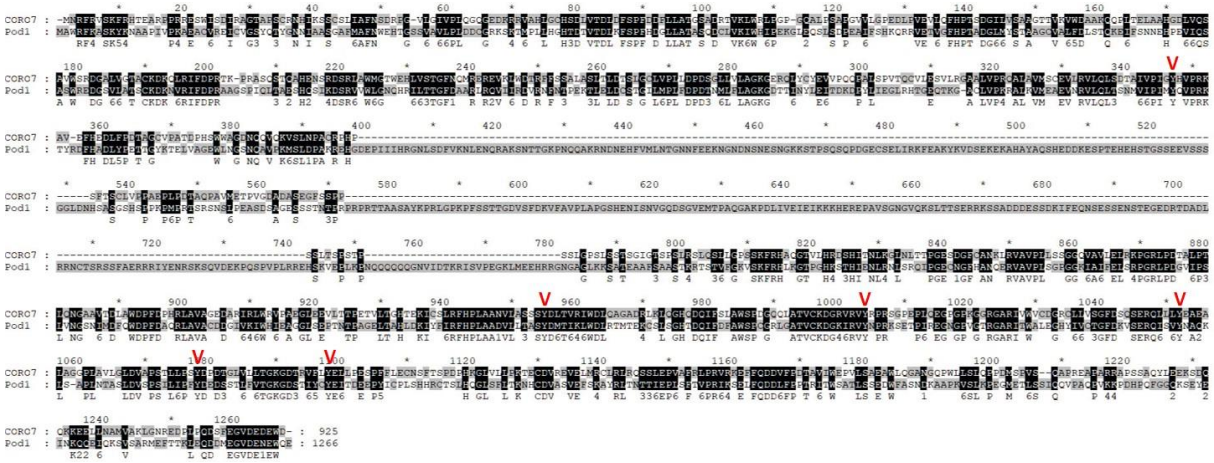

**Figure 25. Evolutionarily conserved tyrosine residues between CORO7 and Pod1.**

Protein sequence alignment between CORO7 and Pod1. Six evolutionarily conserved tyrosine residues (Tyr343, 615, 664, 712, 738, and 758) are indicated.

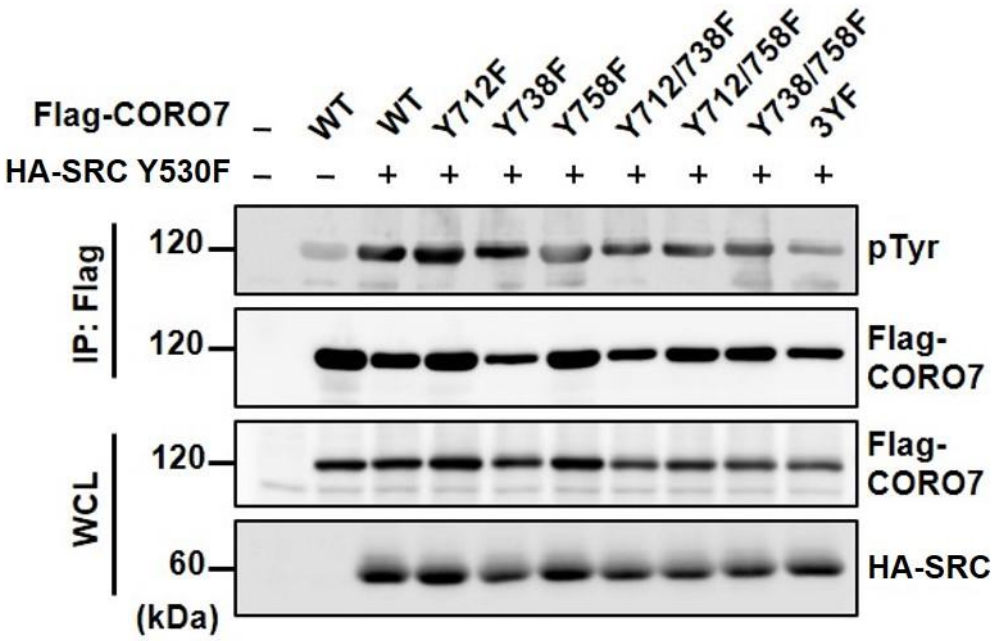


**Figure 26. SRC phosphorylates CORO7 at 712/738/758 tyrosine residues.**

HEK293T cells were transfected with indicated mutant forms of Flag-CORO7 and a constitutively active form of SRC (HA-SRC Y530F). CORO7 3YF indicates that Tyr712, Tyr738, and Tyr758 were all mutated to phenylalanine. The lysate samples were immunoprecipitated (IP) with anti-Flag antibody and immunoblotted with anti-pTyr and anti-Flag antibodies. The WCL samples were loaded for indicating the expression levels. WCL, Whole cell lysates.

# Discussion

In the current study, I identified *pod1* as a novel and positive regulator of the Hippo pathway. From interactome databases, I selected candidate genes that may regulate the Hippo pathway and conducted the genetic screening to validate candidates. *pod1* was the only gene that regulated the eye size of the fly under normal and Hippo pathway-inhibited conditions, suggesting a possible interaction between *pod1* and the Hippo pathway. Further characterization of *pod1* using KO *Drosophila* showed that firstly, *pod1* suppresses the growth of the organism through regulating cell proliferation and death. Secondly, *pod1* controls cell polarity like the Hippo pathway. Thirdly, Pod1 locates in the plasma membrane. By comparing the genetic epistasis between *pod1* and each component of the Hippo pathway, I hypothesized that Pod1 is located between the membrane adapter complex and the core kinase complex on the Hippo pathway. Based on the protein structure of CORO7, a mammalian homolog of Pod1, I discovered that CORO7 directly binds to MST2/SAV1/LATS1, and is essential for the core kinase complex formation. Additionally, I found tyrosine kinase SRC to be a possible upstream regulator of Pod1. In summary, I revealed that Pod1 is a scaffold protein required for the Hippo pathway activation (Figure 27).

### Interaction between *pod1* and *mer*

*pod1* was selected as a candidate regulator of the Hippo pathway due to its interaction with Mer reported in the databases. But, I could only observe the genetic interaction indicating that *pod1* is downstream of *mer* (Figure 20) and not the direct physical interaction between

CORO7 and NF2. However, there is multiple evidence that *pod1* and *mer* may interact to regulate the Hippo pathway. Firstly, Mer is known to physically interact with and activate the core kinase complex that requires Pod1 for the formation (Hamaratoglu et al., 2006). Secondly, Mer and Pod1 both are located in the plasma membrane. Thirdly, Mer is known to recruit the core kinase complex from cytosol to the plasma membrane, but the recruitment mechanism is still unclear. Pod1 regulates protein and vesicle trafficking (Figure 13) (Yuan et al., 2014), which can transport the core kinase complex from cytosol to the plasma membrane. Fourthly, NF2 is reported to bind to SAV1 through FBM motif of SAV1 (Yu et al., 2010). Since CORO7 also binds to SAV1, identification of the CORO7-binding site to SAV1 could clarify the relationship between CORO7/Pod1 and NF2/Mer.

**Interaction between *SRC* and *CORO7*/*pod1***

As mentioned above, *pod1* is reported to interact with *mer* from interactome databases, but both proteins passively modulate the Hippo pathway activity only through binding to other proteins and lack enzymatic activity that rapidly regulates downstream targets in response to external signals. Therefore, I assumed that there would be an upstream molecule with enzymatic activity that rapidly regulates Pod1 in response to external signals. SRC satisfied all of the above conditions. Firstly, it has kinase activity to phosphorylate its substrate. Secondly, many studies already reported that SRC directly regulates the Hippo pathway (Lamar et al., 2019; Li et al., 2016; Si et al., 2017). Thirdly, SRC was also reported to regulate CORO7 by phosphorylation (Rybakin et al., 2008). The 758 tyrosine residue was already known to be phosphorylated by SRC for Golgi association, which was also confirmed in my study. Here I discovered the novel meaning of interaction between SRC and CORO7/Pod1, for SRC to

negatively regulate the Hippo pathway through CORO7/Pod1. I discovered that SRC requires CORO7/Pod1 to inhibit the Hippo pathway and phosphorylates CORO7 at 712, 738, 758 tyrosine residues (Figure 22 – 26). However, there are also remaining questions to be answered about *SRC* and *CORO7*/*pod1*. Whether tyrosine phosphorylation of CORO7/Pod1 is essential for SRC to regulate the Hippo pathway, and if so, what functions of Pod1 are regulated remains to be elucidated. Finding answers to these questions could propose Pod1 as a therapeutic target in oncogene *SRC*-induced cancer pathogenesis.

**Pod1 regulating Actin cytoskeleton and the Hippo pathway**

Mechanical stress such as cell adhesion and cell-cell contact affects actin cytoskeleton homeostasis, thereby activating the Hippo pathway (Panciera et al., 2017). Since *pod1* had been reported to regulate the actin cytoskeleton (Bhattacharya et al., 2016), one may suggest that Pod1 controls the Hippo pathway by regulating actin filament. However, previous studies showed that *CORO7* inhibits F-actin reorganization, and the absence of CORO7 resulted in the actin cytoskeleton depolymerization (Shina et al., 2010). This could be interpreted as *CORO7* negatively regulating the Hippo pathway, an idea inconsistent with this study. Also, neither *pod1* overexpression nor KO showed plasma membrane disruption in the *Drosophila* fat body (Figure 13). Therefore, the function of Pod1 to regulate the Hippo pathway via regulation of actin cytoskeleton does not appear to be relevant.

I have improved our understanding of how body growth is controlled by finding a novel regulator of the Hippo pathway, *pod1*, and elucidating its regulatory mechanisms. Malfunction

of the Hippo pathway has been reported as a major cause of disease development such as cancer (Zheng and Pan, 2019). Mutations and the gene fusion of *CORO7* has been found in several types of cancer cells, which could affect the Hippo pathway-regulatory function of CORO7/Pod1 and thereby causing tumorigenesis (Table 3) (Klijn et al., 2015; Zhu et al., 2018). Further studies about this relationship between mutations and the function of Pod1 will suggest *pod1* as a new therapeutic target for cancer.

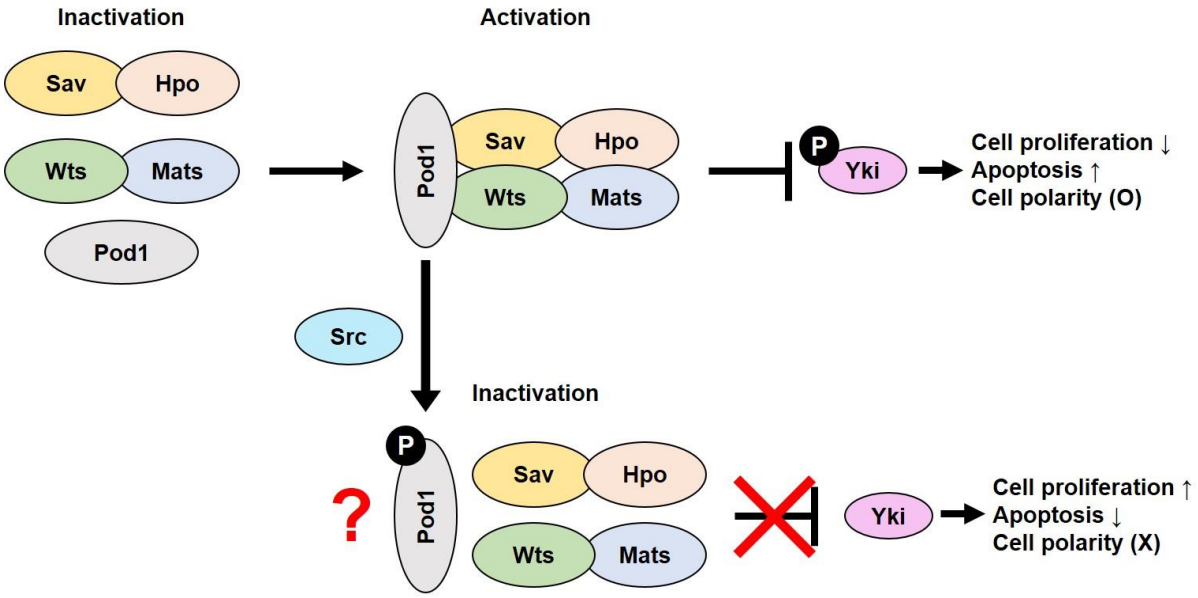


**Figure 27. Proposed model for Pod1 to regulate the core kinase complex formation.**

Under the growth-inhibitory condition, Pod1 acts as a scaffold protein to recruit the core kinase complex components. SRC activation represents the growth-favorable condition, which results in phosphorylation and inhibition of Pod1.

| Gene ID | Consequence | Protein_position | Amino_acids | Conservation in *Drosophila* Pod1 |
|---|---|---|---|---|
| 79585_*CORO7* | NON_SYNONYMOUS_CODING | 13 | E/K | |
| 79585_*CORO7* | NON_SYNONYMOUS_CODING | 217 | R/W | O |
| 79585_*CORO7* | NON_SYNONYMOUS_CODING | 236 | R/H | O |
| 79585_*CORO7* | NON_SYNONYMOUS_CODING | 252 | L/M | |
| 79585_*CORO7* | NON_SYNONYMOUS_CODING | 290 | V/M | O |
| 79585_*CORO7* | STOP_GAINED | 306 | E/* | O |
| 79585_*CORO7* | NON_SYNONYMOUS_CODING | 308 | V/M | |
| 79585_*CORO7* | NON_SYNONYMOUS_CODING | 327 | V/A | O |
| 79585_*CORO7* | NON_SYNONYMOUS_CODING | 345 | V/A | O |
| 79585_*CORO7* | NON_SYNONYMOUS_CODING | 359 | D/N | |
| 79585_*CORO7* | NON_SYNONYMOUS_CODING | 484 | D/N | |
| 79585_*CORO7* | NON_SYNONYMOUS_CODING | 513 | V/M | O |
| 79585_*CORO7* | NON_SYNONYMOUS_CODING | 618 | T/A | O |
| 79585_*CORO7* | NON_SYNONYMOUS_CODING | 661 | V/E | O |
| 79585_*CORO7* | NON_SYNONYMOUS_CODING | 707 | R/C | O |
| 79585_*CORO7* | NON_SYNONYMOUS_CODING | 741 | D/V | O |
| 79585_*CORO7* | NON_SYNONYMOUS_CODING | 766 | F/L | O |
| 79585_*CORO7* | NON_SYNONYMOUS_CODING | 799 | R/Q | O |

**Table 3a. Mutations of *CORO7* in cancer cell lines (Klijn et al., 2015).**

| Gene ID | Consequence | Protein_position | Amino_acids | Conservation in *Drosophila* Pod1 |
|---|---|---|---|---|
| 79585_*CORO7* | NON_SYNONYMOUS_CODING | 817 | R/Q | O |
| 79585_*CORO7* | NON_SYNONYMOUS_CODING,SPLICE_SITE | 819 | R/Q | O |
| 79585_*CORO7* | NON_SYNONYMOUS_CODING | 826 | D/V | O |
| 79585_*CORO7* | NON_SYNONYMOUS_CODING | 836 | E/G | |
| 79585_*CORO7* | NON_SYNONYMOUS_CODING | 900 | M/L | |
| 79585_*CORO7* | NON_SYNONYMOUS_CODING | 904 | L/P | |
| 79585_*CORO7* | NON_SYNONYMOUS_CODING | 921 | E/G | O |

**Table 3b. Mutations of *CORO7* in cancer cell lines (Klijn et al., 2015).**

# Part II

# Characterization of NitFhit as an intestinal enterocyte regulator

# Introduction

## NitFhit is a fusion protein

Rosetta stone theory suggests that separate proteins of one species as a result of gene fission during evolution may consist of a fusion protein of another species (Kummerfeld and Teichmann, 2005; Snel et al., 2000). With the bioinformatics and experimental data, this theory indicates that these individual proteins are likely to participate in the same biological pathways and have physical interactions. Human nitrilase 1 (Nit1) and fragile histidine triad (Fhit) are such examples of this theory as they exist as a fusion protein NitFhit only in *Drosophila melanogaster* and *Caenorhabditis elegans*.

## Fhit

*Fhit* is located on chromosome 3p.14.2, which makes the gene susceptible to genomic deletion, rearrangement, promoter hypermethylation (Zheng et al., 2004). Due to this genomic vulnerability, mRNA/protein expression of *Fhit* is often completely lost, which is commonly observed in various cancer cell types (Karras et al., 2016). Many studies reported *Fhit* as a tumor suppressor gene. One study showed that *Fhit* knockout mice had significantly elevated tumorigenesis rate under ordinary or carcinogen-treated conditions, and gene therapy inducing artificial *Fhit* DNA was sufficient to recover from the disease (Dumon et al., 2001). Other studies reported that *Fhit* expression is lost in human breast and lung cancer, and even in the bronchial epithelial cells of smokers before tumorigenesis (Fu et al., 2019; Tseng et al., 1999). The mechanism by which Fhit suppresses tumorigenesis is well studied. Fhit induces apoptosis

by SRC-dependent phosphorylation (Pekarsky et al., 2004), modulating the Akt pathway (Semba et al., 2006b), inhibiting proteasomal degradation of p53 (Andriani et al., 2012). Chaperone protein HSP60/10 is responsible for the mitochondrial localization of Fhit (Druck et al., 2019). Fhit in the mitochondria enhances mitochondrial calcium uptake and potentiates the apoptotic effect (Rimessi et al., 2009), or generates intracellular radical oxygen species (ROS) to promote apoptosis during electron transfer to ferredoxin reductase (Druck et al., 2019). Fhit also controls cell proliferation by regulating gene transcription through β-catenin (Weiske et al., 2007b). Fhit catalyzes diadenosine triphosphate (Ap3A) and tetraphosphate (Ap4A) into AMP and ADP (Barnes et al., 1996). However, since the induction of apoptosis by Fhit requires only physical binding of Fhit to Ap3A and not the catalytic activity, enzymatic activity does not appear to be related to tumorigenic function (Kowara et al., 2002).

**Nit1**

Nit1 is a member of Nitrilase superfamily but lacks nitrilase activity as other family member does (Pace and Brenner, 2001). Nit2 has ω-amidase activity (Krasnikov et al., 2009) and shows a high similarity of protein sequence to Nit1, up to 40%. But It is revealed that Nit1 cannot catalyze the a-ketoglutaramate, the substrate of Nit2 (Jaisson et al., 2009). Instead, Nit1 hydrolyzes deaminated glutathione (deGSH), a byproduct of glutathione (GSH) produced by transaminases (Peracchi et al., 2017).

*Fhit*, its counterpart homolog of *Drosophila NitFhit* (cg7067), has been thoroughly studied as a tumor suppressor gene, but relatively little was known about *Nit1*. Recent studies showed that Nit1 also has the same tumor suppressor function as Fhit. *Nit1* knockdown in murine kidney cells promoted cell proliferation, increased *cyclin D1* expression, and showed

an increased probability of carcinogen-induced tumorigenesis (Semba et al., 2006a). In addition, a recent study reported lung tumor progression of *Nit1* knockout mice (Wang et al., 2016). Nit1 suppresses tumorigenesis by activating the TGFβ1-Smad2/3 signaling pathway (Lin et al., 2018) or, like Fhit, repressing β-catenin-induced transcription, which is independent of the enzymatic activity of Nit1 (Mittag et al., 2016). Although there is no direct interaction between *Nit1* and *Fhit*, the co-expression of Nit1 and Fhit showed an additive tumor-suppressive effect (Sun et al., 2009), presenting a possible interaction between *Nit1* and *Fhit*.

In this study, I identified the novel function of *Drosophila* NitFhit as a positive regulator of individual growth. *NitFhit* null fly showed a lighter body weight, reduced food uptake, and defect in excretion. Further inspection revealed that NitFhit in the enterocyte positively modulates the thickness of the intestinal wall and resistance to starvation. I found that NitFhit regulates the wall thickness of the intestine via ROS and ferredoxin reductase.

# Result

### Cellular location of NitFhit fusion protein

I observed the location of *Drosophila* NitFhit and its two human homologs, Nit1 and Fhit. Protein sequence analysis revealed that all three proteins have a mitochondria-targeting sequence (MTS) at the N-terminus (Figure 28 A). Indeed, all three proteins were located in the mitochondria, as expected (Figure 28 B). Then, I observed the location of each domain of the NitFhit. The N-terminal Nit domain (dNit) was located in the mitochondria because it contains MTS of the NitFhit. However, I confirmed that the C-terminal Fhit domain (dFhit) lacking MTS was located in the nucleus when expressed alone. Because the dFhit in the NitFhit is located in the mitochondria, not the nucleus, I generated N-terminus MTS-tagged dFhit transgenic fly using MTS of human cytochrome C oxidase subunit VIII. Successfully, MTS-tagged dFhit was located in the mitochondria.

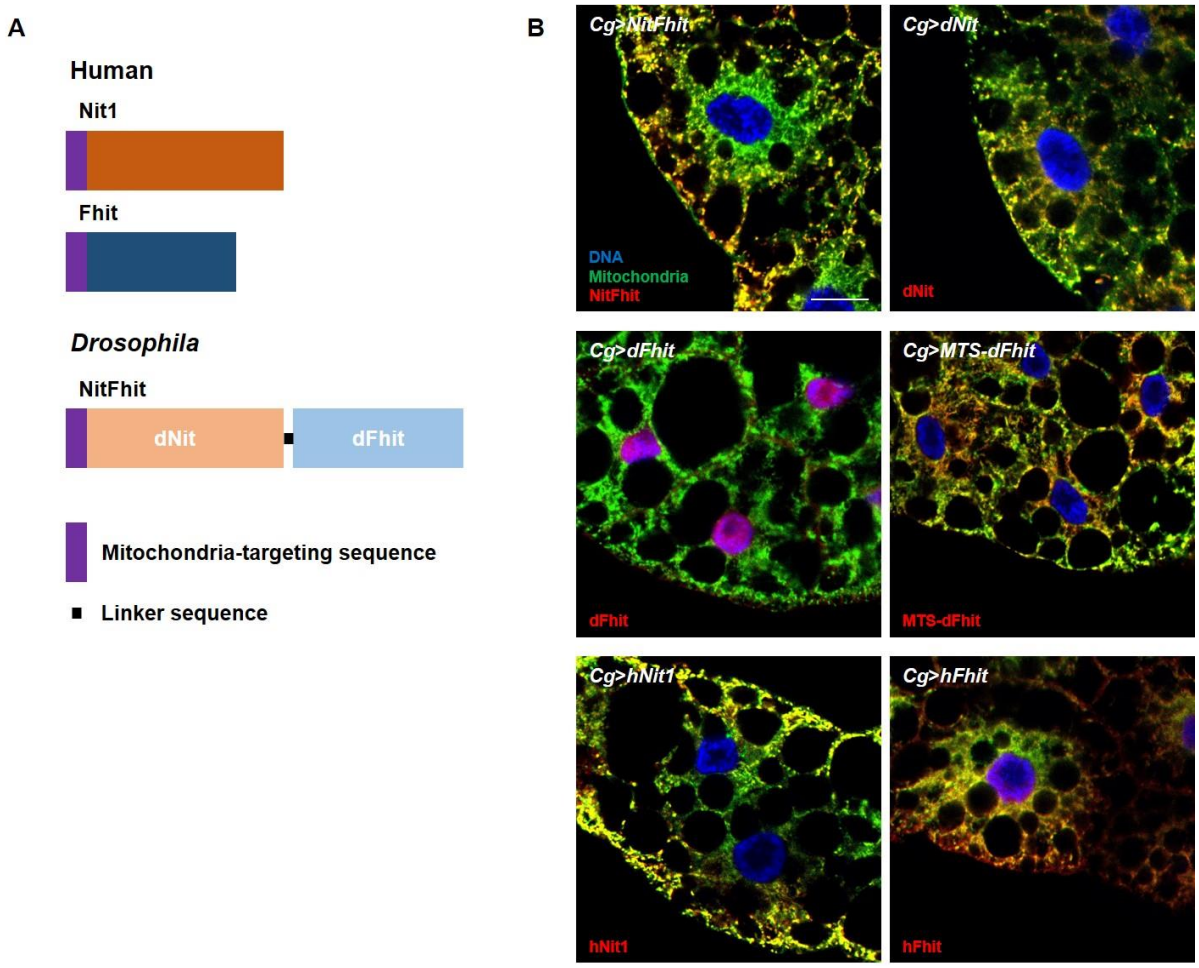


**Figure 28. Protein structure and the localization of NitFhit.**

(A) A schematic diagram of protein structure of Nit1, Fhit, and *Drosophila* NitFhit. dNit, dFhit, MTS, and linker sequence are indicated.

(B) Representative images of NitFhit, dNit, dFhit, MTS-dFhit, Nit1 (hNit1), and Fhit (hFhit) location in the fat body of indicated genotypes respectively. C-terminal HA staining was conducted to observe the location of NitFhit, dNit, dFhit, MTS-dFhit, and hFhit. 488-conjugated streptavidin was used as a mitochondrial marker. Scale bar represents 20 μm.

**Generation of *NitFhit* KO *Drosophila***

I generated the *NitFhit* KO fly to characterize the physiological function of *NitFhit*. Using the CRISPR/Cas9 system, I induced a genomic deletion in exon#1 of *NitFhit*, creating a *NitFhit* KO fly ($NitFhit^{KO}$) that cannot express the normal NitFhit. Frameshift due to the genomic deletion resulted in the expression of an abnormal and shortened form of NitFhit with 59 amino acids (Figure 29). $NitFhit^{KO}$ didn`t show any developmental delay or defects.

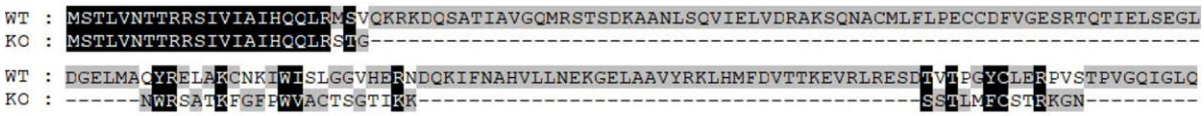


**Figure 29. Comparison of NitFhit amino acids sequence between the wild-type and *NitFhit*$^{KO}$.**

Full protein sequence of abnormal and shortened NitFhit ending with asparagine (N) from *NitFhit*$^{KO}$ (KO) is compared to that of wild-type NitFhit (WT).

### *NitFhit*$^{KO}$ is lighter than the wild-type and intakes less amount of food

I found that NitFhit is located in the mitochondria, a subcellular organelle that makes energy to survive. Nit1 and Fhit have enzymatic activities to produce metabolites, 2-oxoglutarate and L-cysteinylglycine, AMP and ADP, respectively (Barnes et al., 1996; Peracchi et al., 2017), and most of related catalytic sites are evolutionarily conserved in dNit and dFhit of NitFhit (Figures 30 A and B) (Lima et al., 1997; Pace et al., 2000). Besides the enzymatic activity, Nit1 and Fhit are well-known tumor suppressors modulating multiple signaling pathways to promote apoptosis. Taken together, I expected that the absence of NitFhit in *NitFhit*$^{KO}$ would result in metabolism or growth-related defects. To confirm this idea, first, I measured the body weight of *NitFhit*$^{KO}$ to examine the general growth function and metabolism. In contrast to the expectation that the absence of tumor suppressor NitFhit would increase cell proliferation and elevate the body weight of *NitFhit*$^{KO}$, I found that *NitFhit*$^{KO}$ is lighter than the wild-type (Figure 31).

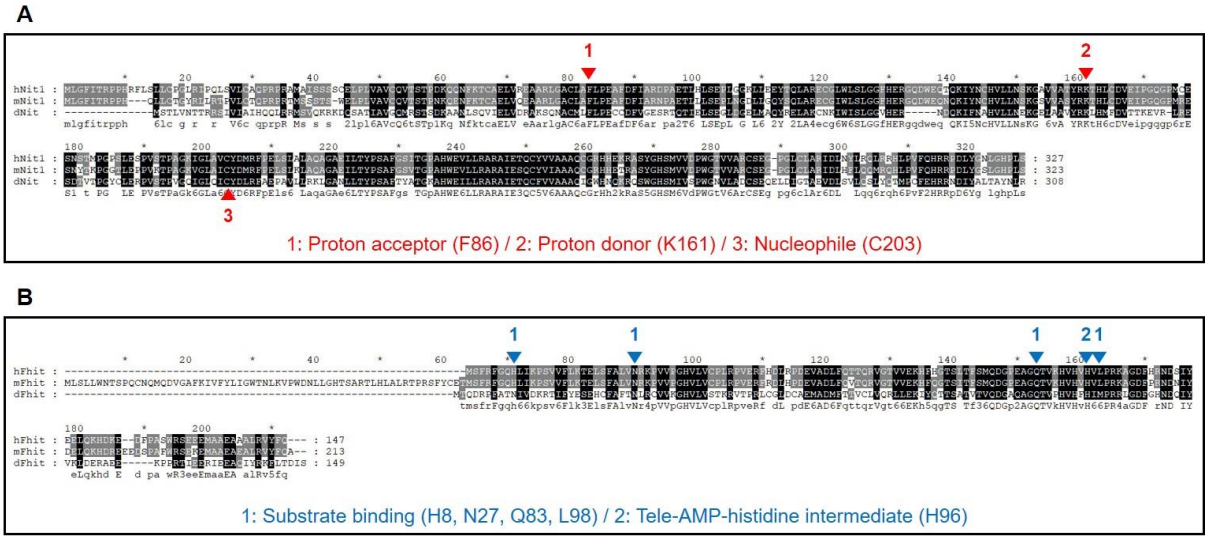


**Figure 30. Protein sequence comparison between Nit1, Fhit, and NitFhit.**

(A) Alignment of human Nit1 (hNit1), mouse Nit1 (mNit1), and Nit domain of *Drosophila* NitFhit (dNit) protein sequence. Catalytic sites are indicated.

(B) Alignment of human Fhit (hFhit), mouse Fhit (mFhit), and Fhit domain of *Drosophila* NitFhit (dFhit) protein sequence. Starting amino acid methionine is added to dFhit for comparison. Catalytic sites are indicated.

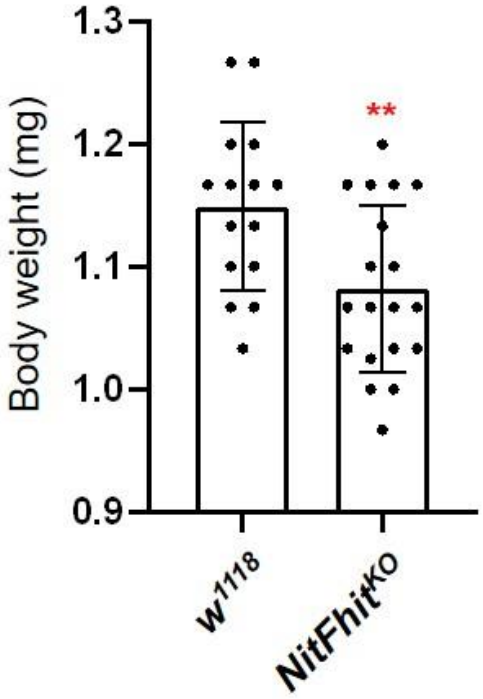


**Figure 31. *NitFhit*$^{KO}$ is lighter than the wild-type.**

Statistical analysis of the body weight of each genotype (**, p<0.01).

In addition to the body weight result, *NitFhit*$^{KO}$ didn`t exhibit any tumorigenesis or abnormal tissue growth, so I excluded the tumor suppressor function of Nit1 and Fhit to analyze the data. Nutrient supply through food uptake is a fundamental factor affecting the growth of all biological organisms. Therefore, I measured the amount of food uptake of *NitFhit*$^{KO}$ to find out whether weight loss of *NitFhit*$^{KO}$ resulted from the lack of nutrient supply due to decreased food uptake. Indeed, I observed that *NitFhit*$^{KO}$ ate less food than the wild-type (Figure 32), which could be a possible explanation for the lighter body weight of *NitFhit*$^{KO}$.

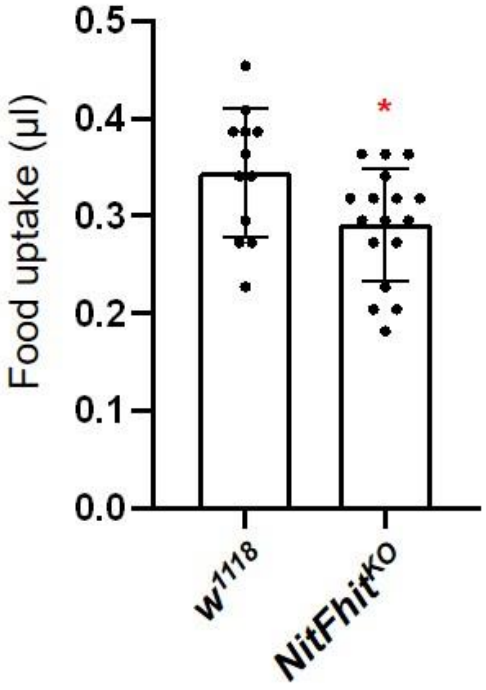


**Figure 32. *NitFhit*$^{KO}$ eats less food than the wild-type.**

Statistical analysis of the food intake of each genotype (*, $p<0.05$). CAFÉ assay was conducted to measure the food uptake.

Next, I measured the ATP level of *NitFhit*$^{KO}$ to see whether the weight loss of *NitFhit*$^{KO}$ resulted from the internal energy shortage. However, the ATP level per unit amount of protein of *NitFhit*$^{KO}$ was the same as that of the wild-type (Figure 33), indicating that weight loss of *NitFhit*$^{KO}$ didn`t result from energy deficiency. In addition, I dissected the thorax of *NitFhit*$^{KO}$, where mitochondria are abundant and most of ATP in *Drosophila* are produced, to observe the mitochondrial morphology. I found that the mitochondrial morphology in the thorax of *NitFhit*$^{KO}$ was ordinary (Figure 34). Combining the ATP level and mitochondrial morphology in the thorax of *NitFhit*$^{KO}$, it is assumed that the ATP-producing function of the mitochondria in *NitFhit*$^{KO}$ is normal. But, since *NitFhit*$^{KO}$ is lighter than the wild-type, the total amount of protein and thus ATP level of *NitFhit*$^{KO}$ is less than that of the wild-type, possibly resulted from decreased food uptake.

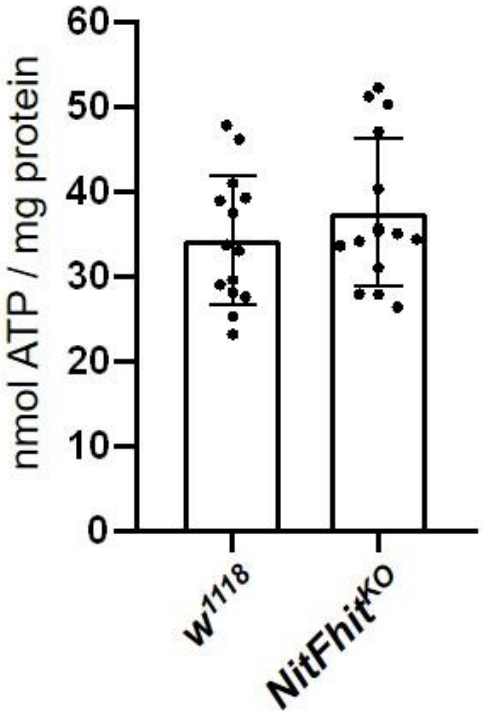


**Figure 33. *NitFhit$^{KO}$* has normal ATP level.**

Statistical analysis of the ATP level of each genotype. The amount of ATP per unit amount of protein was measured.

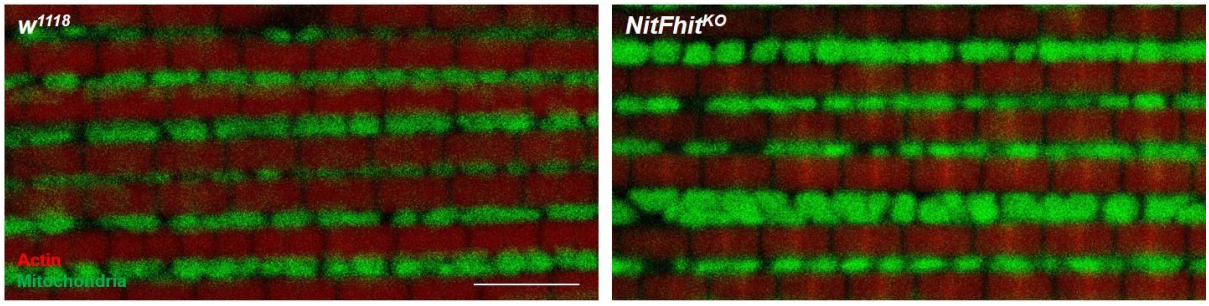


**Figure 34. *NitFhit*$^{KO}$ has normal mitochondrial morphology in the thorax.**

Representative images of actin and mitochondria in the thorax of indicated genotypes. 488-conjugated streptavidin was used as mitochondrial marker. Scale bar represents 5 μm.

### *NitFhit*$^{KO}$ has defects in food uptake and excretion

To find out why *NitFhit*$^{KO}$ eats less food, I examined the food uptake and excretion function of *NitFhit*$^{KO}$. After 24 h of starvation, flies were fed with green-stained 10% sucrose solution for up to 12 h, and the amount of food in the abdomen of the fly was measured at 1, 2, and 12 h using quantification index (Figures 35 A and B). Usually, it takes less than 1 h for *Drosophila* to excrete the newly eaten food (Wong et al., 2008), but it takes longer under the starvation condition (Cognigni et al., 2011). Indeed, very few fecal spots were detected until 2 h of food supply, meaning that the amount of food in the abdomen was equal to the amount of food that fly ate. I observed that *NitFhit*$^{KO}$ ate less food than the wild-type until 2 h (Figure 36 A), indicating a food uptake defect of *NitFhit*$^{KO}$. When the sucrose solution was provided for a period of 12 h to allow for sufficient uptake and excretion, both the wild-type and *NitFhit*$^{KO}$ had the statistically equal amount of food inside (Figure 36 A). I starved these flies that had been fed for 12 h for another 24 h and counted flies that didn`t excrete the sucrose solution after starvation. As a result, I confirmed that twice as many flies of *NitFhit* KO didn`t excrete the food than the wild-type (Figure 36 B), indicating an excretion defect of *NitFhit*$^{KO}$. In conclusion, I found that *NitFhit*$^{KO}$ has defects in food uptake and excretion.

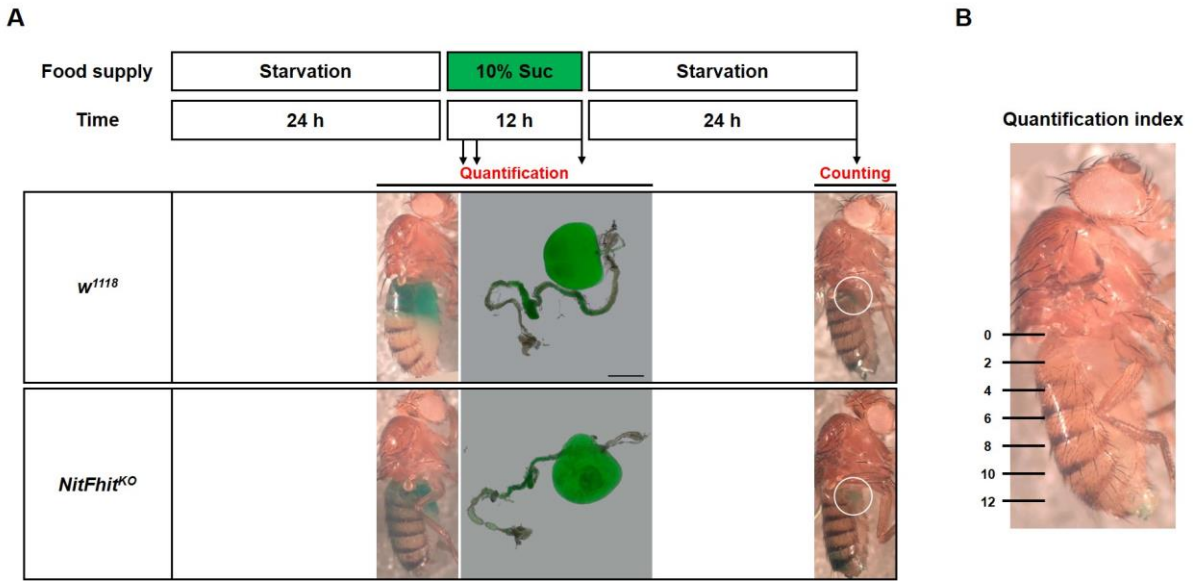


**Figure 35. A schematic diagram to examine the food intake and excretion function of *NitFhit*$^{KO}$.**

(A) A schematic diagram of the food supply timeline. Representative images of flies and intestines after food supply or starvation of indicated genotypes are presented according to time point. Scale bar represents 500 μm.

(B) Quantification index of the amount of food in the abdomen of the fly.

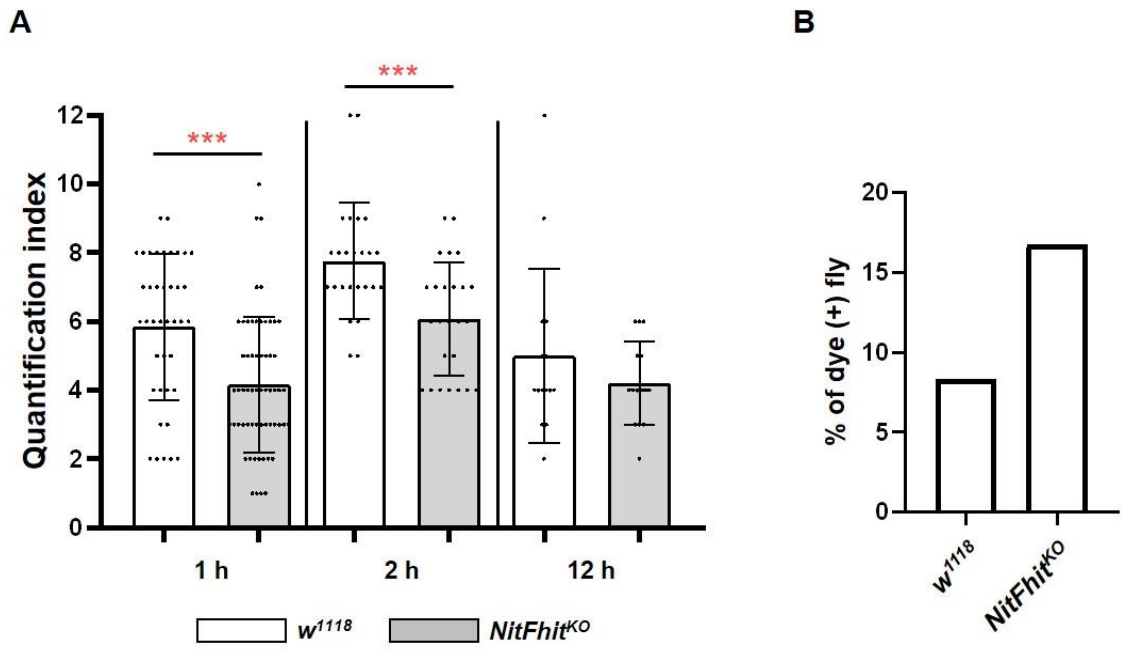


**Figure 36. *NitFhit$^{KO}$* has defects in food uptake and excretion.**

(A) Statistical analysis of the quantification index of each genotype (***, $p<0.001$). Quantification index represents the amount of food in the abdomen of the fly (Note Figure 35 B). Flies fed for 12 h were starved again for 24 h to examine the excretion function in (B).

(B) Percentage of flies that didn`t excrete the food after 24 h starvation.

### *NitFhit*$^{KO}$ has a thin intestinal wall

I analyzed the intestinal structure and morphology of *NitFhit*$^{KO}$ to find the cause of food uptake and excretion defects. *Drosophila* intestine consists of crop, midgut, and hindgut, each representing human stomach, small intestine, and large intestine, respectively. *Drosophila* midgut is divided from R1 to R5 regions according to its shape, function, and transcriptome (Buchon et al., 2013b). *NitFhit*$^{KO}$ didn`t show specific structural abnormalities from crop to hindgut (Figure 37).

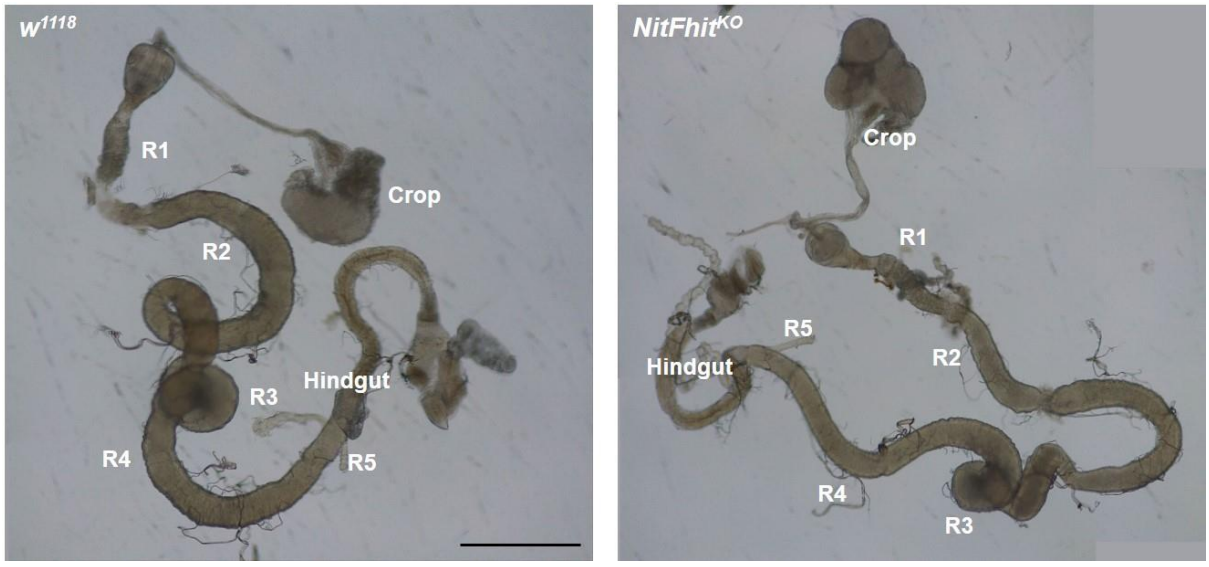


**Figure 37. *NitFhit*$^{KO}$ has normal intestinal morphology.**

Representative images of intestines of indicated genotypes. Crop, midgut from R1 to R5 regions, and hindgut are indicated. Scale bar represents 500 μm.

Next, I tested the function of each intestinal part of *NitFhit*$^{KO}$. First, to find out whether the failure of food transfer from crop to midgut causes the food uptake defect of *NitFhit*$^{KO}$, I counted the number of crop contractions. The crop of *NitFhit*$^{KO}$ contracted statistically the same number of times as that of the wild-type (Figure 38). Also, I observed that after starvation and green-stained sucrose solution feeding, the crop of *NitFhit*$^{KO}$ was full of the solution, and some of the solution was transferred to midgut as the wild-type does (Figure 35 A), indicating no functional abnormality in the crop of the *NitFhit*$^{KO}$. Therefore, I concluded that the crop is not a responsible organ for the food uptake defect of *NitFhit*$^{KO}$.

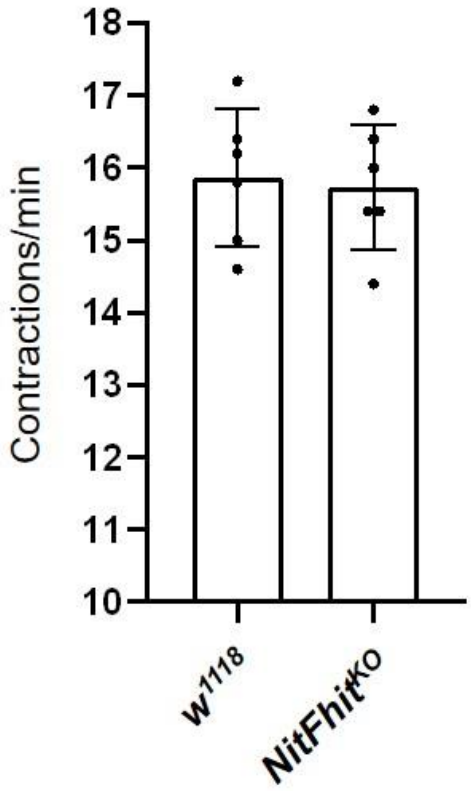


**Figure 38. *NitFhit*$^{KO}$ shows normal crop contraction.**

Statistical analysis of the number of crop contractions per minute of each genotype.

The midgut of the *Drosophila* intestine physically transfers the food by peristalsis using visceral muscle composed of circular and longitudinal actin. A defect in actin structure leads to failure of peristalsis thereby accumulating the food in the midgut and decreasing the food uptake (Min et al., 2017). I observed the actin filament in the midgut of $NitFhit^{KO}$ and found that $NitFhit^{KO}$ has normal circular and longitudinal actin filament structures (Figure 39), indicating no structural defect in the visceral muscle.

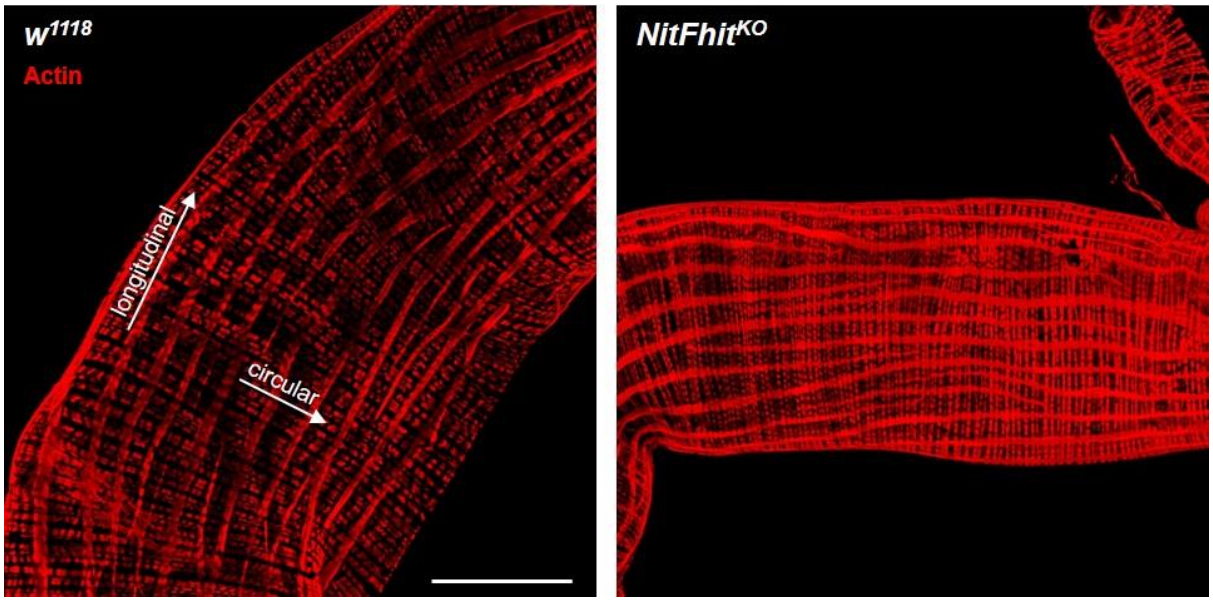


**Figure 39. *NitFhit*$^{KO}$ shows ordinary visceral morphology.**

Representative images of actin structure of midgut of indicated genotypes. Longitudinal and circular actin are indicated. Scale bar represents 500 μm.

However, upon closer inspection of the actin structure in the midgut, I discovered that the intestinal wall of *NitFhit*$^{KO}$ was thinner than that of the wild-type at R2 and R4 regions (Figures 40 A and B; see also Figure 37). The thickness of the intestinal wall refers to the vertical distance crossing the center of the nucleus between actin filaments, that is the thickness of the cell composing the intestinal wall. To confirm that this defect of *NitFhit*$^{KO}$ resulted from the absence of NitFhit, I tested whether RNAi-induced *NitFhit* knockdown exhibited the same phenotype as the knockout. Indeed, *NitFhit* knockdown by *tubulin* (*tub*)-GAL4 driver resulted in the intestinal wall thinning at R2 and R4 regions (Figure 41).

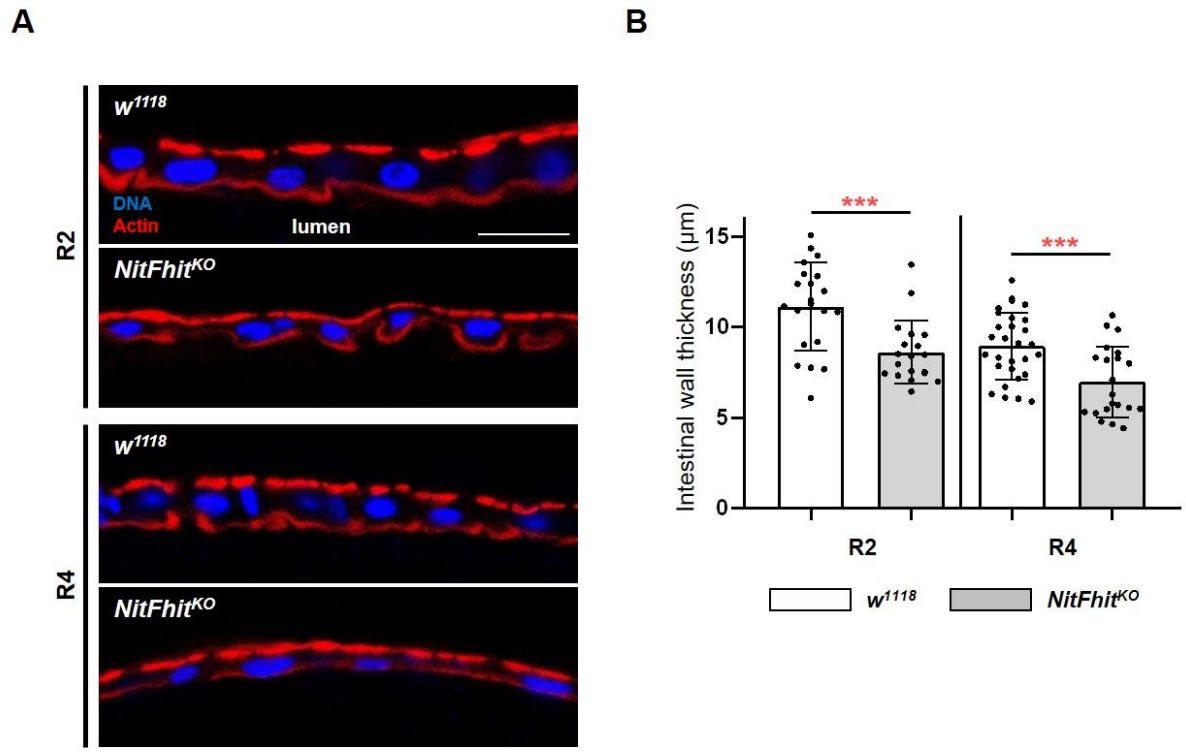


**Figure 40. *NitFhit*$^{KO}$ has a thin intestinal wall.**

(A) Representative images of the intestinal wall of midgut at R2 and R4 regions of indicated genotypes. The lumen is at the bottom of every images. Scale bar represents 20 μm.

(B) Statistical analysis of the thickness of the intestinal wall of each genotype in (A) (***, $p<0.001$).

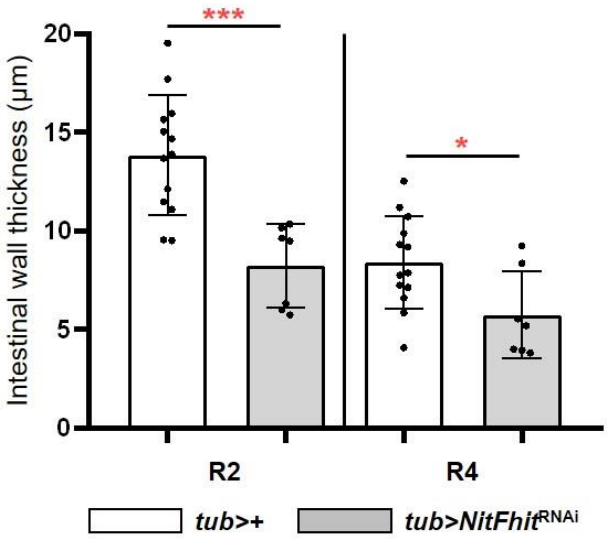


**Figure 41. *NitFhit* knockdown by *tub*-GAL4 results in thinning of the intestinal wall.**

Statistical analysis of the thickness of the intestinal wall of each genotype (*, $p<0.05$; ***, $p<0.001$).

### *NitFhit* in the enterocyte regulates the intestinal wall thickness

The midgut of *Drosophila* is composed of intestinal stem cells (ISC), enteroblasts (EB), secretory enteroendocrine (EE) cells, and absorptive enterocytes (EC) (Figure 42). I investigated the cell type in which NitFhit controls the intestinal wall thickness using *Esg*, *Su(H)GBE*, and *Myo1A*-GAL4 driver, each controlling the gene expression in ISC, EB, and EC respectively (Figure 43). Among three GAL4 drivers, only *Myo1A*-GAL4 driver-induced *NitFhit* knockdown resulted in the decrease of the intestinal wall thickness. Furthermore, FLAG-tagged NitFhit overexpression by *Myo1A*-GAL4 driver restored the intestinal wall thickness of $NitFhit^{KO}$ (Figure 44), indicating that NitFhit in the enterocyte is responsible for the regulation of the intestinal wall thickness. *NitFhit* overexpression didn`t increase the cell number to increase the intestinal wall thickness because cells of the intestinal wall remained in a mono-layer. Rather, *NitFhit* overexpression increased the thickness of each epithelial cell, that is, increased cell growth, thereby increasing the intestinal wall thickness.

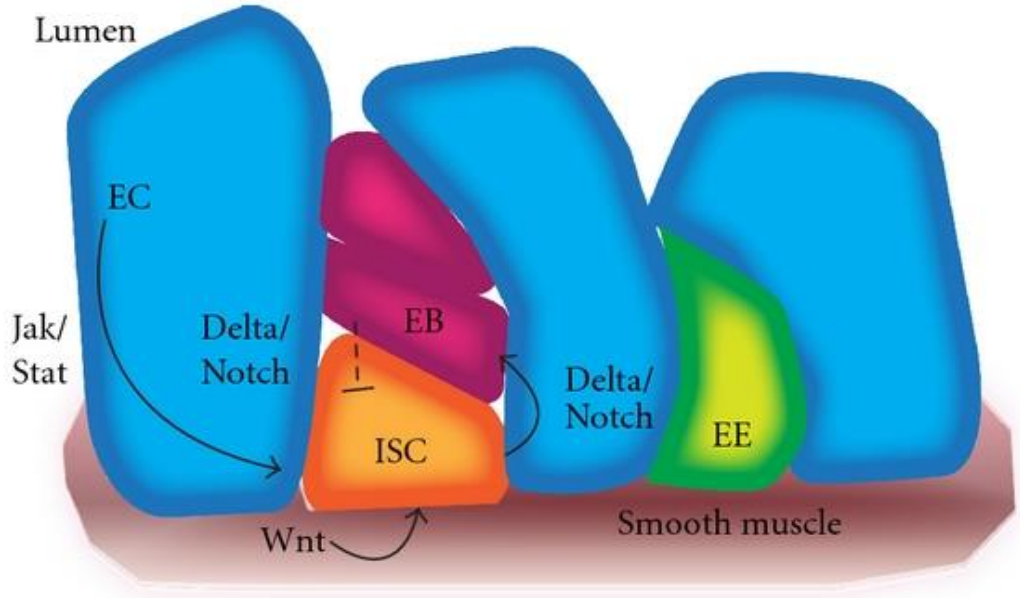


**Figure 42. An overview of intestinal stem cell differentiation of *Drosophila*.**

Intestinal stem cell differentiates into enteroblast which produces enterocytes and enteroendocrine cells. Adopted from Kevin S. Tieu, Ryan S. Tieu, Julian A. Martinez-Agosto, and Mary E. Sehl (Tieu et al., 2012).

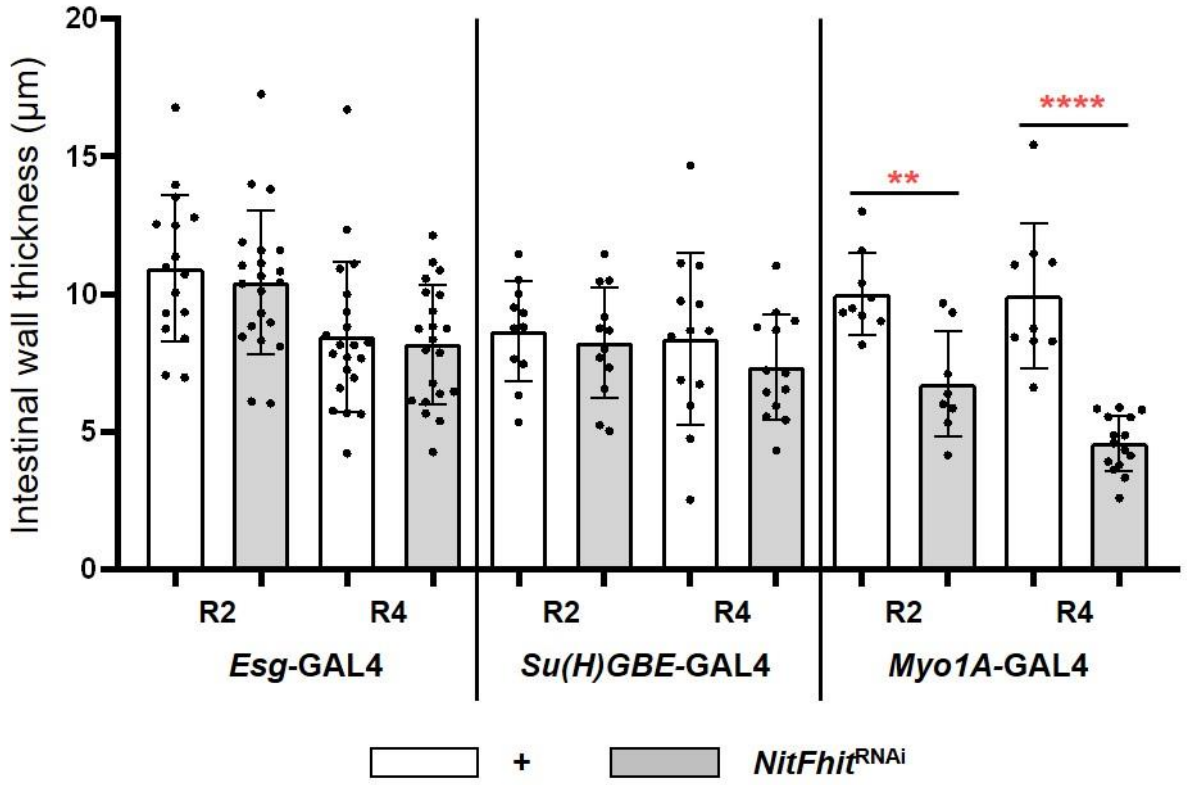


**Figure 43. NitFhit in the enterocyte is responsible for the intestinal wall thinning.**

Statistical analysis of thickness of the intestinal wall of *Esg, Su(H)GBE, Myo1A*-GAL4 of each genotype (**, $p<0.01$: ***, $p<0.001$).

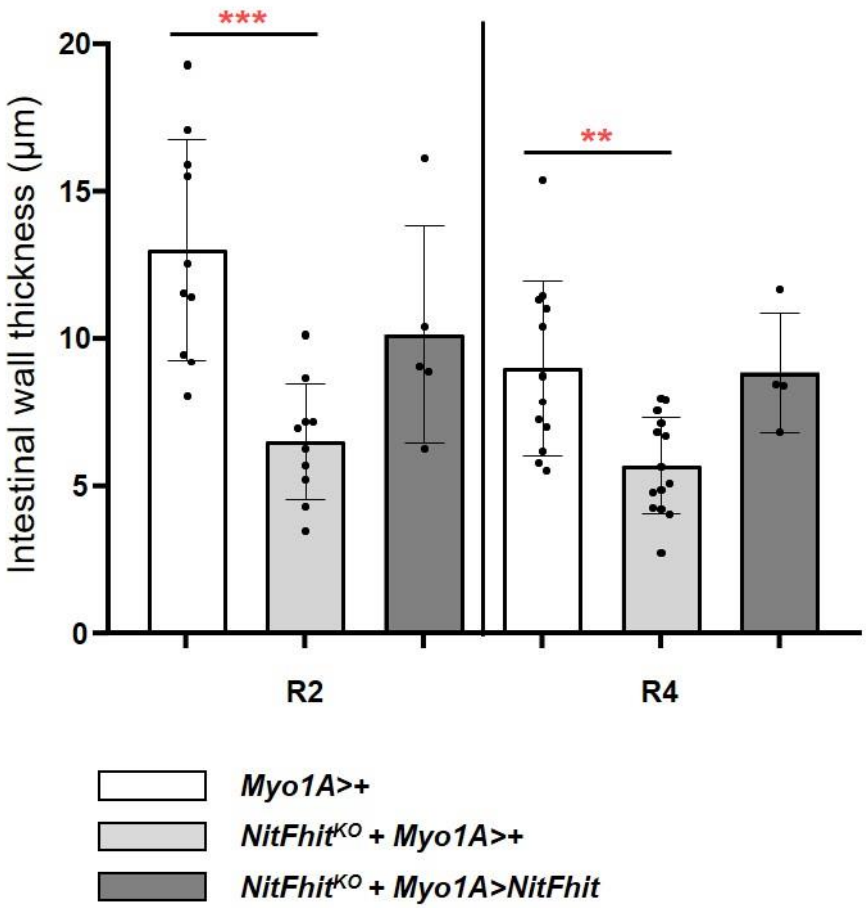


**Figure 44. NitFhit in the enterocyte positively regulates the intestinal wall thickness.**

Statistical analysis of the thickness of the intestinal wall of each genotype (**, $p<0.01$: ***, $p<0.001$).

### *NitFhit* expression in the enterocyte increases the starvation resistance

If the decrease of the intestinal wall thickness in *NitFhit*$^{KO}$ is responsible for the body weight and food uptake decreases, I hypothesized that *NitFhit* would affect the longevity in the starvation condition in which nutrient supply is halted and thereby consuming all energy generated before by food intake is required. Indeed, *NitFhit*$^{KO}$ showed a shorter lifespan under the starvation condition, which was fully restored by *NitFhit* overexpression by *Myo1A*-GAL4 (Figure 45), indicating that NitFhit in the enterocyte modulates the starvation sensitivity.

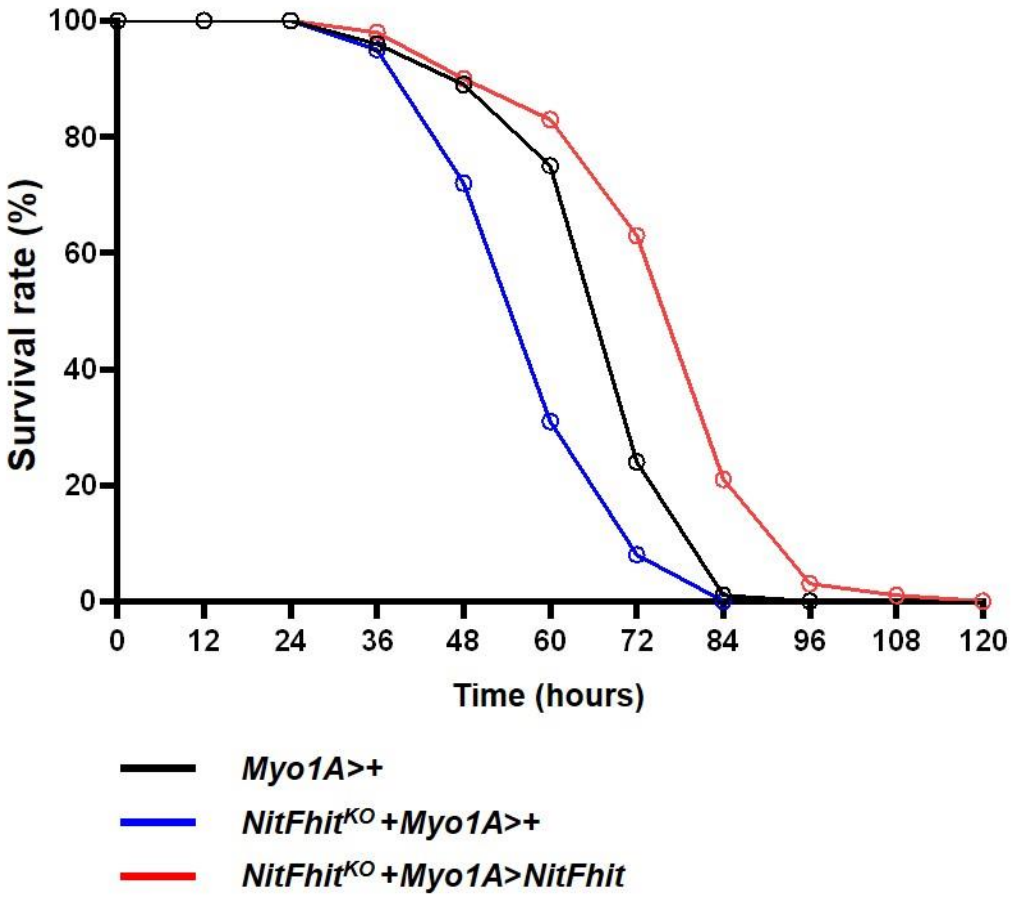


**Figure 45. NitFhit in the enterocyte increase the starvation resistance.**

Life spans of flies of indicated genotypes under starvation (n > 87).

**Catalase restores the intestinal wall defect of *NitFhit$^{KO}$***

A previous study reported that Fhit transfers electrons to ferredoxin reductase (FDXR) and hyper-activation of Fhit results in the ROS level increase (Druck et al., 2019). Nit1 indirectly regulates GSH metabolism by catalyzing deGSH, an unusable form of glutathione, into 2-oxoglutarate and L-cyteinylglycine (Peracchi et al., 2017). GSH is an antioxidant metabolite used for ROS clearance (Gaucher et al., 2018). Putting these ideas together, the NitFhit depletion could result in either elevation or down-regulation of the ROS level. I assumed that the ROS level of *NitFhit$^{KO}$* had changed, and tested whether the ROS level change was responsible for the intestinal wall thinning. Indeed, overexpression of ROS scavenging enzyme Catalase and SOD2 increased the intestinal wall thickness (Figure 46), presenting ROS as one of the factors modulating the intestinal wall thickness. Surprisingly, only Catalase, but not SOD2, was able to restore the thin intestinal wall of *NitFhit$^{KO}$*. Radical oxygen is converted to hydrogen peroxide by SOD2 and hydrogen peroxide is catalyzed into water and oxygen by Catalase (Figure 47). Taken together, it is expected that hydrogen peroxide accumulation may be responsible for the decrease of the intestinal wall thickness of *NitFhit$^{KO}$*.

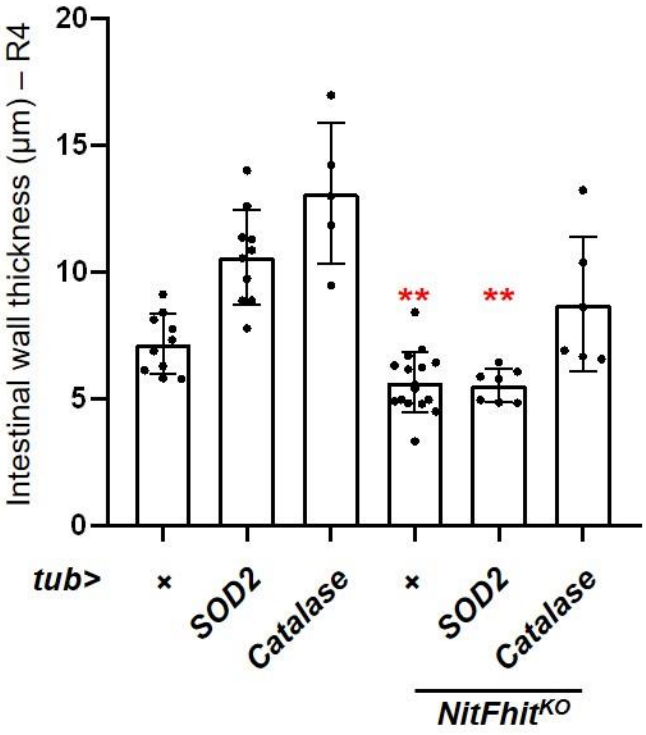


**Figure 46. Catalase can restore the intestinal wall thinning of *NitFhit*$^{KO}$.**

Statistical analysis of the thickness of the intestinal wall of each genotype (**, $p<0.01$).

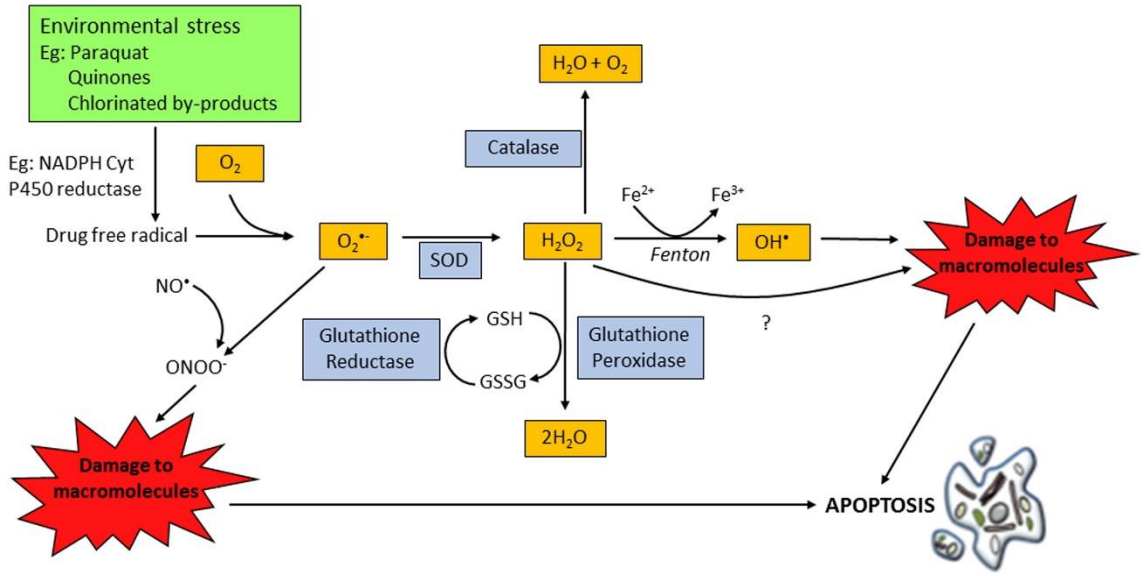


**Figure 47. An overview of ROS scavenging system.**

Adopted from Maureen Redza-Dutordoir and Diana A.Averill-Bates (Redza-Dutordoir and A.Averill-Bates, 2016).

### *dare* is a downstream target of *NitFhit*

As mentioned above, Fhit transfers electrons to FDXR, activating ferredoxin 1 (FDX1) and ferredoxin 2 (FDX2). In addition, I found a report in the interactome database that Nit1 and FDXR may interact. The fact that each separately existing counterpart gene of the fusion protein gene interacts in common with FDXR suggests that FDXR may be an important downstream target of NitFhit. Therefore, I tested whether Dare, *Drosophila* homolog of FDXR, is responsible for the intestinal wall thinning of $NitFhit^{KO}$. Indeed, *dare* knockdown alone was sufficient to reduce the intestinal wall thickness and completely blocked the recovery of the intestinal wall thinning by NitFhit overexpression (Figure 48). In conclusion, Dare is a necessary downstream target of NitFhit for modulating the intestinal wall thickness.

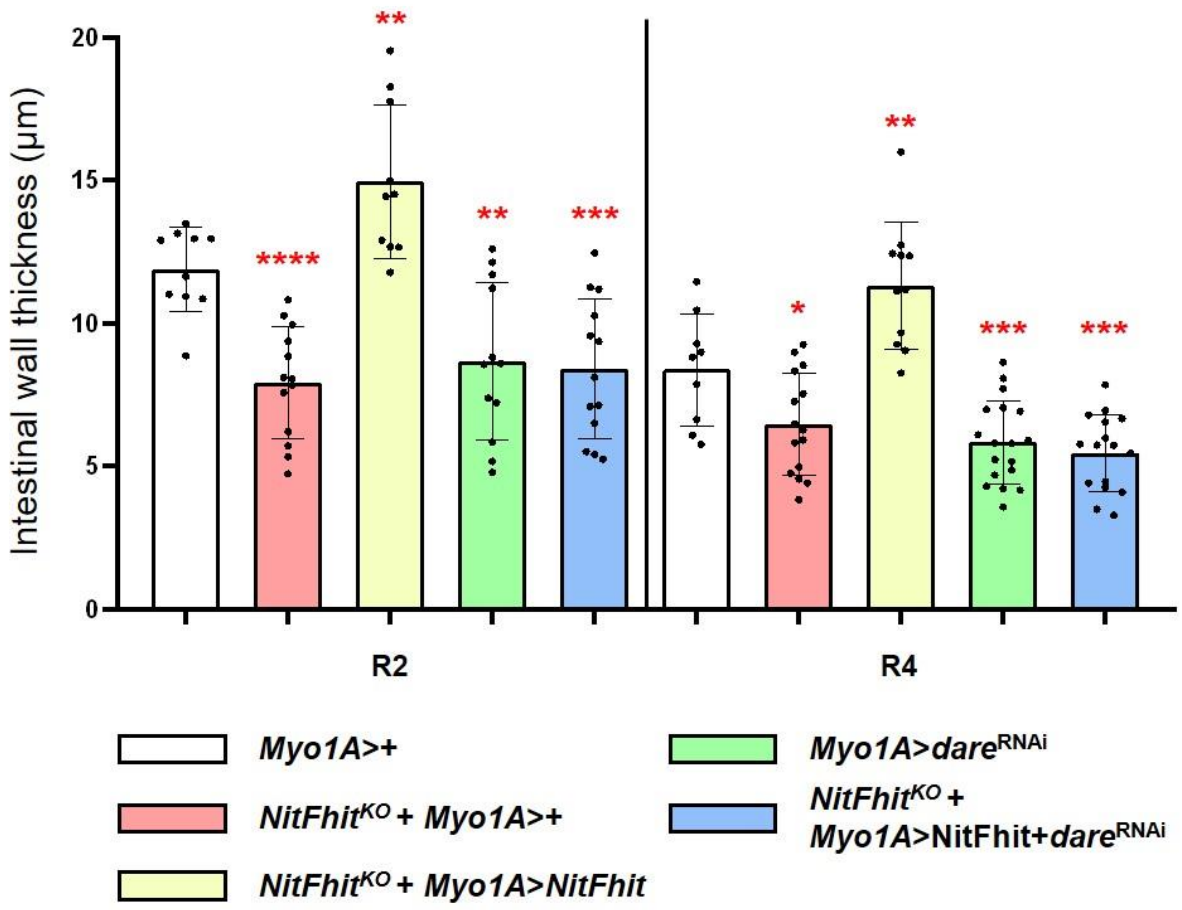


**Figure 48. NitFhit requires Dare to regulate the thickness of the intestinal wall.**

Statistical analysis of the thickness of the intestinal wall of each genotype (*, $p<0.05$; **, $p<0.01$; ***, $p<0.001$).

# Discussion

From this study, I discovered various physiological phenotypes of *NitFhit* associated with intestinal function (Figure 49). I found that the *NitFhit*$^{KO}$ is lighter, eats less amount food slowly, and excretes slowly than the wild-type. After analyzing the intestine structure of *NitFhit*$^{KO}$, I found that NitFhit in the enterocyte modulates the intestinal wall thickness. I also discovered that NitFhit in the enterocyte elevated the resistance to starvation. I found that ROS scavenger enzyme Catalase, but not SOD2, restored the intestinal wall thinning of *NitFhit*$^{KO}$. I confirmed that FDXR is responsible for the modulation of the intestinal wall thickness by NitFhit. However, further experiments are needed to confirm the association between the various phenotypes regulated by NitFhit.

**NitFhit is a fusion protein of Nit1 and Fhit**

NitFhit consists of dNit, the N-terminal Nit domain, and dFhit, C-terminal Fhit domain, each representing the human Nit1 and Fhit, respectively. According to Rosetta stone gene fusion analysis, separate proteins that exist as a fusion protein in other species have a chance to physically interact with and participate in the same biological pathway. One might question whether the physical interaction of human Nit1 and Fhit, which mimic the fusion protein NitFhit, is necessary for two proteins to function properly. Although there is no report of human Nit1 and Fhit proteins physically interacting with each other, there is much evidence that the two proteins likely act in a fused form. Firstly, several studies showed that human Nit1 and Fhit inhibit tumorigenesis in an additional manner (Mittag et al., 2016; Sun et al., 2009).

Secondly, Nit1 and Fhit share two physical interaction partners, β-catenin and FDXR (Druck et al., 2019; Mittag et al., 2016; Weiske et al., 2007a). Thirdly, protein structure analysis of NitFhit revealed that NitFhit forms a tetramer, a Nit tetramer binding to two Fhit dimers (Pace et al., 2000). The fact that both Nit1 and Fhit locates in the mitochondria suggests the chance of physical interaction between two proteins. However, even if Nit1 and Fhit physically interact, it is still unknown why the two separate proteins need to physically interact. The enzymatic activity does not appear to be important for the physiological function of each protein, as the tumor suppressor function of both proteins does not require the enzymatic activity of each protein (Kowara et al., 2002; Semba et al., 2006a). Moreover, enzymatic activities of the two proteins do not appear to be chemically or structurally related, so the enzymatic activity cannot be a clue for the physical association of the two proteins. Briefly, the function of dNit may be to transport MTS-free dFhit to mitochondria, just as HSP60 transports human Fhit to mitochondria in the mammalian system (Druck et al., 2019). I showed that *NitFhit* overexpression is sufficient to restore the intestinal wall thinning of $NitFhit^{KO}$ (Figure 44). We could answer the need for a physical interaction between human Nit1 and Fhit by testing whether independent expression of the dNit and the MTS-tagged dFhit could rescue $NitFhit^{KO}$, as the expression of the fusion protein does.

**The physiological meaning of the intestinal wall thickness in the cell**

Previous studies reported that Nit1 and Fhit act as tumor suppressors, leading to apoptosis upon overexpression and cell proliferation upon downregulation. In this study, I discovered a novel function of NitFhit in regulating intestinal homeostasis. However, the exact mechanism of controlling the intestinal wall thickness by NitFhit is not clear and the tumor-

suppressive function of Nit1 and Fhit cannot be the proper answer to this question. Since enterocytes make up most of the cells in the intestine, the thickness of the enterocyte represents the thickness of the intestinal wall. Indeed, I found that NitFhit in the enterocyte is responsible for modulating the intestinal wall thickness (Figure 44). Therefore, thinning of the intestinal wall seems to result from decreased cell growth of enterocytes, but increased enterocyte apoptosis or the insufficient number of enterocytes due to decreased intestinal stem cell differentiation might be other possible explanations for the defect. Stress signals in the enterocyte, such as integrin loss and microbial infection, promote apoptosis of enterocytes decreasing the enterocyte population (Patel et al., 2015). To replenish the enterocyte, the damaged enterocyte activates the JNK pathway to transmit signals to neighboring intestinal stem cells and promote stem cell proliferation (Herrera and Bach, 2019). If the intestinal wall thinning of *NitFhit*$^{KO}$ represents the damaged status of the enterocyte, investigating the JNK pathway activity might be one way to elucidate the mechanism of NitFhit controlling the intestinal wall thickness.

Serum starvation inhibits the PI3K-Akt pathway and thereby activates the transcription activity of FOXO3a, which is responsible for *Fhit* expression (Kelley and Berberich, 2011; Sard et al., 1999). In response to starvation, *Drosophila* may elevate *NitFhit* expression in the enterocyte to maintain its homeostasis, which is not possible in *NitFhit*$^{KO}$, making *NitFhit*$^{KO}$ more susceptible to starvation. Increased *Fhit* expression under serum starvation induces autophagy (Lee et al., 2017). Although this autophagy inductive function cannot explain the intestinal wall thickening by *NitFhit* overexpression in the enterocyte, it can be another possible explanation for the elevated starvation sensitivity of *NitFhit*$^{KO}$. The absence of Fhit in *NitFhit*$^{KO}$ can lead to the autophagy defect in energy-saving tissues such as fat body under the starvation

condition, resulting in energy deficiency. If *NitFhit* overexpression in other tissues can restore the starvation sensitivity of *NitFhit*$^{KO}$ by increasing autophagy, one can say that *NitFhit* plays different roles upon tissue-context, as a growth activator in the enterocyte and autophagy inducer in other tissues.

There are diseases such as bowel perforation and acute mesenteric ischemia whose pathology is similar to the phenotype of *NitFhit*$^{KO}$, a decrease in the intestinal wall thickness. If other phenotypes of *NitFhit*$^{KO}$, such as defective food excretion, are observed in patients with these diseases, a causal relationship between the intestinal wall thickness and other *NitFhit*$^{KO}$ phenotypes may be revealed.

**Downstream signaling pathway of NitFhit**

Based on the previous study that Fhit transfers electrons to FDXR generating ROS (Druck et al., 2019), the defect in *NitFhit*$^{KO}$ is expected to be due to the depletion of ROS. However, I found that the removal of ROS by Catalase, not by SOD2, restored the intestinal wall thinning of *NitFhit*$^{KO}$ (Figure 46), indicating that the defect in *NitFhit*$^{KO}$ was caused by an increased amount of ROS. *Drosophila* elevates the intestinal ROS level in response to microbiota infection via increasing catabolic pathway and thereby activating NADPH oxidase DUOX (Lee et al., 2018). The elevated ROS level in the *Drosophila* intestine promotes endosome formation via the Hedgehog pathway (Lee et al., 2015) or promotes intestinal stem cell differentiation by activating the Hippo pathway and JNK pathway in the enterocyte (Buchon et al., 2013a). *NitFhit*$^{KO}$ seems to have a high-level of ROS without infection, which could alter the activity of listed pathways thereby decreasing the intestinal wall thickness. Another research revealed that infection by *Lactobacillus plantarum* also triggers ROS-

dependent defense system by activating another NADPH oxidase Nox, which shortens the lifespan of *Drosophila* (Iatsenko et al., 2018). *NitFhit*$^{KO}$ was more sensitive to starvation (Figure 45), which may result from elevated immune response due to a high-level of ROS. Therefore, identifying the pathway that alters its activity due to the elevated ROS level in *NitFhit*$^{KO}$ is one way to explain to defect of *NitFhit*$^{KO}$.

Radical oxygen is converted to hydrogen peroxide by the SOD family (Figure 47). Catalase and Glutathione peroxidase catalyze hydrogen peroxide into water and oxygen, but glutathione peroxidase requires its substrate GSH to remove ROS. A previous study revealed that Nit1 removes deGSH, an unusable form of GSH (Peracchi et al., 2017). Although this report said that accumulation of deGSH in Nit1 knockout cell didn`t alter the GSH level, accumulated deGSH may interfere with the enzymatic function of Glutathione peroxidase. This idea can explain why Catalase succeeded and SOD2 failed to restore the defect of *NitFhit*$^{KO}$ because Catalase but not SOD2 can remove the hydrogen peroxide. Maybe, up-regulating Glutathione peroxidase or GSH metabolism could be another approach to rescue the defect of *NitFhit*$^{KO}$.

I presented FDXR, *Drosophila* homolog of Dare, to be a downstream target of the NitFhit (Figure 48). Dare transfers electrons to its two downstream targets FDX1 and FDX2 (Druck et al., 2019). FDX1 transfers electrons to cytochrome P 450 which synthesizes steroid hormones from cholesterol. FDX2 transfers electrons to Cox15 which converts heme A to heme O or uses electrons to generate the iron-sulfur cluster complex. Specification of the pathway responsible for NitFhit to control the intestinal wall thickness will help to understand the physiological meaning of NitFhit.

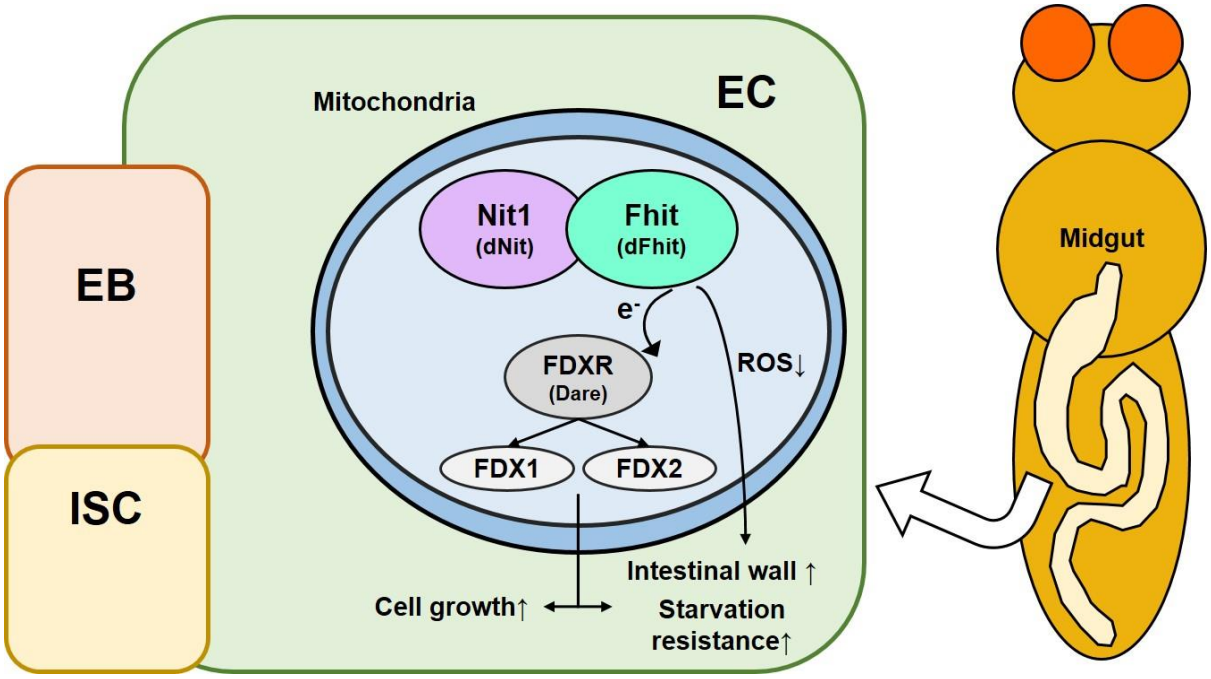


**Figure 49. Proposed model for NitFhit to regulate the enterocyte.**

NitFhit in the enterocyte regulates the cell growth and thereby increasing the intestinal wall thickness. NitFhit in the enterocyte also elevates the starvation resistance. ROS and FDXR is a downstream target for NitFhit to regulate the intestinal wall thickness.

# Conclusion

Among listed genes from interactome databases that may interact with the Hippo pathway, only *pod1* showed the possibility to regulate the Hippo pathway during the screening. Through null fly characterization and genetic interaction with the Hippo pathway components, *pod1* further exhibited the Hippo pathway-activating function. Finally, I discovered the novel scaffold function of Pod1 to recruit the core kinase complex using the mammalian system. Together, these results present *pod1* as a new tissue growth-inhibitory gene. Furthermore, considering that abnormal activity of the Hippo pathway leads to cancer development, that oncogene *SRC* regulates the Hippo pathway through *pod1*, and that there were reports about mutations of *CORO7* in several cancer cell types, I suggest *pod1* as a new therapeutic target for cancer treatment through cell proliferation inhibition.

Besides cell proliferation, cell growth is another way for tissue to grow. I discovered a novel function of NitFhit, a fusion protein of tumor suppressor Nit1 and Fhit, as an activator of cell growth and tissue growth. $NitFhit^{KO}$ showed overall retardation to the growth and survival, such as the lighter body weight, decreased food uptake, thin intestinal wall, and elevated sensitivity to starvation. Restoring the function of NitFhit in the enterocyte rescued the intestinal wall thickness and starvation sensitivity of $NitFhit^{KO}$, presenting NitFhit as a positive regulator of tissue growth and survival.

I discovered novel functions of *pod1* and *NitFhit* regulating cell proliferation and growth, respectively. This research extends our understanding of complicated regulatory mechanisms over tissue growth and proposes new treatment methods for related diseases.

## References


Andriani, F., Roz, E., Caserini, R., Conte, D., Pastorino, U., Sozzi, G., and Roz, L. (2012). Inactivation of Both FHIT and p53 Cooperate in Deregulating Proliferation-Related Pathways in Lung Cancer. Journal of Thoracic Oncology *7*, 631-642.

Bao, L.Y., Shi, B.Y., and Shi, Y.B. (2020). Intestinal homeostasis: a communication between life and death. Cell Biosci *10*.

Barnes, L.D., Garrison, P.N., Siprashvili, Z., Guranowski, A., Robinson, A.K., Ingram, S.W., Croce, C.M., Ohta, M., and Huebner, K. (1996). Fhit, a Putative Tumor Suppressor in Humans, Is a Dinucleoside 5',5'' ''-P1,P3-Triphosphate Hydrolase. Biochemistry *35*, 11529-11535.

Bhattacharya, K., Swaminathan, K., Peche, V.S., Clemen, C.S., Knyphausen, P., Lammers, M., Noegel, A.A., and Rastetter, R.H. (2016). Novel Coronin7 interactions with Cdc42 and N-WASP regulate actin organization and Golgi morphology. Sci Rep *6*, 25411.

Brown, M.T., and Cooper, J.A. (1996). Regulation, substrates and functions of src. Biochimica Et Biophysica Acta-Reviews on Cancer *1287*, 121-149.

Buchon, N., Broderick, N.A., and Lemaitre, B. (2013a). Gut homeostasis in a microbial world: insights from Drosophila melanogaster. Nat Rev Microbiol *11*, 615-626.

Buchon, N., Osman, D., David, F.P., Fang, H.Y., Boquete, J.P., Deplancke, B., and Lemaitre, B. (2013b). Morphological and molecular characterization of adult midgut compartmentalization in Drosophila. Cell Rep *3*, 1725-1738.

Byun, M.R., Hwang, J.H., Kim, A.R., Kim, K.M., Park, J.I., Oh, H.T., Hwang, E.S., and Hong, J.H. (2017). SRC activates TAZ for intestinal tumorigenesis and regeneration. Cancer Lett *410*, 32-40.

Cai, L., Marshall, T.W., Uetrecht, A.C., Schafer, D.A., and Bear, J.E. (2007). Coronin 1B coordinates Arp2/3 complex and cofilin activities at the leading edge. Cell *128*, 915-929.

Callus, B.A., Verhagen, A.M., and Vaux, D.L. (2006). Association of mammalian sterile twenty kinases, Mst1 and Mst2, with hSalvador via C-terminal coiled-coil domains, leads to its stabilization and phosphorylation. FEBS J *273*, 4264-4276.

Chan, E.H., Nousiainen, M., Chalamalasetty, R.B., Schafer, A., Nigg, E.A., and Sillje, H.H. (2005). The Ste20-like kinase Mst2 activates the human large tumor suppressor kinase Lats1. Oncogene *24*, 2076-2086.

Chang, Y.C., Wu, J.W., Wang, C.W., and Jang, A.C. (2019). Hippo Signaling-Mediated Mechanotransduction in Cell Movement and Cancer Metastasis. Front Mol Biosci *6*, 157.

Chen, C.L., Gajewski, K.M., Hamaratoglu, F., Bossuyt, W., Sansores-Garcia, L., Tao, C., and Halder, G. (2010). The apical-basal cell polarity determinant Crumbs regulates Hippo signaling in Drosophila. Proc Natl Acad Sci U S A *107*, 15810-15815.

Cognigni, P., Bailey, A.P., and Miguel-Aliaga, I. (2011). Enteric neurons and systemic signals couple nutritional and reproductive status with intestinal homeostasis. Cell Metab *13*, 92-104.

Day, R.M., and Suzuki, Y.J. (2006). Cell proliferation, reactive oxygen and cellular glutathione. Dose Response *3*, 425-442.

Dey, A., Varelas, X., and Guan, K.L. (2020). Targeting the Hippo pathway in cancer, fibrosis, wound healing and regenerative medicine. Nat Rev Drug Discov *19*, 480-494.

Dong, J., Feldmann, G., Huang, J., Wu, S., Zhang, N., Comerford, S.A., Gayyed, M.F., Anders, R.A., Maitra, A., and Pan, D. (2007). Elucidation of a universal size-control mechanism in Drosophila and mammals. Cell *130*, 1120-1133.

Druck, T., Cheung, D.G., Park, D., Trapasso, F., Pichiorri, F., Gaspari, M., Palumbo, T., Aqeilan, R.I., Gaudio, E., Okumura, H.*, et al.* (2019). Fhit-Fdxr interaction in the mitochondria: modulation of reactive oxygen species generation and apoptosis in cancer cells. Cell Death Dis *10*, 147.

Dumon, K.R., Ishii, H., Fong, L.Y., Zanesi, N., Fidanza, V., Mancini, R., Vecchione, A., Baffa, R., Trapasso, F., During, M.J.*, et al.* (2001). FHIT gene therapy prevents tumor development in Fhit-deficient mice. Proc Natl Acad Sci U S A *98*, 3346-3351.

Eder, N., Roncaroli, F., Domart, M.-C., Horswell, S., Andreiuolo, F., Flynn, H.R., Lopes, A.T., Claxton, S., Kilday, J.-P., Collinson, L.*, et al.* (2020). YAP1/TAZ drives ependymoma-like tumour formation in mice. Nature Communications *11*.

Enomoto, M., and Igaki, T. (2013). Src controls tumorigenesis via JNK-dependent regulation of the Hippo pathway in Drosophila. EMBO Rep *14*, 65-72.

Fallahi, E., O'Driscoll, N.A., and Matallanas, D. (2016). The MST/Hippo Pathway and Cell Death: A Non-Canonical Affair. Genes (Basel) *7*.

Feitelson, M.A., Arzumanyan, A., Kulathinal, R.J., Blain, S.W., Holcombe, R.F., Mahajna, J., Marino, M., Martinez-Chantar, M.L., Nawroth, R., Sanchez-Garcia, I.*, et al.* (2015). Sustained proliferation in cancer: Mechanisms and novel therapeutic targets. Semin Cancer Biol *35 Suppl*, S25-S54.

Fernandez, B.G., Jezowska, B., and Janody, F. (2014). Drosophila actin-Capping Protein limits JNK activation by the Src proto-oncogene. Oncogene *33*, 2027-2039.

Ferrari, G., Langen, H., Naito, M., and Pieters, J. (1999). A coat protein on phagosomes involved in the intracellular survival of mycobacteria. Cell *97*, 435-447.

Fu, Y., Shan, X., Song, W., Xu, K., Jiao, C., and Zhang, Q. (2019). Correlations of breast cancer FHIT gene with the incidence and prognosis of breast cancer. J BUON *24*, 40-47.

Gareth, D., and baser, M.E. (2001). Neurofibromatosis type 2. Journal of Medical Genetics.

Gatfield, J., Albrecht, I., Zanolari, B., Steinmetz, M.O., and Pieters, J. (2005). Association of the leukocyte plasma membrane with the actin cytoskeleton through coiled coil-mediated trimeric coronin 1 molecules. Mol Biol Cell *16*, 2786-2798.

Gaucher, C., Boudier, A., Bonetti, J., Clarot, I., Leroy, P., and Parent, M. (2018). Glutathione: Antioxidant Properties Dedicated to Nanotechnologies. Antioxidants (Basel) *7*.

Goulev, Y., Fauny, J.D., Gonzalez-Marti, B., Flagiello, D., Silber, J., and Zider, A. (2008). SCALLOPED interacts with YORKIE, the nuclear effector of the hippo tumor-suppressor pathway in

Drosophila. Curr Biol *18*, 435-441.

Hamaratoglu, F., Willecke, M., Kango-Singh, M., Nolo, R., Hyun, E., Tao, C.Y., Jafar-Nejad, H., and Halder, G. (2006). The tumour-suppressor genes NF2/Merlin and Expanded act through Hippo signalling to regulate cell proliferation and apoptosis. Nat Cell Biol *8*, 27-U29.

Hao, Y.W., Chun, A., Cheung, K., Rashidi, B., and Yang, X.L. (2008). Tumor suppressor LATS1 is a negative regulator of oncogene YAP. J Biol Chem *283*, 5496-5509.

Harvey, K., and Tapon, N. (2007). The Salvador-Warts-Hippo pathway - an emerging tumour-suppressor network. Nat Rev Cancer *7*, 182-191.

Harvey, K.F., Pfleger, C.M., and Hariharan, I.K. (2003). The Drosophila Mst ortholog, hippo, restricts growth and cell proliferation and promotes apoptosis. Cell *114*, 457-467.

Harvey, K.F., Zhang, X., and Thomas, D.M. (2013). The Hippo pathway and human cancer. Nat Rev Cancer *13*, 246-257.

Hergovich, A., Schmitz, D., and Hemmings, B.A. (2006). The human tumour suppressor LATS1 is activated by human MOB1 at the membrane. Biochemical and Biophysical Research Communications *345*, 50-58.

Herrera, S.C., and Bach, E.A. (2019). JAK/STAT signaling in stem cells and regeneration: from Drosophila to vertebrates. Development *146*.

Huang, J., Wu, S., Barrera, J., Matthews, K., and Pan, D. (2005). The Hippo signaling pathway coordinately regulates cell proliferation and apoptosis by inactivating Yorkie, the Drosophila Homolog of YAP. Cell *122*, 421-434.

Iatsenko, I., Boquete, J.P., and Lemaitre, B. (2018). Microbiota-Derived Lactate Activates Production of Reactive Oxygen Species by the Intestinal NADPH Oxidase Nox and Shortens Drosophila Lifespan. Immunity *49*, 929-942 e925.

Jaisson, S., Veiga-da-Cunha, M., and Van Schaftingen, E. (2009). Molecular identification of omega-amidase, the enzyme that is functionally coupled with glutamine transaminases, as the putative tumor suppressor Nit2. Biochimie *91*, 1066-1071.

Jayachandran, R. (2008). RNA interference in J774 macrophages reveals a role for coronin 1 in mycobacterial trafficking but not in actin-dependent processes. Mol Biol Cell.

Josse, L., Xie, J., Proud, C.G., and Smales, C.M. (2016). mTORC1 signalling and eIF4E/4E-BP1 translation initiation factor stoichiometry influence recombinant protein productivity from GS-CHOK1 cells. Biochem J *473*, 4651-4664.

Justice, R.W., Zilian, O., Woods, D.F., Noll, M., and Bryant, P.J. (1995). The Drosophila tumor suppressor gene warts encodes a homolog of human myotonic dystrophy kinase and is required for the control of cell shape and proliferation. Genes Dev *9*, 534-546.

Kango-Singh, M., Nolo, R., Tao, C., Verstreken, P., Hiesinger, P.R., Bellen, H.J., and Halder, G. (2002). Shar-pei mediates cell proliferation arrest during imaginal disc growth in Drosophila. Development *129*, 5719-5730.

Karras, J.R., Schrock, M.S., Batar, B., and Huebner, K. (2016). Fragile genes that are frequently altered in cancer: players not passengers. Cytogenetic and Genome Research *150*, 208-216.

Kelley, K., and Berberich, S.J. (2011). FHIT gene expression is repressed by mitogenic signaling through the PI3K/AKT/FOXO pathway. Am J Cancer Res *1*, 62-70.

Kim, N.G., and Gumbiner, B.M. (2015). Adhesion to fibronectin regulates Hippo signaling via the FAK-Src-PI3K pathway. J Cell Biol *210*, 503-515.

Klijn, C., Durinck, S., Stawiski, E.W., Haverty, P.M., Jiang, Z., Liu, H., Degenhardt, J., Mayba, O., Gnad, F., Liu, J.*, et al.* (2015). A comprehensive transcriptional portrait of human cancer cell lines. Nat Biotechnol *33*, 306-312.

Kowara, R., Karaczyn, A.A., Fivash, M.J., Jr., and Kasprzak, K.S. (2002). In vitro inhibition of the enzymatic activity of tumor suppressor FHIT gene product by carcinogenic transition metals. Chem Res Toxicol *15*, 319-325.

Krasnikov, B.F., Chien, C.-H., Nostramo, R., Pinto, J.T., Nieves, E., Callaway, M., Sun, J., Huebner, K., and Cooper, A.J.L. (2009). Identification of the putative tumor suppressor Nit2 as ω-amidase, an enzyme metabolically linked to glutamine and asparagine transamination. Biochimie *91*, 1072-1080.

Kummerfeld, S.K., and Teichmann, S.A. (2005). Relative rates of gene fusion and fission in multi-domain proteins. Trends Genet *21*, 25-30.

Lai, Z.C., Wei, X.M., Shimizu, T., Ramos, E., Rohrbaugh, M., Nikolaidis, N., Ho, L.L., and Li, Y. (2005). Control of cell proliferation and apoptosis by Mob as tumor suppressor, Mats. Cell *120*, 675-685.

Lamar, J.M., Xiao, Y., Norton, E., Jiang, Z.G., Gerhard, G.M., Kooner, S., Warren, J.S.A., and Hynes, R.O. (2019). SRC tyrosine kinase activates the YAP/TAZ axis and thereby drives tumor growth and metastasis. J Biol Chem *294*, 2302-2317.

Lee, K.A., Cho, K.C., Kim, B., Jang, I.H., Nam, K., Kwon, Y.E., Kim, M., Hyeon, D.Y., Hwang, D., Seol, J.H.*, et al.* (2018). Inflammation-Modulated Metabolic Reprogramming Is Required for DUOX-Dependent Gut Immunity in Drosophila. Cell Host Microbe *23*, 338-+.

Lee, K.A., Kim, B., Bhin, J., Kim, D.H., You, H., Kim, E.K., Kim, S.H., Ryu, J.H., Hwang, D., and Lee, W.J. (2015). Bacterial uracil modulates Drosophila DUOX-dependent gut immunity via Hedgehog-induced signaling endosomes. Cell Host Microbe *17*, 191-204.

Lee, T.G., Jeong, E.H., Kim, S.Y., Kim, H.R., Kim, H., and Kim, C.H. (2017). Fhit, a tumor suppressor protein, induces autophagy via 14-3-3tau in non-small cell lung cancer cells. Oncotarget *8*, 31923-31937.

Levayer, R. (2020). Solid stress, competition for space and cancer: The opposing roles of mechanical cell competition in tumour initiation and growth. Semin Cancer Biol *63*, 69-80.

Li, P., Silvis, M.R., Honaker, Y., Lien, W.-H., Arron, S.T., and Vasioukhin, V. (2016). αE-catenin inhibits a Src–YAP1 oncogenic module that couples tyrosine kinases and the effector of Hippo signaling pathway. Genes Dev *30*, 798-811.

Lima, C.D., Klein, M.G., and Hendrickson, W.A. (1997). Structure-based analysis of catalysis and substrate definition in the HIT protein family. Science *278*, 286-290.

Lin, C., Zhang, J., Lu, Y., Li, X., Zhang, W., Zhang, W., Lin, W., Zheng, L., and Li, X. (2018). NIT1 suppresses tumour proliferation by activating the TGFbeta1-Smad2/3 signalling pathway in colorectal cancer. Cell Death Dis *9*, 263.

Liu, X., Gao, Y., Lin, X., Li, L., Han, X., and Liu, J. (2016). The Coronin Family and Human Disease. Curr Protein Pept Sci *17*, 603-611.

Machesky, L.M., Reeves, E., Wientjes, F., Mattheyse, F.J., Grogan, A., Totty, N.F., Burlingame, A.L., Hsuan, J.J., and Segal, A.W. (1997). Mammalian actin-related protein 2/3 complex localizes to regions of lamellipodial protrusion and is composed of evolutionarily conserved proteins. Biochemical Journal *328*, 105-112.

Machnicka, B., Czogalla, A., Hryniewicz-Jankowska, A., Boguslawska, D.M., Grochowalska, R., Heger, E., and Sikorski, A.F. (2014). Spectrins: a structural platform for stabilization and activation of membrane channels, receptors and transporters. Biochim Biophys Acta *1838*, 620-634.

Mayer, E.L., and Krop, I.E. (2010). Advances in targeting SRC in the treatment of breast cancer and other solid malignancies. Clin Cancer Res *16*, 3526-3532.

Meignin, C., Alvarez-Garcia, I., Davis, I., and Palacios, I.M. (2007). The Salvador-Warts-Hippo pathway is required for epithelial proliferation and axis specification in Drosophila. Current Biology *17*, 1871-1878.

Min, S., Yoon, W., Cho, H., and Chung, J. (2017). Misato underlies visceral myopathy in Drosophila. Sci Rep *7*, 17700.

Mittag, S., Valenta, T., Weiske, J., Bloch, L., Klingel, S., Gradl, D., Wetzel, F., Chen, Y., Petersen, I., Basler, K.*, et al.* (2016). A novel role for the tumour suppressor Nitrilase1 modulating the Wnt/beta-catenin signalling pathway. Cell Discov *2*, 15039.

Moon, S.-K., Lee, H.-Y., Li, J.-D., Magura, M., Kang, S.-H., Chum, Y.-M., Linthicum, F.H., Ganz, T., Andalibi, A., and Lim, D.J. (2002). Activation of a Src-dependent Raf-MEK1/2-ERK signaling pathway is required for IL-1alpha-induced upregulation of beta-defensin 2 in human middle ear epithelial cells. Biochim Biophys Acta *1590*, 41-51.

Neufeld, T.P., de la Cruz, A.F., Johnston, L.A., and Edgar, B.A. (1998). Coordination of growth and cell division in the Drosophila wing. Cell *93*, 1183-1193.

Ni, L., Zheng, Y., Hara, M., Pan, D., and Luo, X. (2015). Structural basis for Mob1-dependent activation of the core Mst-Lats kinase cascade in Hippo signaling. Genes Dev *29*, 1416-1431.

Oh, H., and Irvine, K.D. (2009). In vivo analysis of Yorkie phosphorylation sites. Oncogene *28*, 1916-1927.

Pace, H.C., and Brenner, C. (2001). The nitrilase superfamily: classification, structure and function. Genome Biol *2*, REVIEWS0001.

Pace, H.C., Hodawadekar, S.C., Draganescu, A., Huang, J., Bieganowski, P., Pekarsky, Y., Croce,

C.M., and Brenner, C. (2000). Crystal structure of the worm NitFhit Rosetta Stone protein reveals a Nit tetramer binding two Fhit dimers. Curr Biol *10*, 907-917.

Panciera, T., Azzolin, L., Cordenonsi, M., and Piccolo, S. (2017). Mechanobiology of YAP and TAZ in physiology and disease. Nat Rev Mol Cell Biol *18*, 758-770.

Pantalacci, S., Tapon, N., and Leopold, P. (2003). The Salvador partner Hippo promotes apoptosis and cell-cycle exit in Drosophila. Nat Cell Biol *5*, 921-927.

Patel, P.H., Dutta, D., and Edgar, B.A. (2015). Niche appropriation by Drosophila intestinal stem cell tumours. Nat Cell Biol *17*, 1182-+.

Pekarsky, Y., Garrison, P.N., Palamarchuk, A., Zanesi, N., Aqeilan, R.I., Huebner, K., Barnes, L.D., and Croce, C.M. (2004). Fhit is a physiological target of the protein kinase Src. P Natl Acad Sci USA *101*, 3775-3779.

Peracchi, A., Veiga-da-Cunha, M., Kuhara, T., Ellens, K.W., Paczia, N., Stroobant, V., Seliga, A.K., Marlaire, S., Jaisson, S., Bommer, G.T.*, et al.* (2017). Nit1 is a metabolite repair enzyme that hydrolyzes deaminated glutathione. P Natl Acad Sci USA *114*, E3233-E3242.

Praskova, M., Xia, F., and Avruch, J. (2008). MOBKL1A/MOBKL1B phosphorylation by MST1 and MST2 inhibits cell proliferation. Curr Biol *18*, 311-321.

Qiao, Y.T., Chen, J.X., Lim, Y.B., Finch-Edmondson, M.L., Seshachalam, V.P., Qin, L., Jiang, T., Low, B.C., Singh, H., Lim, C.T.*, et al.* (2017). YAP Regulates Actin Dynamics through ARHGAP29 and Promotes Metastasis. Cell Reports *19*, 1495-1502.

Redza-Dutordoir, M., and A.Averill-Bates, D. (2016). Activation of apoptosis signalling pathways by reactive oxygen species. BBA *1863*, 2977-2992.

Ren, F.F., Zhang, L., and Jiang, J. (2010). Hippo signaling regulates Yorkie nuclear localization and activity through 14-3-3 dependent and independent mechanisms. Dev Biol *337*, 303-312.

Rimessi, A., Marchi, S., Fotino, C., Romagnoli, A., Huebner, K., Croce, C.M., Pinton, P., and Rizzuto, R. (2009). Intramitochondrial calcium regulation by the FHIT gene product sensitizes to apoptosis. Proc Natl Acad Sci U S A *106*, 12753-12758.

Rothenberg, M.E., Rogers, S.L., Vale, R.D., Jan, L.Y., and Jan, Y.N. (2003). Drosophila pod-1 crosslinks both actin and microtubules and controls the targeting of axons. Neuron *39*, 779-791.

Rybakin, V. (2008). Role of Mammalian coronin 7 in the biosynthetic pathway. Subcell Biochem *48*, 110-115.

Rybakin, V., Rastetter, R.H., Stumpf, M., Uetrecht, A.C., Bear, J.E., Noegel, A.A., and Clemen, C.S. (2008). Molecular mechanism underlying the association of Coronin-7 with Golgi membranes. Cell Mol Life Sci *65*, 2419-2430.

Rybakin, V., Stumpf, M., Schulze, A., Majoul, I.V., Noegel, A.A., and Hasse, A. (2004). Coronin 7, the mammalian POD-1 homologue, localizes to the Golgi apparatus. FEBS Lett *573*, 161-167.

Sard, L., Accornero, P., Tornielli, S., Della, D., Bunone, G., Campiglio, M., Colombo, M.P., Gramegna, M., Croce, C.M., Pierotti, M.A.*, et al.* (1999). The tumor-suppressor gene FHIT is involved

in the regulation of apoptosis and in cell cycle control. P Natl Acad Sci USA *96*, 8489-8492.

Saxton, R.A., and Sabatini, D.M. (2017). mTOR Signaling in Growth, Metabolism, and Disease. Cell *168*, 960-976.

Scheel, H., and Hofmann, K. (2003). A novel interaction motif, SARAH, connects three classes of tumor suppressor. Curr Biol *13*, R899-900.

Semba, S., Han, S.Y., Qin, H.R., McCorkell, K.A., Iliopoulos, D., Pekarsky, Y., Druck, T., Trapasso, F., Croce, C.M., and Huebner, K. (2006a). Biological functions of mammalian Nit1, the counterpart of the invertebrate NitFhit Rosetta stone protein, a possible tumor suppressor. J Biol Chem *281*, 28244-28253.

Semba, S., Trapasso, F., Fabbri, M., McCorkell, K.A., Volinia, S., Druck, T., Iliopoulos, D., Pekarsky, Y., Ishii, H., Garrison, P.N.*, et al.* (2006b). Fhit modulation of the Akt-survivin pathway in lung cancer cells: Fhit-tyrosine 114 (Y114) is essential. Oncogene *25*, 2860-2872.

Shina, M.C., Unal, C., Eichinger, L., Muller-Taubenberger, A., Schleicher, M., Steinert, M., and Noegel, A.A. (2010). A Coronin7 homolog with functions in actin-driven processes. J Biol Chem *285*, 9249-9261.

Si, Y., Ji, X.Y., Cao, X.L., Dai, X.M., Xu, L.Y., Zhao, H.X., Guo, X.C., Yan, H., Zhang, H.T., Zhu, C.*, et al.* (2017). Src Inhibits the Hippo Tumor Suppressor Pathway through Tyrosine Phosphorylation of Lats1. Cancer Research *77*, 4868-4880.

Snel, B., Bork, P., and Huynen, M. (2000). Genome evolution. Gene fusion versus gene fission. Trends Genet *16*, 9-11.

Su, T.T., and O'Farrell, P.H. (1998). Size control: Cell proliferation does not equal growth. Curr Biol *8*, R687-R689.

Sudol, M. (1994). Yes-associated protein (YAP65) is a proline-rich phosphoprotein that binds to the SH3 domain of the Yes proto-oncogene product. Oncogene *9*, 2145-2152.

Sun, J., Okumura, H., Yearsley, M., Frankel, W., Fong, L.Y., Druck, T., and Huebner, K. (2009). Nit1 and Fhit tumor suppressor activities are additive. J Cell Biochem *107*, 1097-1106.

Swaminathan, K., Stumpf, M., Muller, R., Horn, A.C., Schmidbauer, J., Eichinger, L., Muller-Taubenberger, A., Faix, J., and Noegel, A.A. (2015). Coronin7 regulates WASP and SCAR through CRIB mediated interaction with Rac proteins. Scientific Reports *5*.

Tapon, N., Harvey, K.F., Bell, D.W., Wahrer, D.C.R., Schiripo, T.A., Haber, D.A., and Hariharan, I.K. (2002). salvador promotes both cell cycle exit and apoptosis in Drosophila and is mutated in human cancer cell lines. Cell *110*, 467-478.

Thomas, S.M., and Brugge, J.S. (1997). Cellular functions regulated by Src family kinases. Annu Rev Cell Dev Biol *13*, 513-609.

Thompson, B.J. (2010). Developmental control of cell growth and division in Drosophila. Curr Opin Cell Biol *22*, 788-794.

Tieu, K.S., Tieu, R.S., Martinez-Agosto, J.A., and Sehl, M.E. (2012). Stem cell niche dynamics:

from homeostasis to carcinogenesis. Stem Cells Int *2012*, 367567.

Tseng, J.E., Kemp, B.L., Khuri, F.R., Kurie, J.H., Lee, J.S., Zhou, X., Liu, D., Hong, W.K., and Mao, L. (1999). Loss of Fhit is frequent in stage I non-small cell lung cancer and in the lungs of chronic smokers. Cancer Research *59*, 4798-4803.

Udan, R.S., Kango-Singh, M., Nolo, R., Tao, C., and Halder, G. (2003). Hippo promotes proliferation arrest and apoptosis in the Salvador/Warts pathway. Nat Cell Biol *5*, 914-920.

Verghese, S., Waghmare, I., Kwon, H., Hanes, K., and Kango-Singh, M. (2012). Scribble acts in the Drosophila fat-hippo pathway to regulate warts activity. PLoS One *7*, e47173.

Wang, Y.A., Sun, Y., Le Blanc, J.M., Solomides, C., Zhan, T., and Lu, B. (2016). Nitrilase 1 modulates lung tumor progression in vitro and in vivo. Oncotarget *7*, 21381-21392.

Weiske, J., Albring, K.F., and Huber, O. (2007a). The tumor suppressor Fhit acts as a repressor of β-catenin transcriptional activity. PNAS *104*, 20344-20349.

Weiske, J., Albring, K.F., and Huber*, O. (2007b). The tumor suppressor Fhit acts as a repressor of β-catenin transcriptional activity. PNAS.

Willecke, M., Hamaratoglu, F., Sansores-Garcia, L., Tao, C., and Halder, G. (2008). Boundaries of Dachsous Cadherin activity modulate the Hippo signaling pathway to induce cell proliferation. Proc Natl Acad Sci U S A *105*, 14897-14902.

Wong, R., Piper, M.D.W., Blanc, E., and Partridge, L. (2008). Pitfalls of measuring feeding rate in the fruit fly Drosophila melanogaster. Nat Methods *5*, 214-215.

Wu, S., Liu, Y., Zheng, Y., Dong, J., and Pan, D. (2008). The TEAD/TEF family protein Scalloped mediates transcriptional output of the Hippo growth-regulatory pathway. Dev Cell *14*, 388-398.

Xie, X., Hu, H., Tong, X., Li, L., Liu, X., Chen, M., Yuan, H., Xie, X., Li, Q., Zhang, Y.*, et al.* (2018). The mTOR-S6K pathway links growth signalling to DNA damage response by targeting RNF168. Nat Cell Biol *20*, 320-331.

Xu, C., and Min, J. (2011). Structure and function of WD40 domain proteins. Protein Cell *2*, 202-214.

Xu, T., Wang, W., Zhang, S., Stewart, R.A., and Yu, W. (1995). Identifying tumor suppressors in genetic mosaics: the Drosophila lats gene encodes a putative protein kinase. Development *121*, 1053-1063.

Yu, F.X., Zhao, B., Panupinthu, N., Jewell, J.L., Lian, I., Wang, L.H., Zhao, J., Yuan, H., Tumaneng, K., Li, H.*, et al.* (2012). Regulation of the Hippo-YAP pathway by G-protein-coupled receptor signaling. Cell *150*, 780-791.

Yu, J.Z., and Pan, D.J. (2018). Validating upstream regulators of Yorkie activity in Hippo signaling through scalloped-based genetic epistasis. Development *145*.

Yu, J.Z., Zheng, Y.G., Dong, J.X., Klusza, S., Deng, W.M., and Pan, D.J. (2010). Kibra Functions as a Tumor Suppressor Protein that Regulates Hippo Signaling in Conjunction with Merlin and Expanded. Dev Cell *18*, 288-299.

Yuan, W.C., Lee, Y.R., Lin, S.Y., Chang, L.Y., Tan, Y.P., Hung, C.C., Kuo, J.C., Liu, C.H., Lin, M.Y., Xu, M., *et al.* (2014). K33-Linked Polyubiquitination of Coronin 7 by Cul3-KLHL20 Ubiquitin E3 Ligase Regulates Protein Trafficking. Mol Cell *54*, 586-600.

Zhang, L., Ren, F., Zhang, Q., Chen, Y., Wang, B., and Jiang, J. (2008). The TEAD/TEF family of transcription factor Scalloped mediates Hippo signaling in organ size control. Dev Cell *14*, 377-387.

Zhang, N.L., Bai, H.B., David, K.K., Dong, J.X., Zheng, Y.G., Cai, J., Giovannini, M., Liu, P.T., Anders, R.A., and Pan, D.J. (2010). The Merlin/NF2 Tumor Suppressor Functions through the YAP Oncoprotein to Regulate Tissue Homeostasis in Mammals. Dev Cell *19*, 27-38.

Zhao, B., Li, L., Tumaneng, K., Wang, C.Y., and Guan, K.L. (2010). A coordinated phosphorylation by Lats and CK1 regulates YAP stability through SCF(beta-TRCP). Genes Dev *24*, 72-85.

Zhao, B., Tumaneng, K., and Guan, K.L. (2011). The Hippo pathway in organ size control, tissue regeneration and stem cell self-renewal. Nat Cell Biol *13*, 877-883.

Zhao, B., Wei, X., Li, W., Udan, R.S., Yang, Q., Kim, J., Xie, J., Ikenoue, T., Yu, J., Li, L., *et al.* (2007). Inactivation of YAP oncoprotein by the Hippo pathway is involved in cell contact inhibition and tissue growth control. Genes Dev *21*, 2747-2761.

Zheng, S.C., Ma, X.M., Zhang, L.P., Gunn, L., Smith, M.T., Wiemels, J.L., Leung, K., Buffler, P.A., and Wiencke, J.K. (2004). Hypermethylation of the 5 ' CpG island of the FHIT gene is associated with hyperdiploid and translocation-negative subtypes of pediatric leukemia. Cancer Research *64*, 2000-2006.

Zheng, Y., and Pan, D. (2019). The Hippo Signaling Pathway in Development and Disease. Dev Cell *50*, 264-282.

Zheng, Y.G., Liu, B., Wang, L., Lei, H.Y., Prieto, K.D.P., and Pan, D.J. (2017). Homeostatic Control of Hpo/MST Kinase Activity through Autophosphorylation-Dependent Recruitment of the STRIPAK PP2A Phosphatase Complex. Cell Reports *21*, 3612-3623.

Zhu, S., Jin, J., Gokhale, S., Lu, A.M., Shan, H., Feng, J., and Xie, P. (2018). Genetic Alterations of TRAF Proteins in Human Cancers. Front Immunol *9*, 2111.

## Abstract in Korean/국문 초록

# 성장 조절 유전자 *pod1* 과 *NitFhit* 의 기능 규명

세포 증식과 세포 사멸의 적절한 조절을 통해 조직은 모양과 기능을 유지한다. 세포 증식과 세포 사멸 사이의 균형 손실은 종종 암과 같은 질병의 발생을 유래한다. Hippo 경로는 세포 증식과 세포 사멸을 모두 조절하여 조직 항상성을 제어하는 전형적인 신호 메커니즘이다. 1 부에서는 히포 경로의 조절 메커니즘을 연구하였다. 히포 경로의 새로운 조절자를 찾기 위해 유전자-상호작용 데이터베이스에서 Hippo 경로에 대한 잠재적 조절 후보를 나열하고 유효성 확인을 위한 유전자 스크리닝을 수행하였다. 그 결과, *pod1* 이 히포 경로의 이전에 알려지지 않은 조절자일 수 있음을 발견하고 노랑초파리에서의 *pod1* 과발현 또는 돌연변이가 히포 경로와 관련된 표현형을 나타내는지 여부를 조사하였다. 저자는 *pod1* 이 체중, 날개 크기, 세포 증식 및 세포 사멸과 같은 세포 성장 관련 표현형을 억제하는 것을 관찰하였다. 따라서 *pod1* 과 Hippo 경로의 각 구성 요소 사이의 유전적 상호 작용을 시험하였다. 첫째, Pod1 은 Hippo 경로를 통해 Yki 활동을 직접 제어하고 경로의 핵심 키나제 복합체의 상류 조절자이다. 세포막 어댑터 복합체와의 추가 유전적 상호 작용은 Pod1 이 해당 복합체의 하류 표적임을 보여주었다. 노랑초파리에서의 이러한 유전학적 결과를 기반으로 Pod1 의 포유류 동종체인 CORO7 과 Hippo 경로 구성 요소의 물리적 상호 작용을 조사한 결과 CORO7 이 SAV1, MST2 및 LATS1 과 특이

적으로 상호 작용한다는 것을 발견하였다. 또한 CORO7 의 부재 시 핵심 키나제 복합체가 형성되지 않는 것을 관찰하여 CORO7 이 복합체 형성에 필수적임을 나타내었다. 마지막으로, 저자는 티로신 키나아제 SRC 가 Pod1 의 상류 조절자이며 히포 경로를 조절한다는 것을 발견하였다. 2 부에서 저자는 노랑초파리에서 Nit1 과 Fhit 사이에 자연적으로 발생하는 융합 단백질인 NitFhit 이 장 세포의 세포 성장을 긍정적으로 조절한다는 것을 발견하였다. NitFhit 결손 초파리는 야생형보다 가볍고 음식 섭취 및 배설에 결함이 있음을 발견하였다. 장 세포에서의 NitFhit 발현은 장 벽의 두께를 긍정적으로 조절하고 굶주림에 대한 저항성을 증가시켰다. 유전적 실험 증거는 Catalase 에 의한 과산화수소 제거는 NitFhit 결손 모델의 결함을 회복시킬 수 있으며, Ferredoxin reductase 는 NitFhit 이 노랑초파리의 장 벽 두께를 조절하는 데 필요하다는 것을 제안하였다. 결론적으로 저자는 조직 성장을 제어하는 두 개의 독립적인 경로를 발견하였다. *pod1* 은 세포 증식 및 사멸을 조절하는 Hippo 경로의 새로운 조절 자이다. 종양 억제 기능 외에도 장 세포에서의 NitFhit 은 세포 성장을 촉진하여 장 벽 두께를 조절한다. 세포 증식 및 성장의 기능 장애는 암과 같은 여러 질병의 원인이기 때문에, 세포 증식 및 성장의 메커니즘을 밝혀낸 저자의 연구는 위의 질병에 대한 새로운 치료 메커니즘을 제안한다.

주요어: Pod1, 히포 경로, 세포 증식, 핵심 키나제 복합체, NitFhit, 장 세포

학번: 2014-25024